MRC Harwell
Mammalian Genetics Unit

Identification and Characterisation of New Models for Age-Related Hearing Loss

A thesis presented for the degree of Doctor of Philosophy (D.Phil)
Wolfson College, Oxford

Prashanthini Jeyarajan

Mammalian Genetics Unit, MRC Harwell

Department of Physiology, Anatomy & Genetics,
University of Oxford

Supervisors: Dr Michael Bowl (MGU, MRC Harwell)

Professor Steve Brown (MGU, MRC Harwell)

Professor Andrew King (DPAG, Oxford)

Michaelmas Term 2014

Word Count: 23,556

Identification and Characterisation of New Models for Age-Related Hearing Loss

Prashanthini Jeyarajan

Wolfson College, Oxford
Mammalian Genetics Unit, MRC Harwell
Department of Physiology, Anatomy and Genetics, University of Oxford

A thesis presented for D.Phil, Michaelmas term, 2014.

Abstract

Age-related hearing loss (ARHL), or Presbycusis, is the most prevalent sensory impairment observed in the elderly. It is a progressive, symmetrical, age-related sensorineural hearing loss, most pronounced at higher frequencies. ARHL is a multifactorial disease, with contribution from both environmental and genetic factors. To date, little progress has been made in determining the genetic loci involved. The aim of my doctorate studies is to elaborate upon the genetics underlying ARHL through the identification and characterization of ENU-induced mouse models of ARHL.

This approach has identified *trombone*, a recessive model of ARHL arising from the Harwell Ageing Screen. Recurrent auditory phenotyping at 2, 6, 9 and 12 months of age shows that affected animals display elevated ABR thresholds from 9 months of age, when compared to littermates, and these are further increased at 12 months of age. Genome mapping studies identified a 12.5Mb critical region on chromosome 2 and next generation sequencing identified a T>C mutation in the novel deafness gene *Slc4a10*, causing a leucine to proline substitution in the encoded protein. Immunohistochemical staining of cochlear sections demonstrates that Slc4a10 is expressed in the type II and V fibrocytes of the spiral ligament of wildtype mice, whereas no labelling is observed in $Slc4a10^{trmb/trmb}$ mice. In addition, ultrastructural studies show progressive sensory hair cell loss (inner and outer) in the $Slc4a10^{trmb/trmb}$ mice from >6 months of age. Furthermore, histological assessment of the lateral wall identified strial thinning in the $Slc4a10^{trmb/trmb}$ mice. Given the expression pattern and morphological changes observed, endocochlear potentials were measured in these mice. This identified that $Slc4a10^{trmb/trmb}$ mice have a chronically low endocochlear potential compared to their wildtype and heterozygous littermates.

My findings establish the presence of Slc4a10 in the inner ear and suggest an important role for this sodium-coupled bicarbonate transporter in normal auditory function. I hypothesize that *trombone* is a novel model of strial presbycusis and further functional characterization of this model promises to increase our understanding of the pathobiology associated with age-related hearing loss.

To my dearest Amma and Appa,

Thank you for your love, support and for always believing in me.

Acknowledgements

I would like to express my sincere gratitude to my supervisors Dr. Michael Bowl and Professor Steve Brown for their invaluable support and advice over the past four years. Thank you very much Mike in particular for all your words of motivation, support and guidance throughout my DPhil and in helping me write my thesis.

I would also like to thank all the members of the deafness laboratory at Harwell, both past and present for making my past four years a thoroughly enjoyable experience. In particular, I would like to thank Andy Parker, Sue Morse, Carlos Aguilar and Jo Dorning for helping me out in the lab and for being part of the ageing and *trombone* project. I am also extremely grateful to Jeremy Sanderson, Hilda Tateossian and Andy Parker for taking time to read and provide feedback on the first drafts of my chapters.

I have been fortunate enough to have the support of the core services at Harwell who have been very helpful during my DPhil. First and most importantly, I would like to thank all the members of staff in the MLC, especially Ward 3 and Ward 4. In particular, Marie Hutchison, Lucie Vizor and Sara Wells, without whom I could not have carried out all the experiments detailed in this thesis. I am also grateful to GEMS, the histology team, FESA and Jeremy Sanderson (Bioimaging facility) for their invaluable support throughout my DPhil.

I would like to thank Vincent Michel and Alun Barnard for their experimental contributions to the *trombone* project.

Needless to say, this PhD would not have been possible without the support from my family members. Most importantly, I would like to thank my husband Jeyan, for supporting me and encouraging me throughout my DPhil. Whenever things were not working, you were always there to put a smile on my face. I genuinely couldn't have done it without you. I would like to thank my supportive parents, Amma and Appa, without your love and encouragement; I would not be where I am today. I hope you can be proud of my research and I dedicate this thesis to you. I would also like to thank my sister, Thangi for always being there for me and for keeping me sane. I am also extremely thankful to Sinna and Uncle, who have been like my second parents, for supporting me throughout my life and for giving me valuable advice and to Nivashinee and Thambi for always being there when I needed them. In addition, I would like to thank my extended family, my dearest grandma and my uncles: Lumbo mama, Anna mama and Chutta mama for being there for me from day one and by supporting me and encouraging me throughout my life.

I would like to thank Research into Ageing, Age UK, Action on Hearing Loss and the Medical Research Council for funding this research and my DPhil.

Contributions

Animal husbandry was undertaken by the staff at the Mary Lyon Centre.

The embedding, cutting and mounting of wax sections were performed by the histology core services group at MRC, Harwell.

The endocochlear potential measurements of two and twelve month old animals were undertaken with the assistance of Vincent Michel at the Pasteur Institute in Paris. Subsequent measurements of nine month old animals were undertaken by Vincent alone.

The electroretinography measurements of the *trombone* mice were undertaken by Alun Barnard at the Nuffield Laboratory of Opthalmology, University of Oxford.

Table of Contents

Abstract..... i
Acknowledgments..... iii
Contributions..... iv
List of Figures..... ix
List of Tables..... xii
Abbreviations..... xiii

Chapter 1: Introduction..... 1
1.1 The Anatomy of the Ear and Auditory Transduction..... 1
1.1.1 The Outer Ear..... 3
1.1.2 The Middle Ear..... 3
1.1.3 The Inner Ear..... 5
1.1.3.1 Cochlea Structure..... 5
1.1.3.2 Organ of Corti..... 7
1.1.3.3 Cochlea Hair Cells..... 8
1.1.4 Auditory Transduction..... 11
1.1.5 Ion Regulation in the Cochlea..... 15
1.1.5.1 Generation of the EP by the stria vascularis.. 16
1.1.5.2 Potassium Recycling..... 19
1.1.5.3 Gap Junctions..... 25
1.2 The Vestibular System..... 27
1.3 Hearing Loss..... 29
1.3.1 Types of hearing loss..... 30
1.3.1.1 Conductive Hearing Loss..... 30
1.3.1.2 Central Hearing Loss..... 33
1.3.1.3 Sensorineural Hearing Loss..... 33
1.3.2 Classification of Hearing Loss..... 34
1.3.2.1 Syndromic Hearing Loss..... 34
1.3.2.2 Non syndromic Hearing Loss..... 36
1.3.3 Environmental Factors Causing Hearing Loss..... 39
1.4 Presbycusis and its prevalence..... 41
1.5 GWAS to Elucidate Genes Associated with Age-Related Hearing Loss in Humans..... 44
1.6 The Mouse as a Model of Deafness..... 47
1.6.1 The study of presbycusis in inbred mouse models..... 47
1.7 The Harwell Ageing Screen..... 53
1.7.1 Breeding and Phenotyping Strategy..... 53
1.7.2 Auditory Assessment in mice..... 54
1.8 Models identified..... 56
1.8.1 Muta-Ped-90..... 56
1.8.2 Muta-Ped-c3pde-96..... 57
1.9 Project Aims and Objectives..... 58

Chapter 2: Materials and Methods..... 59
2.1 Animal Care and Husbandry..... 59
2.2 ENU Mutagenesis..... 60
2.2.1 Screening for *ahl1*..... 61
2.3 Auditory Assessment..... 64
2.3.1 Click Box..... 64
2.3.2 Auditory-evoked Brainstem Response (ABR)..... 64
2.4 DNA Extraction..... 67
2.4.1 DNA Extraction Using Lysis Solution..... 67
2.4.2 Qiagen Extraction..... 67
2.4.3 Nucleon Extraction..... 68
2.4.4 DNA Quantification..... 68
2.5 PCR (Polymerase Chain Reaction)..... 69
2.5.1 Reddymix..... 69
2.5.2 Amplitaq Gold..... 69
2.5.3 Hot Shot..... 70
2.6 PCR Purification..... 70
2.6.1 QIAquick PCR Purification Kit (Qiagen)..... 70
2.6.2 GeneClean II (MP Biomedicals)..... 71
2.6.3 SureClean (Bioline)..... 71
2.7 Agarose Gel Electrophoresis..... 72
2.8 Gene Identification..... 73
2.8.1 Whole Genome Mapping..... 73
2.8.2 Fine Mapping..... 73
2.8.3 Next Generation Sequencing..... 75
2.8.4 Validating ENU Induced Changes..... 75
2.8.5 Sanger Sequencing..... 77
2.8.6 Gap Analysis..... 77
2.8.7 *in silico* Analysis..... 77
2.9 Genotyping..... 79
2.9.1 Restriction Digest..... 79
2.9.2 Pyrosequencing..... 79
2.9.3 LightScanner..... 81
2.10 Scanning Electron Microscopy (SEM)..... 84
2.10.1 Tissue Collection..... 84
2.10.2 Fine Dissection of the Inner Ear..... 84
2.10.3 OTOTO Processing..... 85
2.10.4 Critical Point Drying and Mounting..... 85
2.10.5 Sputter Coating..... 86
2.10.6 Imaging..... 86
2.10.7 Hair Cell Counts..... 86
2.11 Histology and Morphological Analysis..... 87
2.11.1 Tissue Collection..... 87
2.11.2 Decalcification, Embedding and Sectioning..... 87
2.11.3 H&E Staining..... 88
2.11.4 Spiral Ligament Analysis..... 89

2.11.5 Nuclei Counts and Spiral Ganglion Neuron Count.... 90
2.12 Immunohistochemistry..... 91
2.12.1 Dewaxing..... 91
2.12.2 Blocking..... 91
2.12.3 Antigen Retrieval..... 92
2.12.4 Antibodies..... 92
2.12.5 Detection and Analysis..... 93
2.13 Immunofluorescence..... 94
2.13.1 Dewaxing..... 94
2.13.2 Permeabilisation and Blocking..... 94
2.13.3 Antibodies..... 94
2.13.4 Mounting and Imaging..... 95
2.14 Endocochlear Potential..... 96
2.15 Statistical Analysis..... 97
2.16 Online Tools..... 98
2.17 Stock Solutions..... 99

Chapter 3: Muta-Ped-90..... 100
3.1 Auditory Phenotyping..... 100
3.2 Identifying the causative mutation in Muta-Ped-90.... 102
3.2.1 Mapping..... 102
3.2.2 Next Generation Sequencing..... 102
3.2.3 Validating the ENU lesions..... 103
3.2.4 Gap Analysis..... 103
3.3 Phenotypic Characterisation..... 105
3.3.1 Histological Studies..... 105
3.3.2 Ultrastructural Studies..... 105
3.4 Discussion and Conclusion..... 108

Chapter 4: Identifying the Causative Mutation in Muta-Ped-C3Pde-96..... 110
4.1 Auditory phenotyping..... 110
4.2 Identifying the Causative Mutation in MPC96..... 112
4.2.1 Mapping..... 112
4.2.2 Next Generation Sequencing..... 113
4.2.3 Validating the ENU Lesions..... 114
4.2.4 *in silico* analysis..... 116
4.3 Analysis of Terminal Tissues..... 117
4.3.1 Expression on Slc4a10 in the inner ear..... 117
4.3.2 SEM Analysis of the Hair Cells..... 119
4.3.3 Gross Histological Analysis..... 119
4.4 Discussion and Conclusion..... 122
4.4.1 Slc4a10..... 122
4.4.2 Role of the Spiral Ligament in the Inner Ear..... 125
4.4.3 Future Work and Conclusion..... 126

Chapter 5: Phenotypic Characterisation of *trombone*..... 127
5.1 Longitudinal Studies..... 128
5.1.1 Onset and Progression of Hearing Loss..... 128
5.1.2 Ultrastructural Studies..... 131
5.1.2.1 SEM Analysis of Hair Cells..... 131
5.1.2.2 Hair Cell Counts..... 133
5.1.3 Expression studies..... 136
5.2 Strial Analysis..... 138
5.2.1 Strial Surface Area..... 138
5.2.2 Nuclei Counts..... 142
5.2.3 Analysis of the Different Layers of the Stria Vascularis..... 146
5.3 Endocochlear Potential..... 151
5.4 Discussion and Conclusion..... 153
5.4.1 The role of the stria vascularis in auditory function... 155
5.4.2 *trombone*..... 159
5.4.3 Conclusion..... 162

Chapter 6: Discussion and Conclusion..... 163
6.1 Conclusion..... 169

References..... 170
Supplementary Information..... 189

List of Figures

Figure 1.1: Overview of the mammalian ear..... 2

Figure 1.2: Cross Section of the Cochlea..... 6

Figure 1.3: Cross Section of the Organ of Corti..... 8

Figure 1.4: Stereocilia formation and organisation..... 10

Figure 1.5: Diagrammatic representation of an uncoiled cochlea..... 12

Figure 1.6: Cochlea mechanotransduction..... 13

Figure 1.7: Auditory Transduction..... 14

Figure 1.8: Structures of the stria vascularis and spiral ligament..... 16

Figure 1.9: Potassium recycling in the cochlea..... 21

Figure 1.10: The Vestibular System..... 28

Figure 1.11: Pathology and treatment of otitis media..... 32

Figure 1.12: Effects of noise induced hearing loss..... 40

Figure 1.13: Types of age-related hearing loss (ARHL)..... 43

Figure 1.14: Clickbox and Auditory Brainstem Response (ABR) testing..... 55

Figure 1.15: ABR thresholds of MP90 mice at three and nine months of age..... 56

Figure 1.16: ABR thresholds of MPC96 mice at 9 months of age..... 57

Figure 2.1: Breeding scheme for the Harwell Ageing Screen..... 62

Figure 2.2: Genotyping for the *ahl1* allele..... 63

Figure 2.3: Electrode positioning for ABR measurements..... 65

Figure 2.4: Restriction digest of *Slc4a10*^{trmb}..... 80

Figure 2.5: Genotyping trombone using the pyrosequencing..... 81

Figure 2.6: Genotyping trombone using the LightScanner..... 82

Figure 3.1: ABR thresholds of MP90 mice at 14 months of age and the progression of hearing loss between nine and 14 months of age.. 101

Figure 3.2: Histological analyses of the inner ear from affected (n=3) and unaffected (n=2) animals..... 106

Figure 3.3: Scanning electron micrographs of hair cells from affected (n=3) and unaffected (n=2) MP90 animals..... 107

Figure 4.1: ABR thresholds of MPC96 mice at 12 months of age and the progression of hearing loss..... 111

Figure 4.2: Critical region of interest of chromosome two..... 112

Figure 4.3: The narrowed MPC96 candidate interval contains one high confidence NGS identified ENU-induced lesion..... 113

Figure 4.4: Confirmation of the presence of an ENU-induced lesion in *Slc4a10*..... 115

Figure 4.5: Location of the L647 residue and its conservation across species..... 115

Figure 4.6: Immunolabelling with an anti-Slc4a10 antibody..... 118

Figure 4.7: Scanning electron micrograph of $Slc4a10^{+/+}$ and $Slc4a10^{trmb/trmb}$ hair cells..... 120

Figure 4.8: Gross morphology of 12 month old trombone mice..... 121

Figure 4.9: There are five Na+ coupled HCO3- transporters in the Slc4 family..... 123

Figure 4.10: Splice variants of Slc4a10..... 124

Figure 5.1: Longitudinal ABR assessment of trombone mice at two, six, nine and 12 months of age..... 129

Figure 5.2: The progression of hearing loss in $Slc4a10^{trmb/trmb}$ mice.... 130

Figure 5.3: Longitudinal ultrastructural studies of the hair cells..... 132

Figure 5.4: Quantification of outer hair cells throughout the cochlear. 134

Figure 5.5: Comparison of outer hair cell loss across the genotypes.. 135

Figure 5.6: Immunolabelling of Slc4a10 in trombone mice..... 137

Figure 5.7: Strial vascularis morphometric analysis of $Slc4a10^{+/+}$ and $Slc4a10^{trmb/trmb}$ mice..... 138

Figure 5.8: Analysis of Spiral Ligament Surface Area in trombone Mice..... 140

Figure 5.9: Analysis of Stria Vascularis Surface Area in trombone Mice..... 141

Figure 5.10: Nuclei Counts to Determine the Number of Cells in the Spiral Ligament [A-D] and the Stria Vascularis [E-H] of trombone mice..... 144

Figure 5.11: Analysis of fibrocytes density in the spiral ligament of trombone mice..... 145

Figure 5.12: Immunofluorescence Analysis of the Strial Basal Cells and vasculature in trombone Mice using Glut1 as a marker..... 148

Figure 5.13: Immunofluorescence Analysis of the Intermediate Cells in trombone Mice using Kir4.1 as a marker..... 149

Figure 5.14: Immunofluorescence Analysis of the Marginal Cells in trombone Mice using Acetylated Tubulin as a marker..... 150

Figure 5.15: Endocochlear Potential Measurements of trombone Mice 152

List of Tables

Table 1.1: Classification of hearing loss..... 29

Table 1.2: Genes underlying non-syndromic hearing loss..... 37

Table 1.3: GWAS to elucidate genes associated with AHRL in humans 46

Table 1.4: Genetic factors that contribute to age-related hearing loss in inbred mouse strains..... 52

Table 2.1 Primers and PCR conditions used for ahl1 genotyping..... 63

Table 2.2: Primers used for narrowing the candidate region in the pedigree MPC96..... 74

Table 2.3: Primers used for narrowing the candidate region in the pedigree MP90..... 74

Table 2.4: Primers used to validate the ENU induced changes in pedigree MP90..... 76

Table 2.5: Primers used to validate the ENU induced changes in pedigree MPC96..... 76

Table 2.6: Primers used to sequence the gaps in the pedigree MPC96 78

Table 2.7: Primer sequences and enzyme used for agarose gel based PCR assays and restriction digests..... 82

Table 2.8: Primer sequences used for pyrosequencing based PCR assays trombone..... 82

Table 2.9: Primer sequences used for LightScanner-based PCR assays..... 82

Table 2.10: PCR mix details for agarose gel based, pyrosequencing and LightScanner-based genotyping assays..... 83

Table 2.11: PCR cycling conditions for (A) Reddy mix standard PCR cycling conditions, (B) pyrosequencing PCR cycling conditions and (C) LightScanner PCR cycling conditions..... 83

Table 2.12: Staining procedure using Shandon Varistain 24..... 88

Table 2.13: Primary antibodies used for immunolabelling..... 95

Table 2.14: Secondary antibodies used for immunolabelling..... 95

Table 3.1: ENU-induced lesions identified by NGS..... 103

Table 3.2: Sequencing gaps within NGS data..... 104

Table 4.1: High confidence ENU-induced lesion identified by NGS..... 114

Table 4.2: Protein prediction of the Slc4a10 mutation..... 116

Abbreviations

3D	Three-dimensional
AA	Amino acid
AB	Avidin-Biotin solution
ABR	Auditory-evoked brainstem response
AHRL	Age-related hearing loss
BX	Backcross
cDNA	Complimentary DNA
COME	Chronic otitis media with effusion
CDH23	Cadherin 23
CPD	Critical point dried
DAB	3-3’diaminobezidine
DAPI	4',6-diamidino-2-phenylindole
dB SPL	Decibels sound pressure level
dd	Double deionised
DNA	Deoxyribonucleic acid
dsDNA	Double stranded DNA
EDTA	Ethylenediaminetetraacetic acid
ENU	N-ethyl-N-nitrosourea C3H6N3O2
EP	Endocochlear potential
ERG	Electroretinography
FESA	Frozen embryo and sperm archive
FGFR	Fibroblast growth factor receptor
G	Generation
GWA	Genome-wide association
H&E	Haematoxylin and Eosin

HET	Heterozygous
HOM	Homozygous
Ig	Immunoglobulin
IHC	Inner hair cell
IP	Intraperitoneal
kb	Kilobases
KO	Knock out
Mb	Megabases
MET	Mechano-electrical transduction
MLC	The Mary Lyon Centre, MRC Harwell
MP90	Muta-ped-90
MPC96	Muta-ped-c3pde-96
mRNA	Messenger RNA
NCBE	Na-driven chloride/bicarbonate exchanger (NBCn2 = Slc4a10)
NBCn2	Same as NCBE
NCBT	Na-driven chloride/bicarbonate transporters, subgroup in SLC4 family
NEB	New England Biosystems
NGS	Next generation sequencing
O_sO_4	Osmium tetroxide (1%)
OHC	Outer hair cell
OM	Otitis media
OTOTO	Osmium tetroxide, thiocarbohydrazide processing
P	Postnatal day
PBS	Phosphate-buffered saline
PBS-T	0.1% PBS-Tween
PCR	Polymerase chain reaction

PDZ	Post synaptic density, Disc large tumour suppressor protein and Zonula occludens-1. (A common domain found in signalling proteins)
PFA	Paraformaldehyde
qPCR	Quantitative PCR
qRT-PCR	Quantitative reverse transcription PCR
RAOM	Recurrent acute otitis media
RNA	Ribonucleic acid
rs	Reference SNP
SEM	Scanning electron microscopy
SGN	Spiral ganglion neuron
SLC4	Solute carrier 4 family
Slc4a10	Solute carrier Family 4, Sodium bicarbonate transporter, member 10
SNP	Single nucleotide polymorphism
ssDNA	Single strand DNA
SSRI	Selective serotonin reuptake inhibitor
SL	Spiral Ligament
SV	Stria Vascularis
T	1% Thiocarbohydrazide in ddH2O
TAE	Tris-acetate EDTA
TBS-T	Tris-buffered saline-Tween
TDT	Tucker Davies Technology
TE	Tris-EDTA
TEM	Transmission electron microscopy
Trmb	Trombone
UV	Ultraviolet light
VEGF	Vascular epithelial growth factor
WT	Wildtype

Chapter 1

Introduction

1.1 The Anatomy of the Ear and Auditory Transduction

In mammals, the ear is the primary organ of the auditory system, which not only detects sound, but also aids in the positioning and balancing of the body. The ear is made up of three distinct sections; the outer ear, the middle ear and the inner ear **(Figure 1.1)**.

The outer ear comprises the pinna (also known as the auricle), external auditory canal and the most superficial layer of the tympanic membrane (also known as the ear drum). The middle ear is an air-filled cavity connected to the nasopharynx by the Eustachian tube and contains the ossicular bones which transmit sounds to the inner ear. The inner ear is a fluid-filled space consisting of the cochlea, which is responsible for sound transduction and the vestibular system which senses balance and motion. These three distinct sections of the ear all play vital roles in sound transduction.

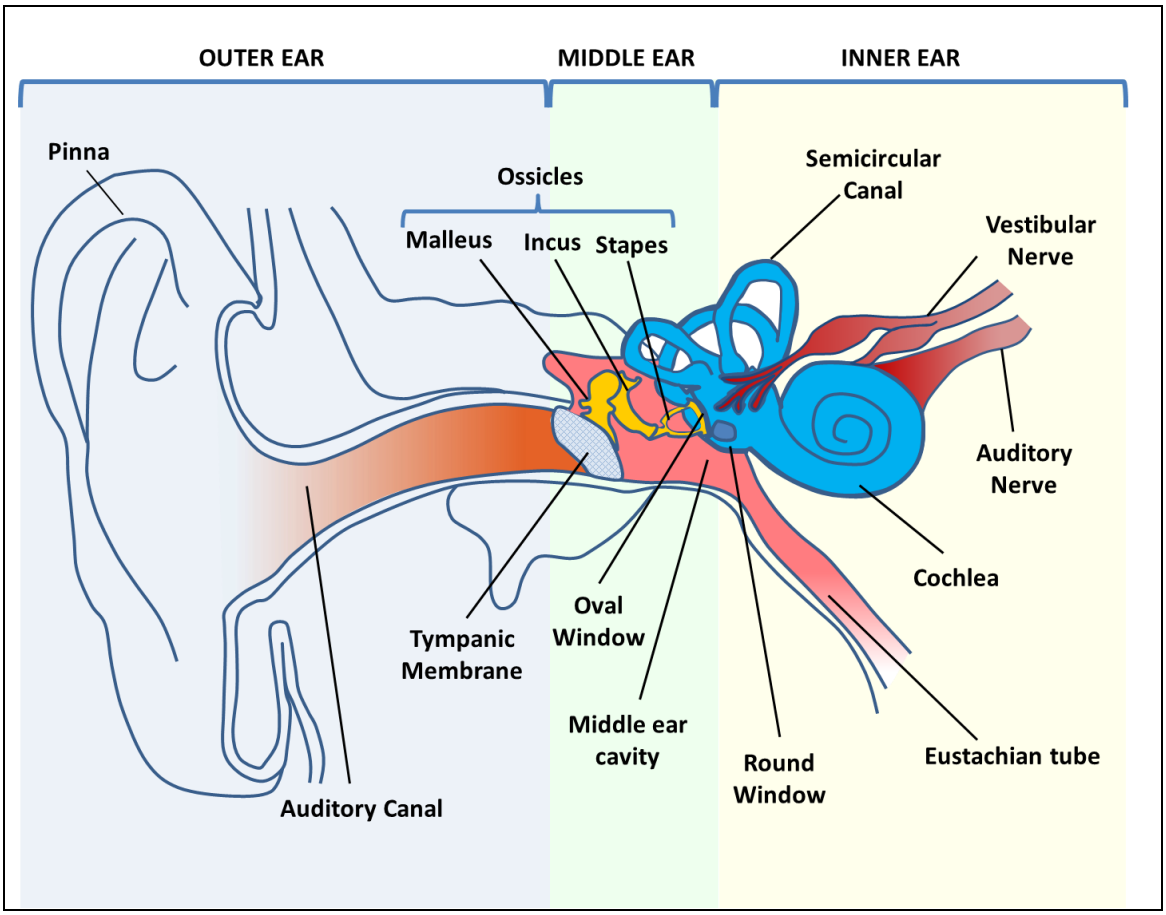

Figure 1.1: Overview of the mammalian ear
The mammalian ear can be divided into three distinct sections; the outer, middle and inner ear. The outer (external) ear contains the pinna and the auditory canal. Sounds waves enter the ear and are channelled to the middle ear through the auditory canal. The middle ear contains the tympanic membrane and ossicles (malleus, incus and stapes). The ossicles transfer the vibrations of the tympanic membrane to the inner ear and generate fluid-membrane waves. The inner ear consists of the cochlear and the vestibular system. The cochlea is responsible for auditory transduction whereas the vestibular organs sense balance and motion.

1.1.1 The Outer Ear

The outer ear is the only visible part of the ear and essentially acts as a resonator and enhances the transmission of sound waves. The pinna collects sound waves and channels them to the tympanic membrane via the auditory canal **(Figure 1.1)**.

Sound waves are longitudinal waves which propagate from a source by the vibration of air molecules along the direction of motion. The pinna plays a pivotal role in sound localisation by reflecting incomings sound depending on the angle of the source. These vibrations pass along the auditory canal, which in turn results in the vibration of the tympanic membrane (Lawrence et al., 1961).

The tympanic membrane is a thin membrane that separates the auditory canal from the middle ear and participates in the first stage of the sound transduction pathway. The tympanic membrane is located at the end of the auditory canal where it is protected from trauma and is maintained at a constant temperature and humidity.

1.1.2 The Middle Ear

The middle ear is an air-filled space enclosed by the temporal bone. The vibrations of the tympanic membrane are transferred through this air-filled cavity to the inner ear. Essentially, the transfer of sound waves encompasses a transition in medium as well – from air to fluid. The middle ear mechanics ensure efficient transfer of acoustic energy to the inner ear.

In order to achieve this, the middle ear contains three of the smallest bones in the human body, the ossicles **(Figure 1.1)**. The ossicular chain comprises the malleus (hammer), incus (anvil) and stapes (stirrup). The ossicles amplify and transfer the sound-induced vibrations of the tympanic membrane to the inner ear via a connection between the stapes footplate and the oval window.

The stapedius muscle and the tensor tympani are attached to the bony capsule encapsulating the inner ear and connect to the stapes and malleus respectively. In response to high intensity sound waves resonating on the tympanic membrane, these muscles contract to decrease the amplification of sound by the ossicular chain, and thus, protecting the inner ear from trauma. This process is known as the tympanic reflex.

The middle ear is the site at which the ear is connected with the nasopharynx to the throat by the Eustachian tube. The Eustachian tube plays an important role in ventilating and equilibrating the pressure of the middle ear. The mucus membrane of the middle ear is lined with ciliated cells which aid in the clearance of particles out of the middle ear and down the Eustachian tube. It is known that optimal sound conduction is only achieved when the middle ear gas pressure is equivalent to the air pressure of the auditory canal (Felding et al., 1987).

1.1.3 The Inner Ear

The inner ear is a membranous labyrinth located in the cavity of the temporal bone. It comprises the cochlea, the auditory sense organ, and five vestibular-end organs which are required for maintaining balance (Hardelin et al., 2001). Vibrations of the tympanic membrane are transferred to the cochlea where the mechanical stimuli are transferred into electrical signals, these signals then travel along the eighth cranial nerve to the brain allowing for auditory perception. The cochlea and the vestibule are both derived from the otic placode during embryonic development, and they share several structural and functional features (Hardelin et al., 2001).

1.1.3.1 Cochlea Structure

The cochlea is a fluid-filled coiled structure which is encapsulated in a membranous bony labyrinth (the otic capsule) and is spiralled around a central bone called the modiolus. The Reissner's membrane and the basilar membrane divide the cochlear duct into three fluid filled sections **(Figure 1.2)**. The two outer sections are, the scala tympani which is connected to the round window, and the scala vestibuli which is connected to the oval window. Both the scala tympani and the scala vestibuli are filled with fluid known as perilymph. Although separated along the length of the cochlea, the scala tympani and scala vestibuli meet at the helicotrema (apex of the cochlea), thus forming a continuous duct that surrounds the third section- the scala media.

The scala media is a triangular-shaped duct filled with endolymph. The ionic composition of the endolymph is very similar to that of an intracellular fluid.

It contains a high potassium (150 mM) concentration and a low sodium (1 mM) and calcium (0.02 mM) concentration. Tight junctions present in the epithelium of the scala media prevent the leakage of the endolymph into the intercellular space (Raphael and Altschuler, 2003). The perilymph is an extracellular-like fluid, high in sodium (140 mM), and low in potassium (3.5 mM). The perilymph also has a higher calcium concentration (1 mM) than the endolymph.

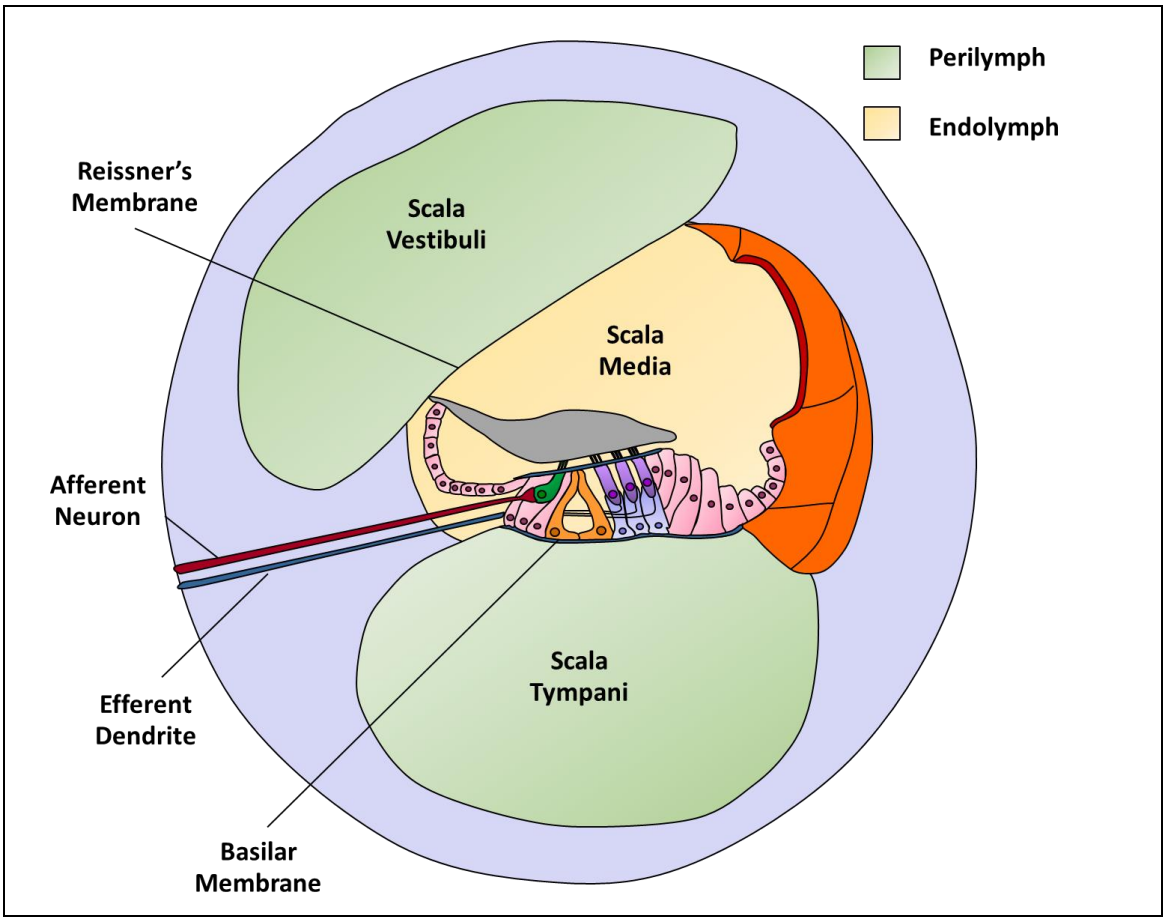

Figure 1.2: Cross Section of the Cochlea
The cochlea is separated into three fluid filled sections, the scala vestibuli, scala media and scala tympani. The scala vestibuli and scala tympani are filled with an extracellular like fluid, perilymph, whereas the scala media is filled with endolymph. Separating the scala vestibuli from the scala media and the scala media from the scala tympani are the Reissner's membrane and basilar membrane respectively. Located within the scala media is the organ of Corti made of up sensory cells and supporting cells. There are two types of sensory hair cells within the organ of Corti; the inner and outer hair cells. Afferent neurons form synapses with the inner hair cells and relay signals to the spiral ganglion neurons. The outer hair cells are innervated by efferent dendrites.

1.1.3.2 Organ of Corti

The organ of Corti, found within the scala media, is made up of an array of sensory cells, also known as hair cells, and different types of supporting cells **(Figure 1.3)**. There are two types of sensory cells: a single row of inner hair cells (IHCs) and three rows of outer hair cells (OHCs) which sit on the basilar membrane, anchored by a series of supporting cells. On the apical surface of the hair cells are specialised structures known as stereocilia.

These are actin-rich organelles that project out into the endolymph and play an important role in auditory transduction. The OHCs and IHCs are physically separated by supporting cells known as pillar cells, which form an arch known as the tunnel of Corti. In addition, supporting cells such as Dieters' cells, Hensen cells and Claudius cells are also located in the Organ of Corti. The Hensen cells and the Deiter's cells are thought to play a structural role and be involved with ionic regulation in the cochlea. Lateral to the Hensen cells are Claudius cells which again provide support for the organ of Corti and provide a barrier between the endolymph and the perilymph (Fechner et al., 1998).

The tectorial membrane is an extracellular matrix which extends along the length of the cochlea in parallel to the basilar membrane overlying the OHCs and the IHCs.

The basilar membrane extends along the length of the cochlear, separating the scala media from the scala tympani. The basilar membrane is narrowest (and stiffest) at the base of the cochlea (closest to the oval window) and

gets wider and less stiff towards the apical end of the cochlea, at the helicotrema. This gradient in physical properties along the length of the cochlea allows different areas of the cochlea to be stimulated in a frequency specific manner (von Békésy and Wever, 1960) and is known as tonotopic organisation. The high frequencies stimulate the base of the cochlea whereas the low frequencies stimulate the apex.

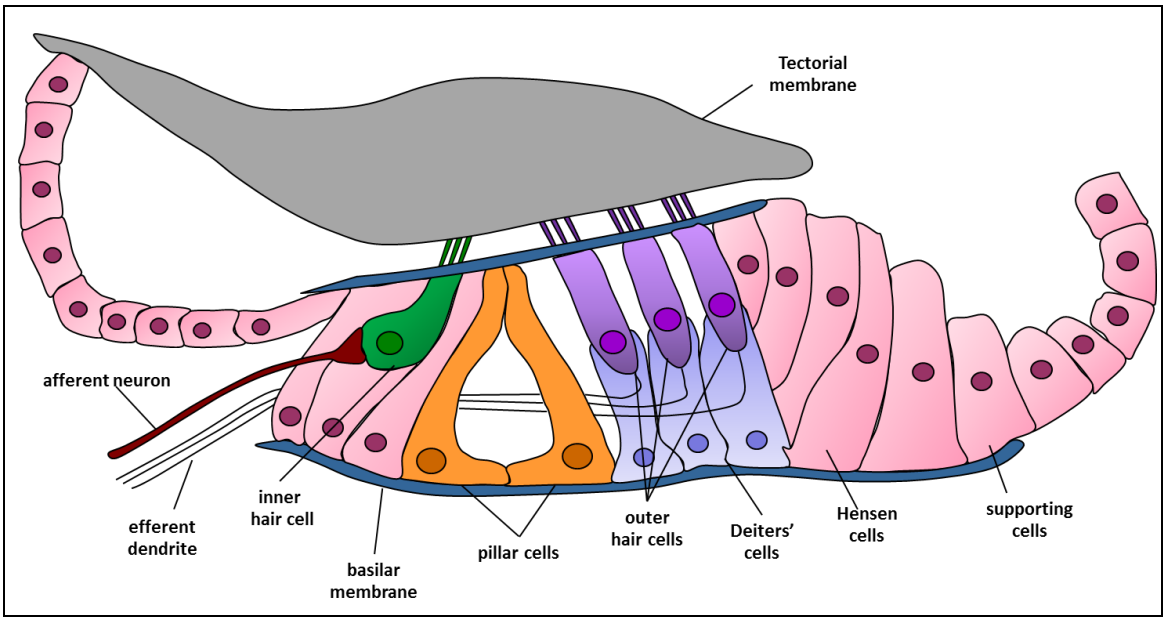

Figure 1.3: Cross Section of the Organ of Corti
The organ of Corti contains the sensory epithelium which sits on top of the basilar membrane in the scala media. The sensory cells of the organ of Corti are made up of three rows of outer hails and one row of inner hair cells which are surrounded by supporting cells. The tectorial membrane is a collagen rich extracellular matrix which lies on top of the hair cells making contact with the stereocilia.

1.1.3.3 Cochlea Hair Cells

Cochlear hair cells develop from epithelial progenitor cells in the otocyst (Morsli et al., 1998), and prior to birth share similar characteristics and are biophysically indistinguishable (Housley et al., 2006). Hair cells first start to differentiate at ~E14.5, however, they mature and exhibit cell-type specific

properties around E19 or P0 (Pujol and Lavigne-Rebillard, 1995). The presence of functionally mature OHCs and IHCs can be seen at p8 and p12, respectively.

The stereocilia are composed of actin filaments and approximately 30-300 stereocilia form a bundle (Rzadzinska et al., 2004). Stereocilia grow towards a kinocilum specialised cilia found at the apex of the stereocilia. The kinocilia, however, tend to regress once the stereocilia bundle becomes fully mature. The stereocilia form into a staircase pattern in which a row of shorter stereocilia is connected to the next row of taller stereocilia by tip links **(Figure 1.4 [A])**. There are also additional connecting links along the rows of stereocilia, known as lateral links.

The OHCs are arranged as three rows of hair cells, with each cell having a stereocilia bundle forming a V shape **(Figure 1.4 [B&C])**, whereas the IHCs are arranged in a single row of cells with a more linear stereocilia bundle **(Figure 1.4 [B&D])**.

The IHCs are the primary acoustic sensors responsible for transforming sound vibrations into electrical signals. Afferent neurons form synapses with IHCs and relay the electrical signals to the spiral ganglion neurons (SGN). These neurons transmit the signals to the auditory centres of the brain via the eighth cranial nerve. Efferent neurons relay signals from the brain into the ear to influence cochlear function in a feedback loop (Raphael and Altschuler, 2003).

The outer hair cells (OHC) behave as cochlea amplifiers responsible for sharpening the frequency-specific response of the cochlea (Purves, 2001) and are innervated by efferent dendrites.

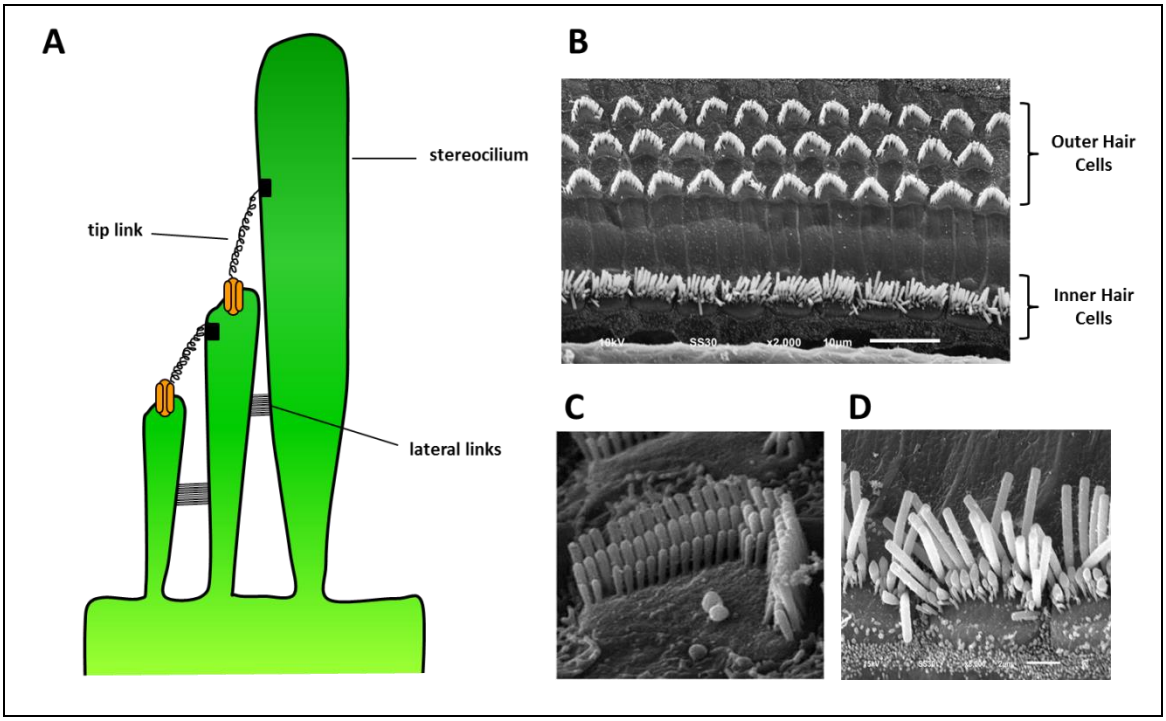

Figure 1.4: Stereocilia formation and organisation
[A] Stereocilia are actin rich organelles which protrude from the apex of cochlea hair cells. Bundles of stereocilia are often formed with several rows of stereocilia in increasing height, forming a staircase pattern. Tip links connect the apex of the stereocilia in adjacent bundles and in addition, there are lateral links along the length of the stereocilia. [B] A scanning electron micrograph (SEM) showing stereocilia arrangement in the cochlea. There are three rows of outer hair cells and one row of inner hair cells. [C] Higher magnification SEM images show the V shaped bundle of the stereocilia in the outer hair cell. [D] The SEM micrograph of the inner hair cells shows the arrangement of the stereocilia in a bundle.

1.1.4 Auditory Transduction

As previously mentioned, in response to auditory stimuli, sound waves enter the outer ear and are channelled along the auditory canal to the tympanic membrane causing it to vibrate. This in turn causes the ossicular bones to articulate.

The malleus is attached to the tympanic membrane on one end and to the incus on the other end. The incus essentially acts as a bridge between the malleus and the stapes, the latter of which rests on the oval window of the inner ear. In response to vibrations in the tympanic membrane, the malleus vibrates and these movements are passed via the incus to the stapes. The footplate of the stapes presses against the oval window in response to these vibrations inducing a change in pressure within the inner ear. This mechanism of auditory transduction is known as ossicular coupling (Merchant et al., 1997).

The stapes-induced pressure waves propagate along the scala vestibuli and the scala tympani, exiting via the round window, and results in the vibration of the basilar membrane **(Figure 1.5)**.

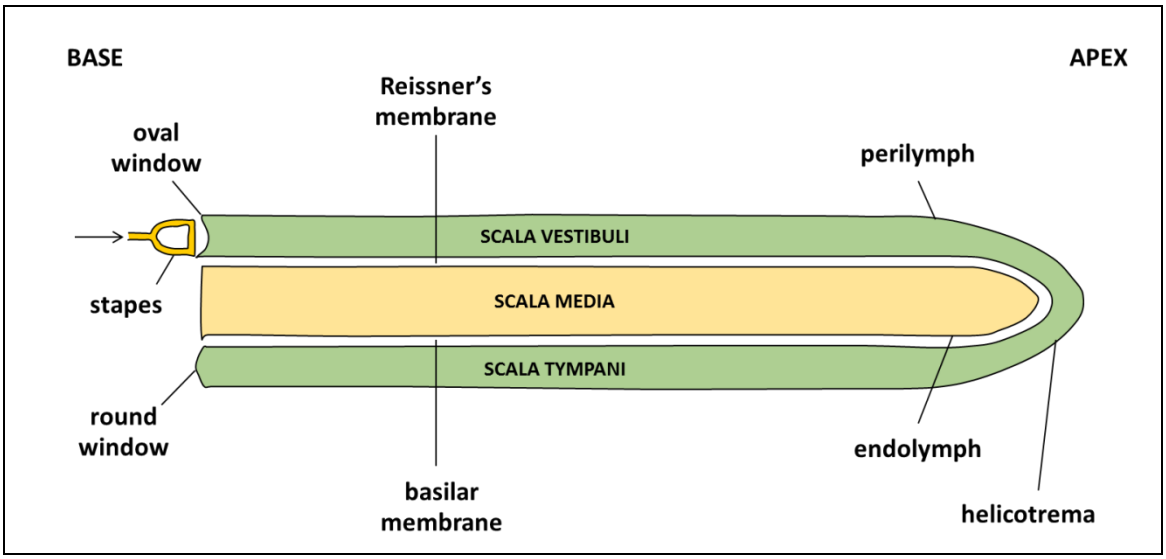

Figure 1.5: Diagrammatic representation of an uncoiled cochlea
During auditory transduction, vibration of the tympanic membrane triggers ossicular coupling. The footplate of the stapes presses against the oval window resulting in the pressure waves to propagate through the perilymph in the scala vestibule and scala tympani, exiting through the oval window.

Adapted from (http://www.bioon.com/bioline/neurosci/course/audvest.html)

Oscillations of the basilar membrane cause the organ of Corti to rise up against the tectorial membrane. This results in the shearing movement of the stereocilia against the tectorial membrane and thus triggering mechanotransduction (Fettiplace and Hackney, 2006).

The shearing force acts on the stereocilia causing a deflection of the hair bundle towards the tallest row. This deflection stretches the tip links resulting in the opening of non-selective cation channels known as mechanotransduction (MET) channels **(Figure 1.6)** (Assad et al., 1991, Corey and Hudspeth, 1979, Shotwell et al., 1981).

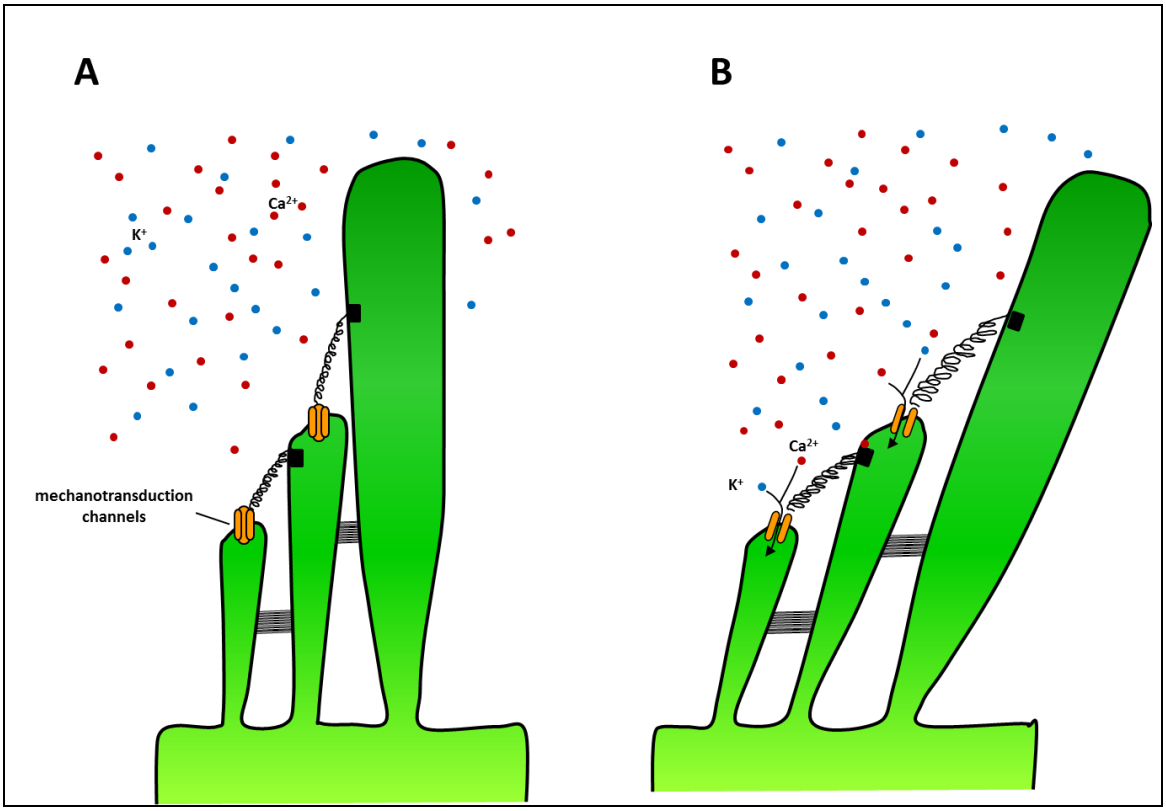

Figure 1.6: Cochlea mechanotransduction
The stereocilia are connected to one another via tip links found on the apex. The stereocilia are bathed in endolymph, which has a high potassium concentration. During mechanotransduction, oscillations of the basilar membrane results in the movement of the stereocilia against the tectorial membrane. [B] This shearing movement between the stereocilia and the tectorial membrane deflects the stereocilia which in turn leads to the opening of non-specific mechanotransduction channels in the apex of the stereocilia. This allows K^+ and Ca^{2+} ions to flood into the cell.

At the resting state, hair cells possess a membrane potential of approximately -60mV (Hudspeth, 1989), whereas the potential of the surrounding endolymph is higher in comparison. The opening of MET channels as a result of stereocilia deflection therefore triggers K^+ and Ca^{2+} to flood into the hair cells down a concentration gradient. This influx leads to cell depolarisation (Shotwell et al., 1981).

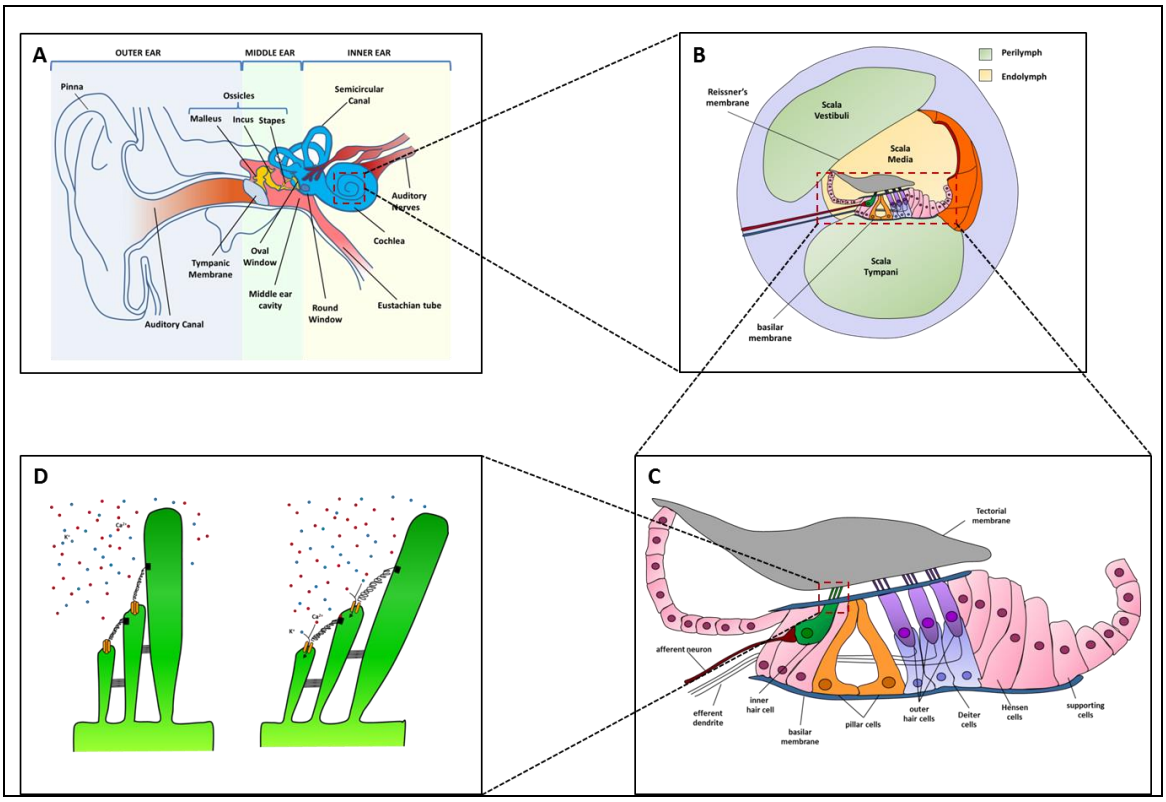

Figure 1.7: Auditory Transduction
[A] Sound waves are collected by the outer ear (pinna) and are channelled down the auditory canal to the tympanic membrane and transmitted via the ossicular chain in the middle ear to the oval window of the inner ear. [B] The cochlea duct is divided into three fluid filled sections, the scala vestibuli, the scala media and the scala tympani. The organ of Corti contains sensory hair cells (outer and inner) and supporting cells. [C] The sensory hair cells are organised into three rows of outer hair cells and one row of inner hair cells. Both contain microvilli like projections known as stereocilia, which project from the apical surface of the hair cells into the potassium rich endolymph. Overlying the hair cells is an extracellular matrix known as the tectorial membrane which is in contact with the apex of the stereocilia. Vibrations from the oval window propagate through the scala vestibuli and scala tympani causing the oscillation of the basilar membrane. This in turn causes movement of the stereocilia which brushes against the tectorial membrane causing a shearing force. [D] The stereocilia are linked to one another via tip links found along the apex. The shearing force between the stereocilia and the tectorial membrane results in the deflection of the stereocilia, stretching the tip links and thus opening mechanotransduction channels. This allows K^+ and Ca^{2+} ions to flood into the cell triggering cell depolarisation and subsequent neurotransmitter release.

In OHCs, the increase in the ionic potential causes the body of the cell to expand and contract due to the presence of the voltage-sensitive motor protein, prestin (Zheng et al., 2000). In IHCs, however, the increase in the membrane potential activates voltage-gated calcium channels in the lateral wall of the hair cell, triggering neurotransmitter release from the base of the cell to the spiral ganglion neurons (SGN) (Raphael and Altschuler, 2003) **(Figure 1.7)**.

1.1.5 Ion Regulation in the Cochlea

Auditory transduction relies on a complex system of ion-transport processes across multiple cell layers within the cochlea (Hibino and Kurachi, 2006). There are three main ionic fluids identified in the cochlea: the endolymph, the perilymph and intrastrial fluid. As previously mentioned (section 1.1.3.1), the endolymph fills the scala media and the perilymph is found in the scala tympani and the scala vestibuli.

The endolymph contains 150 mM K^+, 1 mM Na^+, and 20 μM Ca^{2+}, and possesses a highly positive potential of approximately +80 mV relative to blood plasma and perilymph (Von Bekesy, 1952). This is known as the endocochlear potential (EP), and is necessary to drive mechanotransduction. The endocochlear potential varies in magnitude along the length of the cochlea from base to apex. EP is highest in the basal turn and decreases in magnitude towards the apex.

During auditory transduction, the basilar membrane oscillates causing deflection of the stereocilia and the subsequent opening of mechanotransduction channels. This allows K^+ to enter the hair cells

causing excitation (Hudspeth, 1997, Hudspeth, 1989). It is the role of the endocochlear potential to provide the ideal environment for the K^+ to influx into the hair cells and therefore is imperative for hearing.

1.1.5.1 Generation of the EP by the stria vascularis

The main driving force for mechanotransduction is provided by the endocochlear potential, which is generated by the stria vascularis (Wangemann, 2002, Von Bekesy, 1952). Early research showed that guinea pigs which lacked the stria vascularis do not have an endocochlear potential (Tasaki and Spyropoulos, 1959), highlighting the importance of this specialised epithelium in generating the potential.

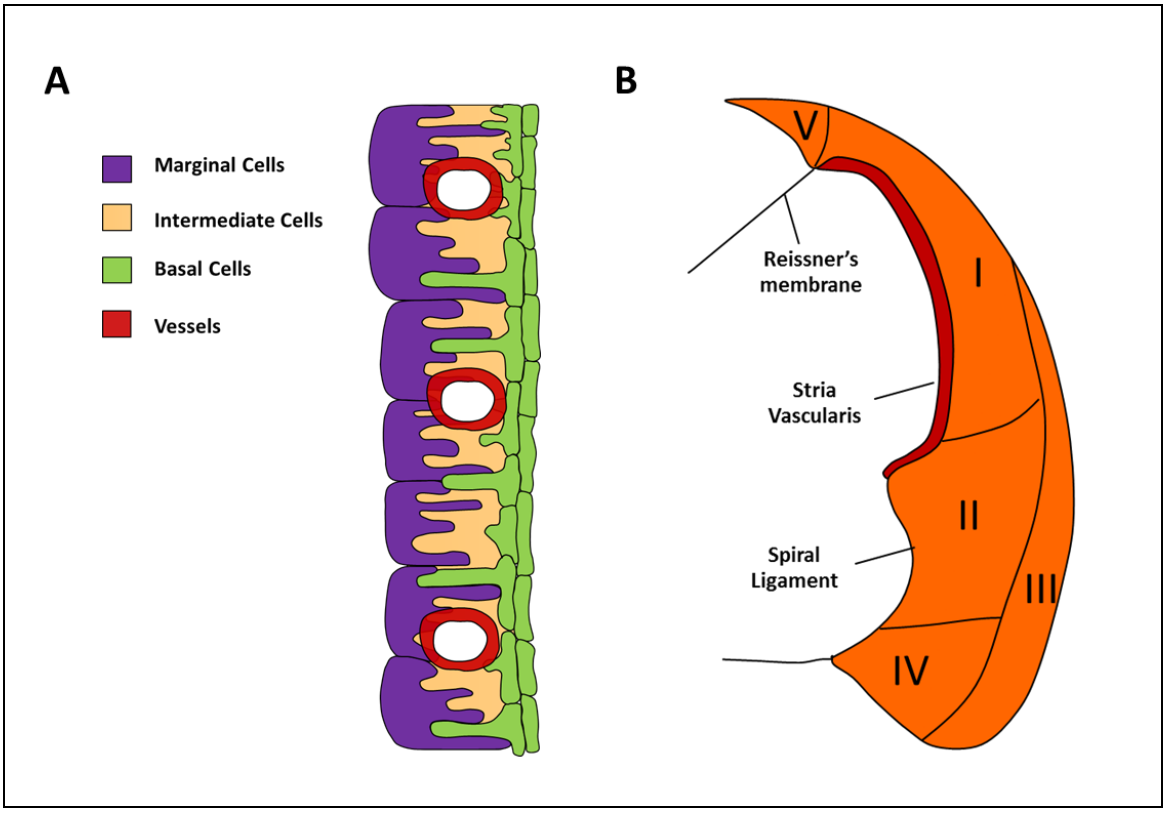

Figure 1.8: Structures of the stria vascularis and spiral ligament
[A] The stria vascularis is responsible for generating the endocochlear potential and is thus pivotal in auditory transduction. It is made up of three layers of cells; from medial to lateral, marginal cells, intermediate cells and basal cells. [B] The spiral ligament contains five distinct groups of fibrocytes (Types I-V). They are functionally specialised due to their location, morphological appearance and marker expression.

Adapted from(Trowe et al., 2008)

The stria vascularis contains a double layered epithelium with cells forming barriers by tight junctions (Jahnke, 1975). It is made of up three distinct layers, from medial to lateral: marginal cells, intermediate cells and basal cells **(Figure 1.8 [A])**.

The first layer consists of basal cells with the inner membrane facing the intrastrial space and the outer membrane facing the fibrocytes of the spiral ligament. They form a continuous layer of flat cells (Raphael and Altschuler, 2003) containing a complex network of junctions between neighbouring basal cells and also with other cells (Forge, 1984). The outer membrane of the basal cells is connected to the fibrocytes via gap junctions. In addition, gap junctions comprised of Gjb2 (Cx26) (gap junction protein, beta 2) and Gjb6 (gap junction protein, beta 2) (Cx30) connect the basal cells to the next layer of cells – the intermediate cells. The gap junctions between the basal cells and the intermediate cells ensure that the intermediate cells play a role in the maintenance of the basal cell barrier (Kikuchi et al., 2000b, Lautermann et al., 1998, Xia et al., 2001).

The intermediate cells are thought to be derived from the neural crest. Due to the presence of melanin in these cells, they are often referred to as melanocytes (Hilding and Ginzberg, 1977). The endocochlear potential is essentially thought to be the K^+ equilibrium potential generated by the potassium channel *Kcnj10* (Kir4.1) found in the intermediate cells (Wangemann, 2006).

Medial to the intermediate cells are the marginal cells which are a layer of polarised epithelial cells which are arranged as one layer that lines the scala

media (Raphael and Altschuler, 2003). The cells are hexagonal shaped with a microvilli-covered surface suggesting interaction with the luminal fluid (Anniko, 1976). Several molecules associated with channels and ionic pumps have been identified in marginal cells. Studies have shown the presence of Na^+ channels in the luminal and lateral membranes of the marginal cells which suggest that they could participate efficiently in the uptake of Na^+ from the endolymph (Iwasa et al., 1994).

It has long been known that Na^+/K-ATPase α1 plays a crucial role in the stria vascularis in generating the endocochlear potential (EP) and thus maintaining the ionic composition of the scala media (Raphael and Altschuler, 2003). This enzyme has been found to be localised to the stria vascularis (Crouch and Schulte, 1995, Erichsen et al., 1996). In addition, studies have also shown the localisation of a Na-K-Cl co-transporter (NKCC1) (Delpire and Mount, 2002) in the basolateral membrane of marginal cells (Mizuta et al., 1997). A similar expression pattern of NKCC1 and Na^+/K-ATPase α1 was seen at both during development and in adults suggesting that the two transporters function together to generate and maintain the K^+ levels and thus the endocochlear potential (Sakaguchi et al., 1998).

Studies have also shown that absence of the intermediate cells in the stria vascularis due to defects in neural cell migration leads to disruption in the generation of the endocochlear potential causing severe hearing impairment (Steel and Barkway, 1989). This suggests that along with the marginal cells, the intermediate cells also play a role in the generation and regulation of the endocochlear potential. The basal cells, however, have

not shown to play a role in ion transport, suggesting that their main function is in creating a physical barrier between the stria vascularis and the spiral ligament.

Research conducted by Salt and colleagues identified a unique extracellular space between the marginal cells and the basal cells known as the intrastrial space (Salt et al., 1987). This fluid-filled space has a K^+ concentration of 1-2 mM. The electrochemical potential of this fluid is ~100mV greater than that of the perilymph and therefore termed the "intrastrial potential" (Salt et al., 1987, Ikeda and Morizono, 1989). This intrastrial space is separated from the endolymph in the scala media and the perilymph in the spiral ligament by the marginal cells and basal cells respectively (Hibino and Kurachi, 2006).

1.1.5.2 Potassium Recycling

Potassium recycling in the inner ear is maintained via a large intercellular pathway in which K^+ ions are brought back to the hair cells and secreted into the scala media via basolateral channels.

Potassium is the most important ion responsible for mechanotransduction and the generation of the endocochlear potential (Konishi et al., 1978, Johnstone et al., 1989, Zidanic and Brownell, 1990). Mutations in several molecules involved in this potassium recycling pathway have been identified as leading to deafness.

The endocochlear potential drives the K^+ from the endolymph into the sensory hair cells via the apical mechanotransduction channels and out into

the perilymph via the basolateral K^+ channels including *Kcnq4*, *Kcnn2* and *Kcnma1 (Kros, 1996)*. The K^+ then cycles through the perilymph to the fibrocytes and the stria vascularis in the lateral wall **(Figure 1.9)**. This circulation of K^+ in the cochlea is thought to essential for maintaining the high K^+ concentration in the endolymph and the endocochlear potential (Hibino and Kurachi, 2006).

The mechanisms underlying K^+ circulations was originally proposed by (Konishi et al., 1978, Sterkers et al., 1982) who showed that radioactive K^+ applied to the perilymph was detected in the endolymph much more efficiently than radioactive K^+ perfused to blood. Further studies by (Marcus et al., 1981, Wada et al., 1979) reiterated this when they showed that perfusion of K^+-free solution in the blood did not affect the endocochlear potential, whereas when the perilymph was perfused with K^+ free solution, the endocochlear potential decreased significantly.

Entry of K^+ into hair cells during auditory transduction, leads to opening of these channels, allowing K^+ to be released into the perilymph. The K^+ is rapidly removed from the perilymph into the supporting cells via the K^+,Cl^- cotransporters, Kcc3 (Boettger et al., 2003) and Kcc4 (Boettger et al., 2002). In addition, supporting cells also express Kir4.1, an inward rectifying K^+ channel which facilitates K^+ uptake (Hibino et al., 1997).

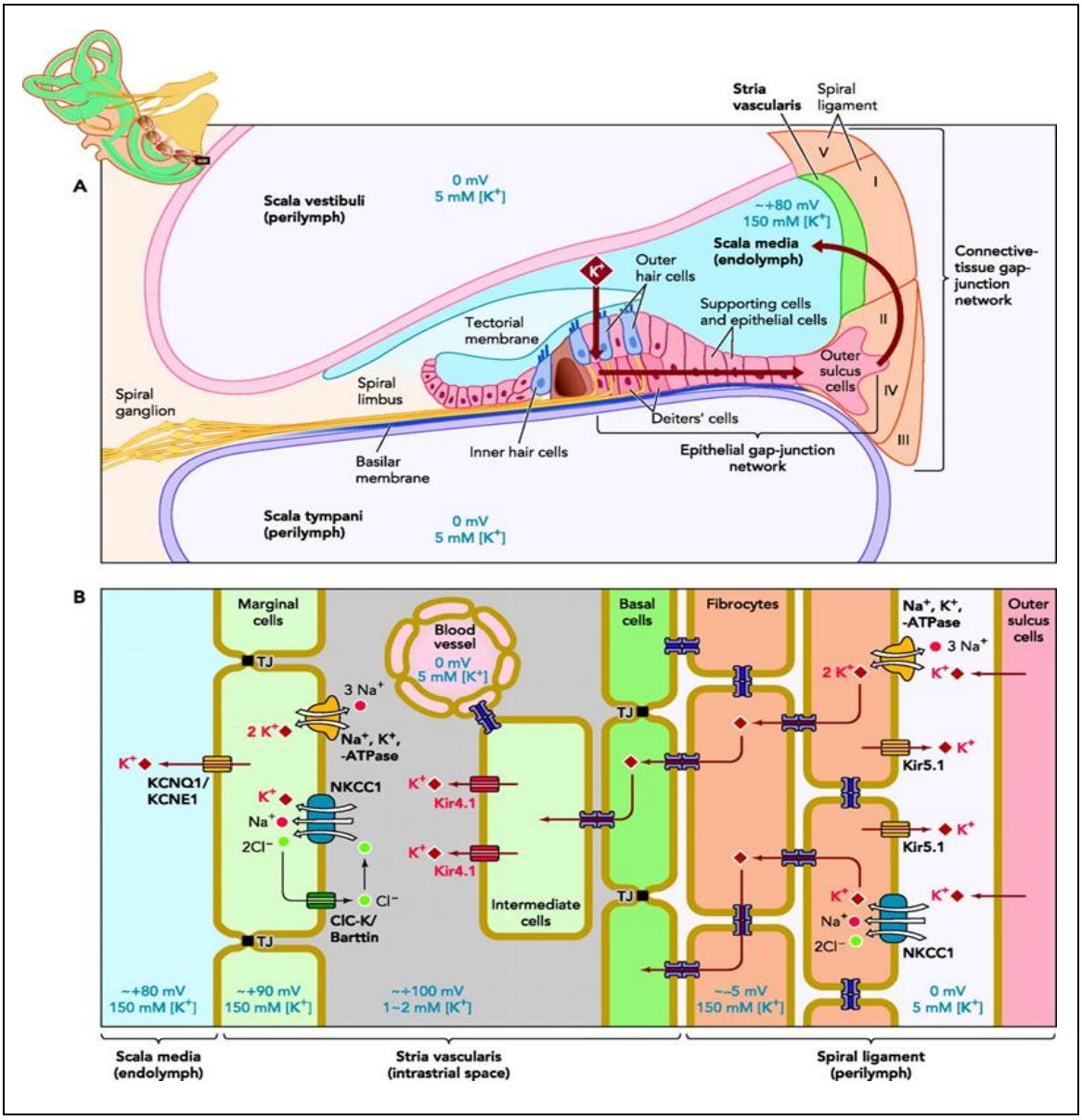

Figure 1.9: Potassium recycling in the cochlea
[A] Potassium recycling in the cochlea in maintained via a large intracellular pathway. K^+ ions enter the hair cells during auditory transduction and are taken up by the supporting. The K^+ ions are then circulated to the fibrocytes in the spiral ligament through the "epithelial gap-junction network", composed of the epithelial and supporting cells on the basilar membrane. Potassium ions are then taken up by the fibrocytes and transported to the stria vascularis via the "connective-tissue gap-junction network", comprising the fibrocytes, basal cells and intermediate cells, where it is released back into the endolymph. K^+ is then released to the endolymph in the scala media across the stria vascularis. **[B]** The stria vascularis is composed of three layers: the basal, intermediate and marginal cells. Several ion transport apparatuses are expressed in the stria vascularis and the spiral ligament which participate in potassium recycling. The K^+ ions cycle through the fibrocytes to the stria vascularis where they transported from the basal cells to the intermediate cells via gap junctions. The K^+ ions are transported from the intermediate cells to the intrastrial space via Kir 4.1 channels due to the low concentration of K^+ in this space. The K^+ is then taken up from the intrastrial space to the marginal cells via NKCC1. The high K^+ concentration in the marginal cells drives the movement of potassium into endolymph via the KCNQ1/KCNE channel.

Image taken from (Hibino and Kurachi, 2006)

Studies have shown that *Kcnq4* knockout mice exhibit degeneration of the outer hair cells leading to progressive hearing loss (Kharkovets et al., 2006). In addition, research has also shown that *Kcc4* knockout mice become deaf at approximately four weeks due to degeneration of the hair cells (Boettger et al., 2002). These studies highlight the importance of potassium recycling for hearing function.

The spiral ligament contains five distinct types of fibrocytes (I-V) which are all bathed in perilymph **(Figure 1.8 [B])**. Type II and type IV fibrocytes have been characterised by numerous extensions of their plasma membrane (Hibino and Kurachi, 2006). There is no cellular connection between the fibrocytes and the supporting cells and therefore K^+ is passed between the two cellular components by a series of K^+ transporters. The K^+ transporters Na^+/K-ATPase α1 (Schulte and Adams, 1989, Schulte and Steel, 1994) and NKCC1 (Crouch et al., 1997, Sakaguchi et al., 1998) have both been found to be expressed in the fibrocytes. Studies have shown that ouabain and furosemide, specific blockers for Na^+/K-ATPase α1 and NKCC1, respectively, suppress the endocochlear potential dramatically when applied to perilymph (Konishi and Mendelsohn, 1970, Marcus et al., 1981, Kusakari et al., 1978). This suggests that both of these transporters contribute to the generation of the endocochlear potential by facilitating K^+ circulation.

In addition to K^+ recycling, Cl^- recycling is also thought to play a role in generating the endocochlear potential (Wangemann, 2006). It is recycled through the basolateral membrane via the Cl^- channel *Clcnka* (Clck-1), *Clcnkb* (Clck-2) and *Bsnd* (barttin). Mutations in the aforementioned Cl^-

channels have been known to cause Bartter syndrome type 4 which is associated with renal failure and deafness (Estevez et al., 2001, Birkenhager et al., 2001, Schlingmann et al., 2004).

The mechanisms of K^+ recycling through the stria vascularis and hair cells have been well characterised. However, there are two different concepts for the uptake of K^+ from the perilymph to the fibrocytes (Wangemann, 2006). Studies by (Salt and Ohyama, 1993, Zidanic and Brownell, 1990) analysing flux and current measurements suggest that, K^+ in the perilymph flows towards the spiral ligament. However, studies by (Spicer and Schulte, 1996) propose that K^+ is taken up by the spiral ligament fibrocytes through a network of gap junctions.

There are several transporters which play a role in K^+ recycling and absence of them leads to a disruption in the ionic composition of the endolymph and the failure to generate the endocochlear potential (Wangemann, 2006).

As previously mentioned, the K^+ channel *Kcnq1/Kcne1* is known to play an important role in transporting K^+ across the membrane of the strial marginal cells (Wangemann et al., 1995). In mice lacking a functional copy of this gene, K^+ secretion is reduced. Severe mutations of this gene have been shown to cause Jervell and Lange-Nielsen syndrome which is a rare autosomal recessive disorder causing sensorineural deafness (Wang et al., 2002, Schulze-Bahr et al., 1997, Baek et al., 2010). Mouse models of Jervell and Lange–Niele syndrome also show a collapsed endolymphatic space as observed in human patients (Friedmann et al., 1966). Less severe

mutations of *Kcnq1*/*Kcne1* lead to the more frequently observed autosomal dominant disorder Romano-Ward syndrome leading to heart defects but not affecting hearing (Casimiro et al., 2004).

The Na^+-$2Cl^+$-K^+ transporter *Slc12a2* is known to be expressed in the strial marginal cells and is essential for uptake of K^+ from the perilymph and the intrastrial space and therefore the generation of the endocochlear potential (Mizuta et al., 1997, Crouch et al., 1997). Mice lacking a copy of this gene show a fall in K^+ in secretion and a collapsed endolymphatic space. In addition, studies where *Slc12a2* is inhibited by a loop-diuretic show that the endocochlear potential is obliterated (Dixon et al., 1999, Delpire et al., 1999, Flagella et al., 1999).

The K^+ channel *Kcnj10* is expressed in the intermediate cells of the stria vascularis (Ando and Takeuchi, 1999) and its onset of expression during development parallels the development of the endocochlear potential (Hibino et al., 2004). Pharmacological studies have identified *Kcnj10* as the channel responsible for the generation of the endocochlear potential (Marcus et al., 1985, Takeuchi and Ando, 1998b). Indeed, mice lacking *Kcnj10* do not generate an endodoclear potential (Marcus et al., 2002) and in addition, the endolymphatic volume and K^+ were reduced. Suggesting that *Kcnj10* not only plays a pivotal role in the generation of the endocochlear potential but is also crucial for K^+ cycling.

Channels and other regulatory mechanisms in the epithelia enclosing the scala media are responsible for maintaining the volume and ionic composition of the endolymph. Ionic imbalance may lead to enlargement of

the scala media as seen in Menière's diseases and Pendred syndrome or lead to the collapse of the endolymphatic compartment as seen in Jervell and Lange-Nielsen syndrome (Paparella et al., 1992, Friedmann et al., 1966, Johnsen et al., 1986). However, the mechanism for detecting the volume within the scala media is still largely unknown. In addition, the K^+ channels and gap junctions within the stria vascularis also play a pivotal role in K^+ cycling. Failure to maintain the K^+ concentration within the cochlea can lead to accumulation of K^+ ions in the intrastrial space thereby abolishing the endocochlear potential (Wangemann, 2006).

1.1.5.3 Gap Junctions

There are two main gap-junctions systems within the cochlea (Kikuchi et al., 2000b). The first system involves the supporting cells of the organ of Corti whereas the second system is associated with the stria vascularis and the fibrocytes of the spiral ligament (Wangemann, 2006) **(Figure 1.9)**. The supporting cells are connected to the epithelial cells in the spiral ligament through an electrical syncytium called the "epithelial gap-junction network". The other syncytium known as the "connective-tissue gap-junction network" is formed by gap junctions between fibrocytes of the spiral ligament and the stria vascularis. It is proposed that these two networks work in conjunction to mediate K^+ cycling in the cochlea (Kikuchi et al., 2000a). Most cells in the cochlea are connected by gap junctions, with the exception of the cochlear hair cells and the strial marginal cells (Takeuchi and Ando, 1998a, Kikuchi et al., 2000b).

The gap junctions *Gjb2* (Cx26) and *Gjb6* (Cx30) connect the stria intermediate cells to the neighbouring basal cells which play a role in the generation of the endocochlear potential. Existing studies show that mice which lack functional expression of *Gjb6* lack the endocochlear potential and are therefore profoundly deaf (Teubner et al., 2003). In addition, mutations in both *GJB2* and *GJB6* have been associated with childhood deafness (Zelante et al., 1997, Del Castillo et al., 2003).

In addition, several other gap junctions have been found to be expressed in the cochlea. *Gja1* and *Gja7* are expressed in the developing mouse cochlea and mutations in *GJA1* have been found to be associated with non-syndromic deafness (Liu et al., 2001, Cohen-Salmon et al., 2004). In adult mice, *Gja1* is expressed in the capillaries of the stria vascularis (Cohen-Salmon et al., 2004) whereas *Gja7* expression is limited to the capillaries of endothelial cells. Mice which lack a functional copy of *Gje1* (Cx29) have been reported to have auditory impairment (Tang et al., 2006).

1.2 The Vestibular System

The vestibular system is responsible for sensing motion, orientation and balance. In consists of five main structures; the sacculus, the utriculus and three semi-circular canals. The sacculus and utriculus are responsible for sensing vertical movement and linear acceleration respectively, whereas the semicircular canals are specialised in responding to the rotational accelerations of the head (Purves, 2001).

The vestibular system is physically connected to the cochlea and shares the same ionic environment as the cochlea. The membranous cavity is filled with the high K^+, low Na^+ intracellular fluid – endolymph.

The vestibular hair cells are located on the sensory epithelium named the crista at the base of the semicircular canals. They are arranged in three swellings known as ampullae (Purves, 2001). The vestibular hair cells extend their hair bundles into the endolymph-filled membranous cavity (Purves, 2001). The vestibular hair cells, unlike cochlear hair cells, form on spots called maculae. They are also much taller than cochlear stereocilia and retain the kinocilium. A gelatinous structure known as the cupula is attached to the top of the hair cells and acts as a barrier to prevent the flow of endolymph.

The sacculus and utriculus are known as otolithic organs due to the presence of otoconia. These are calcium carbonate particles which lay on top of the hair cells. In response to movement, the otoconia are displaced,

causing inertia. This results in the deflection of the hair cells and thus the opening of the channels of the stereocilia.

Rotational movement is perceived by the movement of the endolymph in the semicircular canals (Brown, 1874). Inertia from rotational movements pushes the cupula and depending on the direction of movement, depolarises or hyperpolarises the hair cells.

The vestibular ganglion cells transmit the neural signals from all five sensory area to the brain, enabling the sensation of motion and rotation (Purves, 2001).

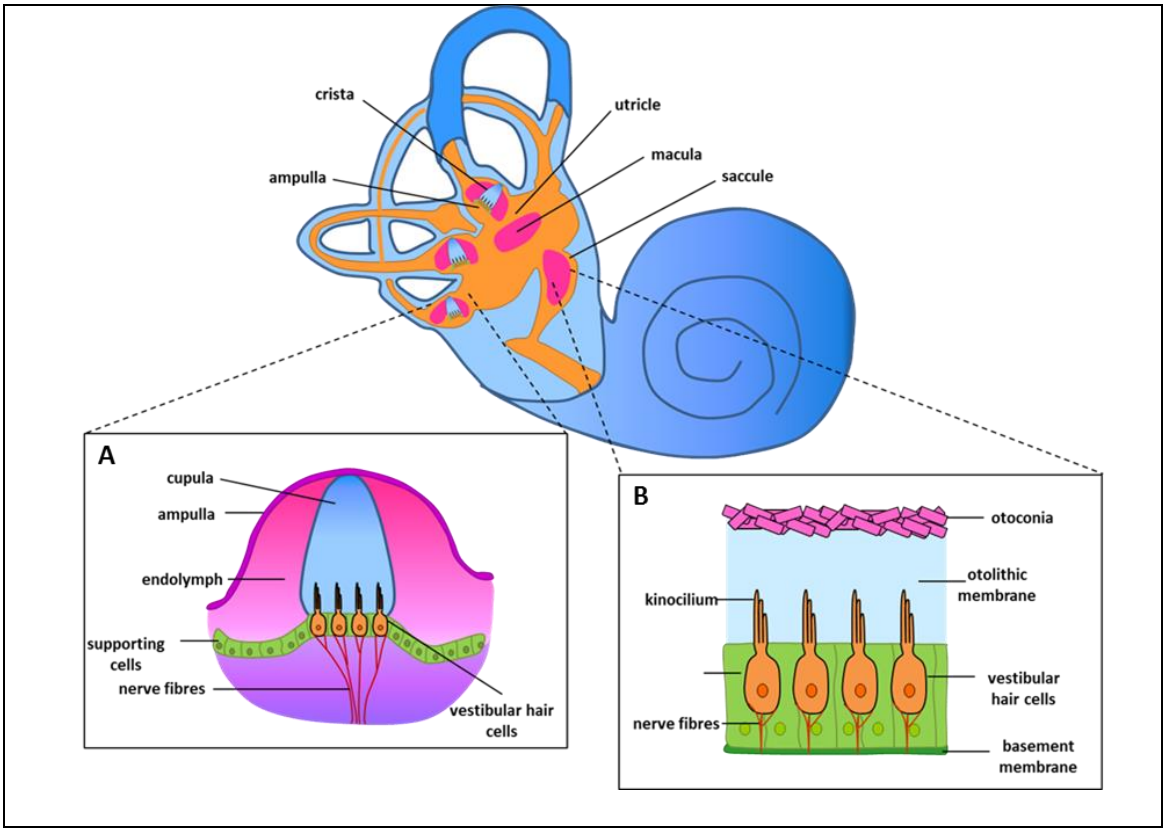

Figure 1.10: The Vestibular System
The vestibular system is responsible for sensing balance and motion in the body. It is made up of five main structures: the utricle, the saccule and the three semi-circular canals. The function of the crista [A] within the semi-circular canals is to sense angular acceleration and deceleration. The macula of the utricle and the saccule [B] allow for the perception of longitudinal accelerations.

Adapted from (http://www.britannica.com/EBchecked/topic/626968/vestibular-system)

1.3 Hearing Loss

Auditory impairment (deafness) is thought to be the most common sensory defect in humans and a huge financial burden on the world economy (JP Holley 2005). The complexity of the auditory apparatus and auditory transduction is echoed in the various classifications of hearing loss. Hearing loss can be classified by a number of different factors such as age of onset, severity, aetiology, and pathobiology **(Table 1.1)**.

Table 1.1: Classification of hearing loss (Dror and Avraham, 2009, Rehm and Morton, 1999, Smith et al., 1993)

Classification	**Description**
Onset of hearing loss	Congenital, pre-lingual or post lingual (including age-related hearing loss)
Severity of hearing loss	Mild (26-40 dB HL), moderate (41-55 dB HL), moderately severe (56-70 dB HL), severe (71-90 dB HL) or profound (>90 dB HL)
Aetiology	Genetic or acquired (environmental)
Site of defect	Conductive (outer and/or middle ear), central (nervous system and auditory cortex), sensorineural (inner ear) or mixed
Presentation	Syndromic (associated with additional clinical features) or non-syndromic (hearing loss is the only clinical abnormality)
Frequency affected (in humans)	Low (<500 Hz), Middle (501-2000 Hz), High (>2000 Hz)
Sidedness of hearing loss	Unilateral (one ear) or bilateral (both ears)

1.3.1 Types of hearing loss

Hearing loss can be broadly classified into three categories; conductive hearing loss, central hearing loss and sensorineural hearing loss.

1.3.1.1 Conductive Hearing Loss

The poor conduction of sound waves into the inner ear is known as conductive hearing loss and can be caused by damage to either the outer ear or the middle ear. The effects of conductive hearing loss can manifest in only one ear or in both ears, causing unilateral or bilateral hearing loss respectively.

Causes of conductive hearing loss include otitis media (OM), otosclerosis (Ramsay and Linthicum, 1994), perforated tympanic membrane, tumours (Verillaud et al., 2011) and impacted cerumen (ear wax) (Subha and Raman, 2006).

The most common cause of conductive hearing loss is otitis media (OM). OM is characterised by effusion in the middle ear accompanied by inflammation of the middle ear epithelial lining. The effusion increases the pressure on the tympanic membrane which restricts the movements of the ossicles and thus preventing efficient sound transduction (Isaacson and Vora, 2003). There are three major types of OM: acute otitis media, otitis media with effusion and chronic suppurative otitis media.

Acute otitis media (AOM) is the most common form of OM, especially in children. Studies have shown that approximately 80% of children

experience one or more episodes of AOM by the age of three (Teele et al., 1989) with approximately 40% experiencing more than six episodes by the age of seven (Casselbrant et al., 1999). It is associated with inflammation of the middle ear lining frequently preceded by an upper respiratory tract infection.

Otitis media with effusion (OME) is more commonly known as "glue ear" and refers to a collection of fluid within the middle-ear space as a result of the negative pressure produced by a dysfunctional Eustachian tube **(Figure 1.11)**.

Chronic suppurative OM occurs as a result of prolonged inflammation of the middle ear. As a result, perforation of the tympanic membrane can occur, causing a bacterial infection in the middle ear for several weeks.

In the majority of cases, AOM will resolve without any specific treatment. In the case of OME and chronic suppurative OM, a tympanostomy tube ("grommet") is inserted through the tympanic membrane to aerate and drain the fluid from the middle ear **(Figure 1.11 [F])**.

Population studies have shown that environmental factors such as frequent swimming, duration of breast feeding and public day care appear to have a significant effect on the development of OM (Zielhuis et al., 1989). Studies on murine models of OM, *Jeff* and *Junbo*, have identified that mice with mutations in the genes *Fbxo11* (Hardisty-Hughes et al., 2006) and *Evi1* (Parkinson et al., 2006) develop OM and conductive hearing loss.

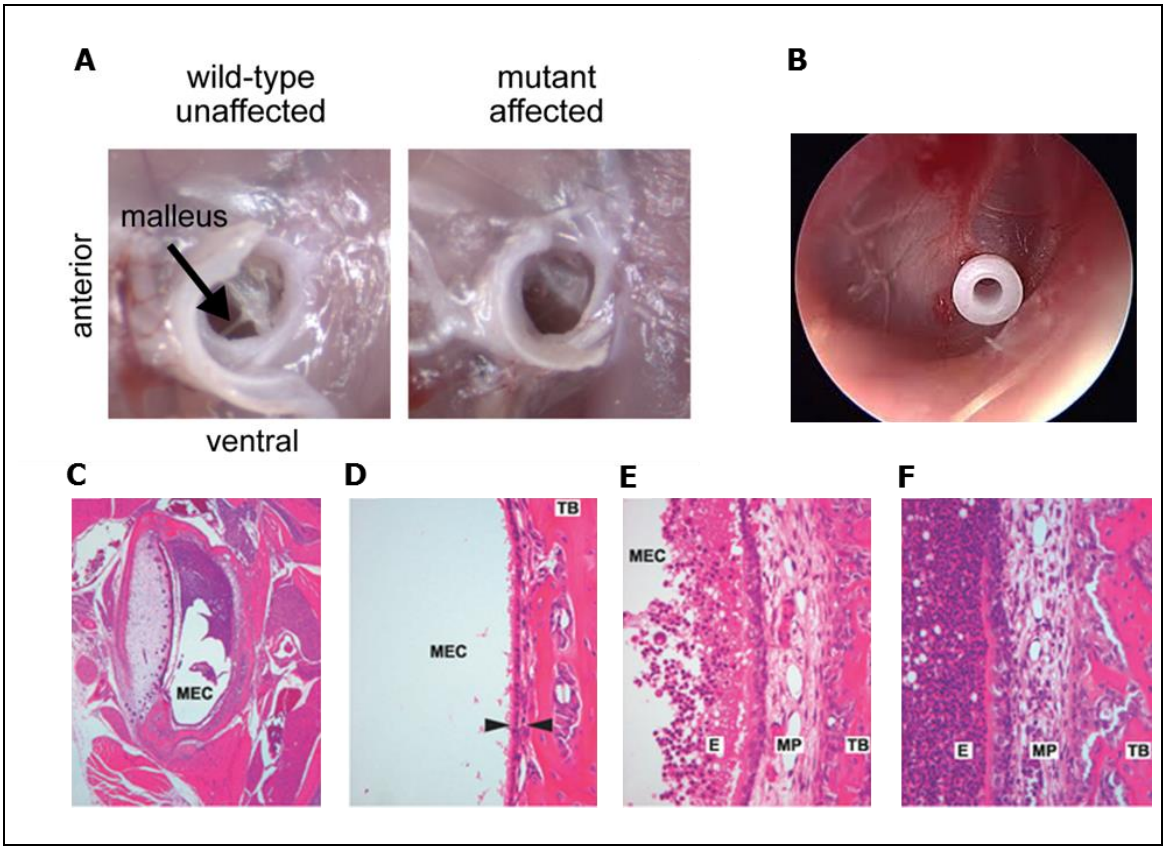

Figure 1.11: Pathology and treatment of otitis media
[A] An unaffected middle ear is clear and therefore the malleus can be seen clearly, however, otitis media results in cloudy eardrums. Otitis media can be treated with the insertion of a tympanostomy tube through the tympanic membrane to drain the fluid from the middle ear [B]. [C-F] Histology sections show that in models of otitis media, the middle ear cavity (MEC) is partly filled with exudate [C]. A normal middle ear contains the temporal bone (TB) covered with a thin mucoperiosteum [D]; however, inflammation of the mucoperiosteum (MP) is seen in model of otitis media [E]. This inflammation can also lead to severe suppurative exudation (E) into the MEC [D].

Adapted from (Cheeseman et al., 2011, Parkinson et al., 2006, http://www.michellewyatt.com/ent-surgery/ear-surgery/grommet-surgery)

1.3.1.2 Central Hearing Loss

Central hearing loss is generally thought to be a rare occurrence when compared to sensorineural and conductive hearing loss. However, recent studies show that it is more prevalent than originally thought (Gates et al., 1996, Gates, 2012).

It is associated with the inability to interpret speech and results from dysfunction of parts of the central nervous system and auditory cortex. One of the conditions frequently associated with central hearing loss is central auditory processing disorder. This affects a person's ability to filter out competing auditory signals, including, problems hearing when there are several conversations simultaneously occurring or the inability to read whilst background noise is present.

Currently, there is no specific treatment for central hearing loss; however, using hearing devices can help by reducing noise signals and thus focussing attention on the main sound source.

1.3.1.3 Sensorineural Hearing Loss

Sensorineural hearing loss occurs due to defects in the inner ear or the cochlear nerve. Due to the complex nature of auditory transduction, many factors can lead to sensorineural hearing loss. These include: developmental failure/delay of the cochlear apparatus, ionic imbalance, degeneration of key structures in the cochlea or disruption of the spiral ganglion neurons and the cochlear nerve. The most common cause of sensorineural hearing loss is the loss or damage of the cochlear hair cells (both OHCs and IHCs). This can be due to environmental factors such as

noise and ototoxic drugs, or due to genetic predispositions. Mammalian cochlear hair cells are terminally differentiated and therefore are not able to regenerate when damaged, resulting in a permanent loss of hearing.

1.3.2 Classification of Hearing Loss

Genetic causes of hearing loss can be further categorised as to whether the gene causes hearing impairment alone (non-syndromic) or whether the hearing impairment is associated with multiple clinical features (syndromic).

1.3.2.1 Syndromic Hearing Loss

The term syndromic hearing loss refers to the manifestation of hearing loss alongside other abnormalities. Approximately 300 syndromes have been described where hearing loss is associated with defects in other systems e.g. renal, ocular, endocrine, nervous and musculoskeletal (Gorlin et al., 1995). Of these syndromes, the causative gene for only approximately 100 have been identified (Petit et al., 2001).

Of those identified, very few are thought to affect only the outer and middle ear. Examples of such syndromes include Treacher-Collins-Franceschetti syndrome and Fanconi pancytopenia which belong to a group of genes encoding DNA-repair proteins. The former, Treacher-Collins-Franceschetti syndrome is a rare, autosomal, dominant, congenital disorder where mutations in the genes *TCOF1* (*Treacle)*, *POLR1C* or *POLR1D* leads to craniofacial abnormalities and ear anomalies, resulting in the manifestation of conductive hearing loss (Group, 1996) (Dauwerse et al., 2011).

The two major classes of syndromic hearing loss are due to (1) middle ear defects associated with or without inner ear defects and (2) isolated inner ear defects (Petit and Weil, 2001).

Examples of syndromes which fall into the first category include: Crouzon facial dysostosis, Stickler syndrome and mucopolysaccharidoses. This often involves defects in the genes encoding fibroblast growth factor receptors (FGFR), transcription factors, lysosomal enzymes and other extracellular matrix components (Petit and Weil, 2001).

Examples of syndromic hearing loss associated with inner ear defects include: Usher, Pendred, Alport and Jervell and Lange Nielsen syndromes. The causative genes encode a large spectrum of molecules including ion channels, transcription factors and lysosomal enzymes.

Studies have shown that defects in a single gene may be responsible for multiple pathologies. Examples of such include Pendred syndrome which is an autosomal recessive disease caused by mutations in the gene *SLC26A4* where an iodine organification defect in the thyroid gland results in early-onset hearing loss, an enlarged vestibular aqueduct and goitre, with occasional hypothyroidism (Hardelin et al., 2001).

However, research has also highlighted that several of the aforementioned syndromes are genetically heterogeneous; therefore, the phenotype may be caused by defects in several different genes. For example, Usher syndrome is a deaf-blind syndrome associated with mutations in 11 known genes. Type I Usher syndrome, characterised by profound congenital

deafness, vestibular dysfunction and progressive retinitis pigmentosa, can be caused by at least six different genes (Jaworek et al., 2012, Millan et al., 2011). Similarly, Alport syndrome, which is associated with deafness and nephropathy, may be due to defects in three different alpha-chains of collagen IV (Petit and Weil, 2001).

1.3.2.2 Non syndromic Hearing Loss

Non-syndromic forms of hearing loss are classified by their mode of inheritance. Deafness which has been inherited on the X-chromosome-linked, autosomal dominant and autosomal recessive modes of transmission are known as DFN, DFNA and DFNB respectively. Approximately 80% of prelingual deafness are DFNB forms whereas, most of the late onset deafness cases are DFNA forms (Hardelin et al., 2001). The different types of non-syndromic hearing loss are further categorised according to the primary target of the inner ear defect; myosin defects, other sensory hair cell defects, tectorial membrane defects and further defects where the primary target is unknown **(Table 1.2)**.

Table 1.2: Genes underlying non-syndromic hearing loss
Adapted from (Petit et al., 2001)

Primary defect	Gene	Protein	Human deafness	Deaf mouse mutant	Type of molecule
Hair cells	*MYO7A*	Myosin VIIA	DFNB2 ± retinopathy	*shaker-1*	Motor protein
			(Usher 1B)[b]		
			DFNA11		
	MYO15	Myosin XV	DFNB3	*shaker-2*	Motor protein
	MYO6	Myosin VI	DFNAi	*Snell's waltzer*	Motor protein
	USH1C	Harmonin	DFNB18 ± retinopathy		PDZ domain-containing
			(Usher 1C)[b]		protein
	CDH23	Cadherin-23	DFNB12 ± retinopathy	*waltzer*	Cell adhesion protein
			(Usher 1D)[b]		
	Espn[a]	Espin	?	*jerker*	Actin-bundling protein
	KCNQ4	KCNQ4	DFNA2		K^+ channel subunit
	Atp2b2/Pmca2[a]	Ca^{2+}-ATPase 2	?	*deafwaddler*	Calcium pump
	OTOF	Otoferlin	DFNB9		Vesicle trafficking protein
	POU4F3	POU4F3	DFNA15	*Brn3c*$^{-/-}$[c]	Transcription factor
Nonsensory cells	*CX26/GJB2*	Connexin 26	DFNB1		Gap junction protein
			DFNA3		
			± keratodermia[b]		
	CX30/GJB6	Connexin 30	DFNA3′		Gap junction protein
			± keratodermia[b]		
	CX31/GJB3	Connexin 31	DFNA2′		Gap junction protein
			DFNBi		
			± peripheral neuropathy[b]		
	Slc12a2/Nkcc1[a]	NKCC1	?	*sy*^{ns}; *Nkcc1*$^{-/-}$[c]	$Na^+K^+2Cl^-$ cotransporter
	PDS	Pendrin	DFNB4 ± thyroid goitre[b]	*Pds*$^{-/-}$[c]	Iodide/chloride transporter
	CLDN14	Claudin-14	DFNB29		Tight junction component

	COCH	Cochlin	DFNA9		Extracellular matrix
					component
	EYA4	EYA4	DFNA10		Transcriptional coactivator
	POU3F4	POU3F4	DFN3	*Brn4*$^{-/-c}$	Transcription factor
Tectorial membrane	*COL11A2*	Collagen XI	DFNA13	*Col11a2*$^{-/-c}$	Extracellular matrix
		(α2 chain)	± osteochondrodysplasia[b]		component
	TECTA	α-tectorin	DFNA8/12	*Tecta*$^{-/-c}$	Extracellular matrix
			DFNB21		component
	Otog[a]	Otogelin	?	*twister*; *Otog*$^{-/-c}$	Extracellular matrix
					component
Unknown	*TMPRSS3*	TMPRSS3	DFNB8/10		Transmembrane serine
					protease
	PCDH15	Protocadherin-15	DFNB23 ? ± retinopathy	*Ames waltzer*	Cell adhesion protein
			(Usher 1F)[b]		
	HDIA1	Diaphanous-1	DFNA1		Regulator of actin
					cytoskeleton
	DFNA5		DFNA5		?
	MYH9	Myosin IIA	DFNA17 ± giant		Motor protein
			platelets[b]		
	MTRNR1				Mitochondrial 12srRNA
	MTTS1				Mitochondrial
					tRNA$^{ser(UCN)}$

[a]Murine deafness genes for which the human orthologue has not yet been implicated in isolated deafness
[b]Syndromic deafness.
[c]Deaf mouse mutant obtained by targeted disruption of the gene.

1.3.3 Environmental Factors Causing Hearing Loss

Auditory impairment can occur as a result of environmental factors or a genetic predisposition. Environmental hearing loss occurs independent to any other associated symptoms. The major causes of environmental hearing loss are exposure to noise, ototoxic drugs, viral and bacterial infections and interactions between these factors (Mills and Going, 1982).

Noise exposure can cause damage to the inner ear resulting in temporary or permanent sensorineural hearing loss. Both laboratory and field studies indicate that the risk of hearing loss is present when noise levels exceeds 75-80 dB (decibel). As the noise levels, duration and number of exposures increase, so do the risks (Mills and Going, 1982). Noise exposure has been shown to damage the hair cells in the cochlea **(Figure 1.12 [A-C])** and also lead to pathological changes in the stria vascularis and the spiral ligament (Henderson et al., 2006) **(Figure 1.12 [D,E])**.

Aminoglycoside antibiotics are known to causes ototoxicity in the ear (Fee, 1980). These antibodies are used frequently in the treatment of tuberculosis and serious gram negative infections. Cochlear toxicity from aminoglycoside antibiotics are shown to affect the cochlear hair cells, the stria vascularis and the spiral ligament. Several theories of the mechanism of damage have been proposed, including disruption of potassium recycling in the stria vascularis leading to changes in the ionic composition of the endolymph and perilymph, thus causing deafness (Fee, 1980).

A large number of viral infections have also been associated with sensorineural hearing loss; the most prevalent being rubella and mumps. In

both cases, the hearing loss is unilateral with significant degeneration of the sensory hair cells, stria vascularis, tectorial membrane and spiral ganglion neurons (Mills and Going, 1982).

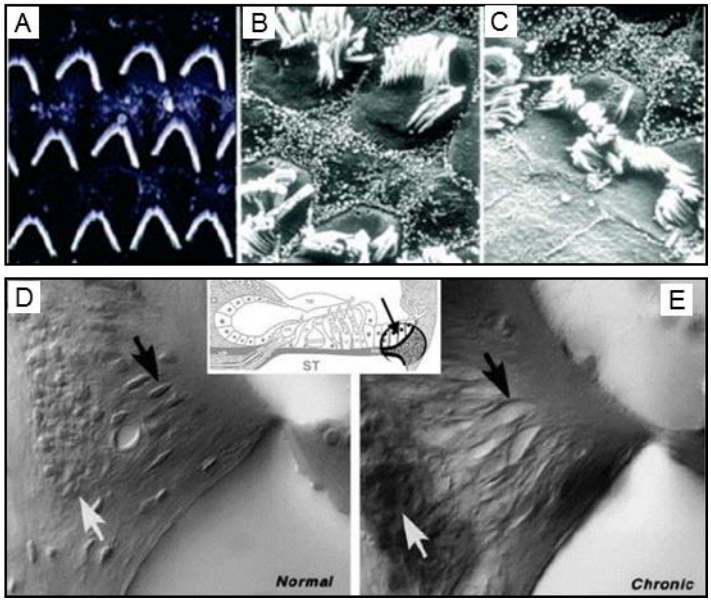

Figure 1.12: Effects of noise induced hearing loss
Scanning electron microscopy images of a normal cochlea show outer hair cells displaying no dysmorphology [A]. However, upon exposure to noise, the stereocilia do not maintain the rigid "V" formation appear to separated [B]. In addition, the stereocilia appear to be damaged and are therefore considerably shorter [C]. Comparison of the spiral ligament shows that in comparison to normal mice [D], mice exposed to noise lose type IV fibrocytes. (Loss of type IV fibrocytes marked in black arrows)

Adapted from: (Henderson et al., 2006)

1.4 Presbycusis and its prevalence

The effect of ageing on the development of hearing loss is a major health concern and prevalence of which is increasing every year. Age-related hearing loss (Presbycusis) is a significant health and social burden on the population and is one of the four leading chronic health conditions experienced by the elderly. Greater than 25% of adults aged 50 and over have a hearing loss of 30dB or more (increasing to 70-80% of people aged 75 and over) (Gates and Mills, 2005). Given current projections that by 2050 the world's population aged 60 and over will be ~2 billion; this is a major public health problem. The loss of hearing sensitivity usually begins at the higher frequencies which often means that warning sounds such as buzzers are not heard (Gates and Mills, 2005). Overall, presbycusis leads to social isolation, depression and loss of self-esteem. Presbycusis has also been implicated as a cofactor in senile dementia (Uhlmann et al., 1989). The onset and progression of presbycusis is known to be influenced by environmental factors such as ototoxic medication and noise exposure (Liu and Yan, 2007), however, the genetic component of presbycusis is thought to account for approximately 50% (Fransen et al., 2003, Christensen et al., 2001).

The pathology of presbycusis was first characterised by (Schuknecht, 1955) where four main subtypes were proposed; sensory presbycusis, associated with hair cell degeneration, strial (metabolic) presbycusis as a result of the degeneration of the stria vascularis, neural presbycusis, caused by the loss of spiral ganglion neurons and mechanical presbycusis resulting from the stiffening of the basilar membrane **(Figure 1.13)**. However, mechanical

presbycusis is now thought to be a manifestation of strial presbycusis (Schuknecht, 1955, Schuknecht and Gacek, 1993, Ohlemiller, 2004).

Sensory presbycusis is associated with degeneration of cells within the organ of Corti. It is primarily caused by epithelial atrophy and loss of hair cells and supporting cells. This loss occurs towards the basal turn of the cochlea, gradually progressing towards the apex. This morphological change correlates with a loss in the high frequency thresholds and therefore, speech frequencies are not affected.

Neural presbycusis is caused by degeneration of nerve cells (especially the VIIIth cranial nerve). This results in a broad hearing loss with an emphasis on high frequencies resulting in a severe decrease in speech discrimination.

Strial presbycusis (also known as metabolic presbycusis) occurs as a result of degeneration of the stria vascularis. The stria vascularis is responsible for maintaining the ionic composition of the endolymph and therefore degeneration and dysfunction of the stria results in a flat hearing loss across all frequency ranges.

Research suggests that a combination of pathology from the three different subtypes is present in most people exhibiting age-related hearing loss (Schuknecht and Gacek, 1993, Ohlemiller, 2004).

Given the prevalence of ARHL (age-related hearing loss) in the human population, very little is known about the genetic determinants that contribute to this condition. In the human, GWAS (genome wide association

studies) have been undertaken to assess this. However, to date, little progress has been made towards this. Therefore, the mouse has been employed to study the genetics of ARHL.

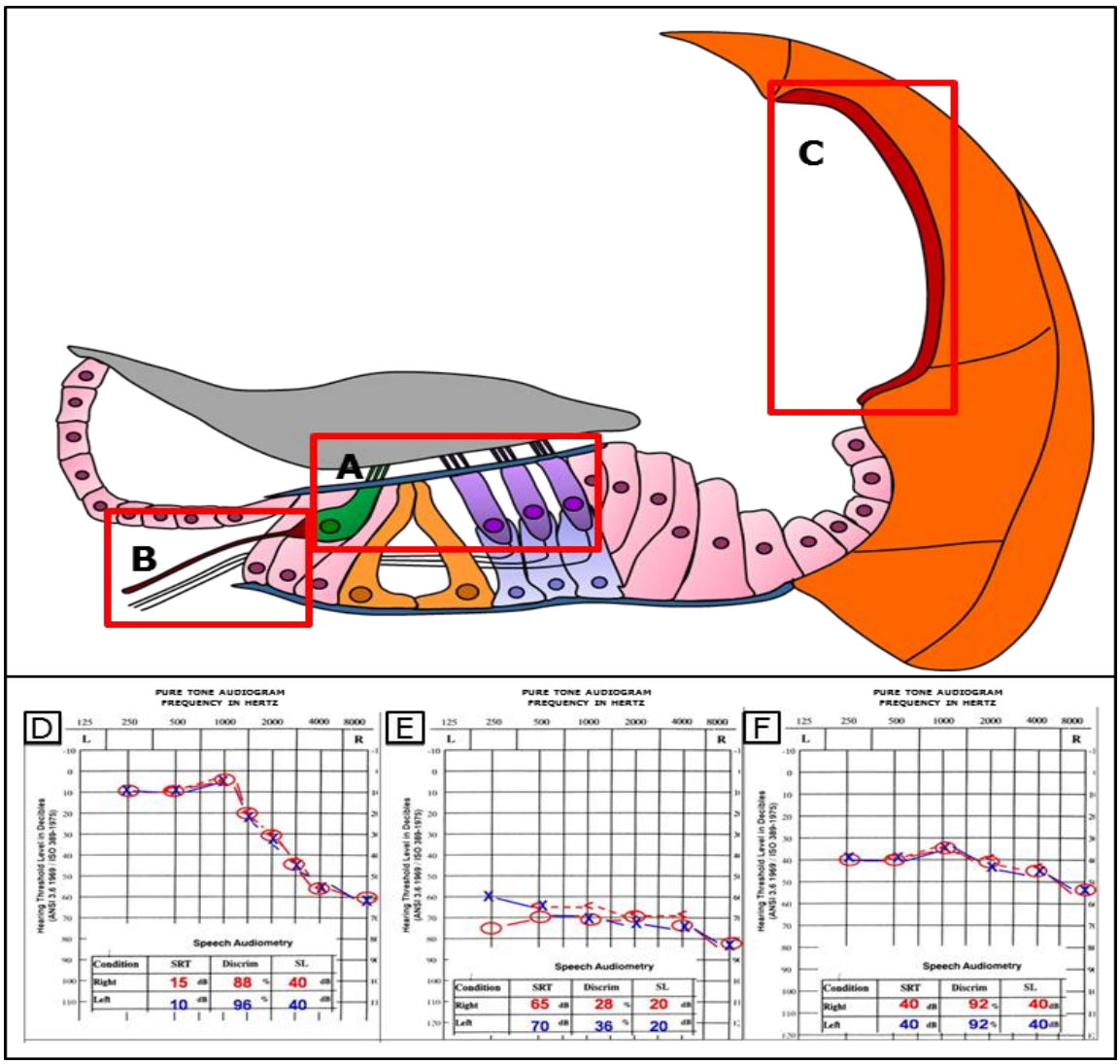

Figure 1.13: Types of age-related hearing loss (ARHL)
There are three types of ARHL characterised by Schnknecht all exhibiting characteristic audiograms. [A,D] Sensory presbycusis refers to epithelial atrophy with loss of sensory hair cells and supporting cells in the organ of Corti. [B,E] Neural presbycusis refers to atrophy of nerve cells in the cochlea and central neural pathways. [C,F] Strial presbycusis results from atrophy of the stria vascularis.

Adapted from: (Bielefeld et al., 2010)

1.5 GWAS to Elucidate Genes Associated with Age-Related Hearing Loss in Humans

Due the complexity and heterogeneous nature of presbycusis, little is known about the genetics underlying age-related hearing loss, despite considerable efforts in performing genome-wide association studies (GWAS). To-date, five major GWAS have been conducted **(Table 1.3)**, hoping to elucidate genetic variants associated with presbycusis, however, no association of statistical significance has been found (Bowl and Dawson, 2014).

The first study was conducted in 2009 by (Friedman et al., 2009) where a total of 3434 individuals, collected across eight different centres in Europe were analysed. The results obtained showed an association between single nucleotide polymorphisms (SNPs) in the gene *GRM7* and age-related hearing loss. GRM7 is a metabotropic glutamate receptor, and the role of such receptors in the ear is not well understood. It is proposed that this gene may be required for afferent auditory nerve firing. Although the results were not above the genome wide significance parameters set to validate such studies, the results were replicated in two population cohorts.

The second study was conducted in 2010 by (Van Laer et al., 2010) analysed samples from a small, ancient genetically-isolated population in the Finnish Saami. DNA samples and audiometric measurements were collected from 352 individuals for analyses. Results showed no significant genome wide association for age-related hearing loss, however, two SNPs were identified which were located in or near genes which could be considered as reasonable biological candidates (*PC3* and *GRM7*). One of the SNPs was immediately

downstream of the *GRM7* gene which had been previously shown to be associated with age-related hearing loss (Friedman et al., 2009).

The third study in 2011 by (Girotto et al., 2011) used meta-analysis to study data from six isolated populations of European ancestry for an overall number of 3417 individuals. The study identified eight genes which include *DCLK1*, *PTPRD*, *GRM8* and *CMIP*, which were found to be expressed in the inner ear whose function has not been previously linked to hearing.

As part of the 1958 British Birth Cohort study, analysis of auditory function was conducted on 3164 individuals between the ages of 44-45. Analyses failed to identify any associations with genome wide significance. However, subsequent analyses of the data lead to the discovery that the estrogen-related receptor gamma (*ESRRG*) gene plays a role in the maintenance of hearing in both humans and mice (Nolan et al., 2013).

A more recent study by (Fransen et al., 2014) analysed a sample set of 2161 individuals originating from Antwerp. Analysis of common variants showed no variants with genome wide significance. There was also no evidence for replication of any of the previously reported genes.

Although the results of the GWA studies have not provided any conclusive outcomes, it has elucidated an array of candidate genes which can be studied further to interrogate their role in the auditory apparatus. However, moving forward, due to the complexity of the auditory system, the study of the pathology and the biochemical processes which take place within the ear is imperative for the understanding of auditory transduction. Conducting such

analysis in humans is challenging as only post mortem analyses can take place and even so, the ear is embedded in the temporal bone and is therefore not easily accessible. As such, the use of animal models, such as the mouse, plays a key role in deciphering the genetics and pathobiology underlying age-related hearing loss.

Table 1.3: GWAS to Elucidate Genes Associated with AHRL in Humans

GWA Study	**Number of individuals analysed**	**Genes identified**
(Friedman et al., 2009)	3434	*GRM7*
(Van Laer et al., 2010)	352	No significant association with any genes
(Girotto et al., 2011)	3417	8 genes including *DCLK1, PTPRD, GRM8* and *CMIP*
British Birth Cohort Study 1958 and (Nolan et al., 2013)	3164	No genes identified Subsequentyl analysis showed possible association with *ESRRG*
(Fransen et al., 2014)	2161	No sgenes identified

1.6 The Mouse as a Model of Deafness

The mouse is the choice organism used to study the genetics and pathways of various human diseases and has proven to be an invaluable model in studying hearing loss due to its anatomical and genetic similarities to humans (Brown et al., 2008) both structurally and physiologically. Studies identify that the mouse genome has an 80% homology to the human genome with 99% of the genes found in mice having a human ortholog (Waterston et al., 2002). The murine inner ear however, is significantly smaller than the human ear and as such the frequency response is also altered. Humans respond to frequencies between 20Hz – 20kHz, whereas in mice it is approximately 1-97 kHz. The murine ear is easy accessible and unlike humans, can be assessed or excised at any stage of pre/postnatal development for physiological or pathological analysis.

From a practical stand point, the lifespan and gestational period of mice is very short in comparison to other animal models, and, the housing costs are relatively low.

1.6.1 The study of presbycusis in inbred mouse models

To date, in mice, most age-related hearing loss research has focused on the loci underlying variation between inbred strains. Towards this, 20 loci have been defined as contributing age-related hearing loss in particular inbred strains (http://hearingimpairment.jax.org/table2.html) **(Table 1.4)**. However, the genes of only four of these loci have been identified: *ahl1, a* hypomorphic allele of the *Cadherin 23* gene (Noben-Trauth et al., 2003), *ahl4* (*citrate synthase*) (Johnson et al., 2012), *ahl5* (*GIPC PDZ domain*

containing family, member 3) (Charizopoulou et al., 2011) and *ahl8* (*Fascin actin-bundling protein 2, retinal*) (Shin et al., 2010).

The first age-related hearing loss locus, *ahl1*, has been determined to be a hypomorphic allele of the *Cadherin 23* gene (*Cdh23*) and has been described as an accelerating allele of the disease (Noben-Trauth et al., 2003). The *Cdh23* gene encodes a cell-cell glycoprotein, which is essential for the development and function of the stereocilia hair bundles in the inner ear. The widely used inbred strain C57BL/6J inbred strain contains the recessive $Cdh23^{ahl1}$ allele, and therefore, mice display hearing loss from as early as three months of age (Johnson et al., 2000). The hearing loss is first observed in the higher frequency, and with age, develops across all frequencies. Mice which are homozygous for *ahl1* display hair cell loss (both outer and inner) which develops at three months and progresses with age (Hequembourg and Liberman, 2001). This loss of cochlea hair cell correlated with Scnuknechts theory of sensory presbycusis. By seven months of age, homozygous mice also display a loss in spiral ganglion cells which is a feature of neural presbycusis. In addition, thinning of the stria vascularis and loss of fibrocytes in the spiral ligament are also seen, which is consistent with the theory of strial presbycusis (Ohlemiller, 2006). The inbred strain C57BL/6J is therefore an ideal model to demonstrate the theory of how a combination of all three different subtypes of presbycusis is present in age-related hearing loss.

Studies by Jonson and colleagues on A/J mice has identified *ahl4* – an AHL locus on distal chromosome ten with a mutation in the gene *citrate synthase* (Cs) (Johnson et al., 2012). Auditory testing has identified hearing loss immediately following weaning, which progresses to severe hearing

impairment by 25 days of age. This differs from the previously identified model *ahl1* which only exhibited evidence of hearing impairment at three months of age. In addition, *ahl4* mice exhibit inner and outer hair cell loss which is most pronounced at the basal region of the cochlea. Hair cell counts reveal that this loss begins at 14 days of age and progressed rapidly during the following 2-5 months. Unlike the *ahl1* model however, there is no lateral wall dysmorphology or spiral ganglion loss identified.

In 2011 research by Charizopoulou and colleagues identified a sequence polymorphism in the PDZ domain of *Gipc3* as the cause of sensorineural hearing loss *(ahl5)* (Charizopoulou et al., 2011). Gipc3^{ahl5} mice show a moderate hearing impairment at four weeks of age which progress to profound hearing loss at 52 weeks of age, most pronounced at 16 kHz. Mice also exhibit reduced distortion product otoacoustic emissions (DPOAEs), which is an indicator of outer hair cell dysfunction, and a reduced endocochlear potential (EP) suggesting a defect in the stria vascularis. Histopathological studies identified an irregular structure of the stereocilia bundle from postnatal day three with significant degeneration of the organ of Corti and loss of spiral ganglion neurons seen at 52 weeks of age. Together, these observations suggest that *Gipc3* plays a pivotal role in signal acquisition and propagation in cochlear hair cells (Charizopoulou et al., 2011).

Research by Shin and colleagues in 2010 identified a non-synonymous nucleotide substitution in the mouse *Fascin-2* gene (*Fscn2*) as a key contributor to the early-onset, age-related hearing loss of DBA/2J mice (Shin et al., 2010). The DBA/2J mouse is used widely in hearing research because

it harbours both the *ahl1* mutation of *Cadherin 23*, which leads to age-related hearing loss and *ahl8*, a locus on distal chromosome 11 that leads to very-early onset hearing loss when in combination with $Cdh23^{ahl1}$ (Johnson et al., 2008). ABR testing identified that DBA/2J exhibit elevated thresholds by five weeks of age. Pathological studies also identify that the stereocilia appear normal at two weeks of age, but progressively degenerate between one and six months of age. FSCN2 is the most abundant actin crosslinking protein in hair bundles and is thought to play a pivotal role in the maturation and elongation of the stereocilia. The results obtained by (Shin et al., 2010) highlight the critical role that hair-bundle proteins play in auditory transduction.

The mouse has been used as a model to study hearing loss due its genetic architecture. The simplicity of targeted mutagenesis (Thomas and Capecchi, 1987, Xiao et al., 2011) has enabled gene-driven approaches to studying known human deafness disorders in mice.

Phenotype-driven screen are also being employed utilising the chemical mutagen *N*-ethyl-*N*-nitrosourea (ENU) which causes random point mutations throughout the genome (Popp et al., 1983). Following random mutagenesis, mutant mice are screened for phenotypes of interest. The development of phenotyping tests such as click box and auditory evoked brainstem response (ABR) enables rapid, high throughput screening of mice to identify auditory phenotypes.

The mouse genome has been sequenced and can be found online through genome browsers such as Ensembl and Vega. Breeding mutagenised mice

with a second inbred strain with known single nucleotide polymorphism (SNP) differences to the ENU-treated strain will helps to map the phenotype-causing gene.

This is a phenotype driven approach, therefore, no *a priori* assumptions are made about the genetic loci underlying the disease and hence this is a powerful approach for discovering novel genes and pathways (Brown et al., 2008).

Table 1.4: Genetic factors that contribute to age-related hearing loss in inbred mouse strains
Adapted from (http://hearingimpairment.jax.org/table2.html)

AHL locus	Gene	Chromosome	Location	References
ahl	*Cdh23*	10	60 Mb	(Johnson et al., 1997, Johnson et al., 2000, Noben-Trauth et al., 2003)
ahl2		5	65-100 Mb	(Johnson and Zheng, 2002)
ahl3		17	65-69 Mb	(Nemoto et al., 2004, Morita et al., 2007)
ahl4	*Cs*	10	120-130 Mb	(Zheng et al., 2009, Johnson et al., 2012)
ahl5	*Gipc3*	10	81 Mb	(Drayton and Noben-Trauth, 2006, Charizopoulou et al., 2011)
ahl6		18	64-76 Mb	(Drayton and Noben-Trauth, 2006)
ahl8	*Fscn2*	11	120 Mb	(Johnson et al., 2008, Shin et al., 2010)
ahl9		18	73-77 Mb	(Nagtegaal et al., 2012)
Hfhl1		7	20-38 cM	(Keller et al., 2011)
Hfhl2		8	20-32 cM	(Keller et al., 2011)
Hfhl3		9	30-50 cM	(Keller and Noben-Trauth, 2012)
Phl1		17	8-29 Mb	(Mashimo et al., 2006)
Phl2		10	48-70 Mb	(Mashimo et al., 2006)
Snhl1		10	54-60 Mb	(Noben-Trauth et al., 2010)
Snhl2		1	133-172 Mb	(Latoche et al., 2011)
Snhl3		6	121-143 Mb	(Latoche et al., 2011)
Snhl4		10	49-90 Mb	(Latoche et al., 2011)
mtDNA(*mt-Tr*)		mitochondria		(Johnson et al., 2001)

1.7 The Harwell Ageing Screen

1.7.1 Breeding and Phenotyping Strategy

At MRC Harwell a major new initiative to generate mouse models of age-related disease is currently underway. Under this programme, male mice (G0) from a C57BL/6J (BL6) inbred strain are injected intraperitoneally with *N*-ethyl-*N*-nitrosourea (ENU), a potent alkylating agent that randomly introduces point mutations in the DNA of spermatogonial stem cells (Russell et al., 1979, Russell et al., 1982). The C57BL/6J strain is utilised because they possess a known homogeneous reference genome sequence. Previous studies have identified that the optimal dose results in one mutation every 1-1.5Mb (Concepcion et al., 2004, Quwailid et al., 2004).

After a period of infertility, the C57BL/6 mice are bred to wildtype female C3H.Pde6b^{+} mice to produce the G1 offspring. The G1 mice carry approximately 30-50 coding mutations that have been inherited from their G0 father (Keays et al., 2006). The G1 male mice are then mated to wildtype C3H.Pde6b^{+} females and their female (G2) offspring are then mated back to the original G1 in order to homozygose the ENU-induced mutations.

The resulting G3 offspring undergo various phenotypic assessments which can be screened for diseases of interest. Over the course of this programme, approximately 200 G3 pedigrees (~100 mice/pedigree) will be generated and aged to 18 months. These mice undergo recurrent phenotypic assessment at several defined time points throughout their life across a wide range of disease areas including, diabetes and metabolism, neurobehaviour, bone

analysis, renal/hepatic function, cardiac disease, clinical chemistry and sensory.

Each G3 pedigree enters an auditory phenotyping pipeline. This consists of a clickbox test at three, six, nine and 12 months of age (~50 mice/pedigree), with the addition of auditory-evoked brainstem response (ABR) tests at three and nine months (~25 mice/pedigree). If a pedigree with an interesting ABR phenotype is identified, an additional ~25 animals from that pedigree are available to test.

1.7.2 Auditory Assessment in mice

The clickbox test is a simple test to assess hearing loss. The clickbox emits a high-frequency (~20 kHz) tone stimulus at a level of 90 dB sound pressure level (dB SPL) when positioned 30 cm above the animal **(Figure 1.14 [A])**. Mice with normal hearing display a startle response recognised by a flick of the ear – the Preyer Reflex (Nolan et al., 2000). The test is a preliminary assessment, most useful for detecting profound hearing loss in mice. The ABR test which records the auditory-evoked brainstem potential is a more robust test and allows estimation of frequency-specific auditory thresholds (Zheng et al., 1999, Hardisty-Hughes et al., 2010) **(Figure 1.14 [B])**. The ABR test measures the response of the VIIIth cranial nerve and brainstem to an auditory stimulus. The resultant trace consists of five peaks (P I-V) relating to the different neuronal populations along the cranial nerve and the brainstem. PI; auditory nerve, PII; cochlear nucleus, PIII; superior olivary complex, PIV; the vicinity of the periolivary and lateral lemniscal nuclei and PV; contralateral inferior colliculus (Henry, 1979) **(Figure 1.14 [C])**. In the

ageing screen, ABR thresholds are measured in relation to a click stimulus and pure tone stimuli at an 8, 16 and 32 kHz.

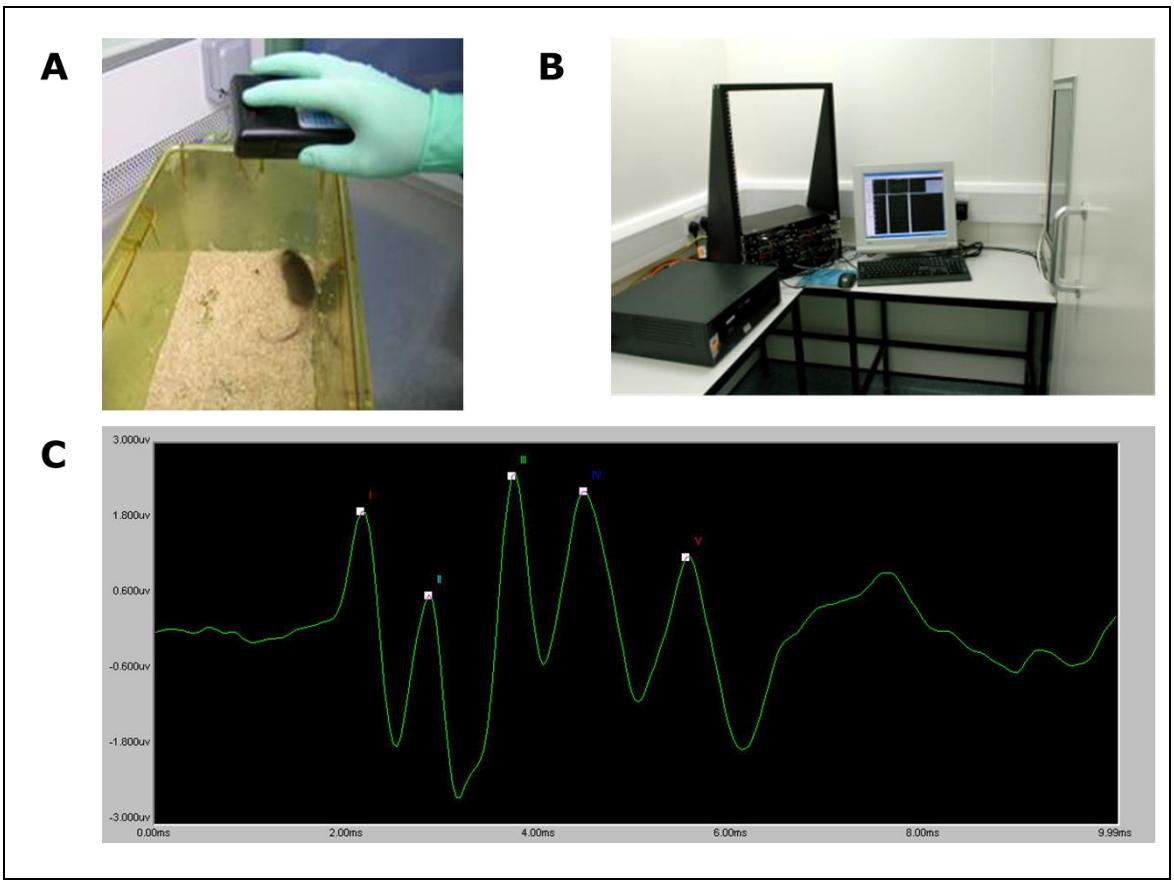

Figure 1.14: Clickbox and Auditory Brainstem Response (ABR) testing
[A] The clickbox test is a crude test for hearing function, inducing a startle response in hearing mice, but not in mice with profound hearing loss. [B] The apparatus used for ABR assessment, consisting of a computer, a display, the Tucker Davis Technology (TDT hardware system and a sound attenuated booth. [C] A normal ABR trace from a wildtype mouse with no auditory impairment, showing the five distinct peaks observed.

1.8 Models identified

As of July 2014, 150 pedigrees have entered the phenotyping pipeline, of which 130 have completed auditory screening. To date, several pedigrees have confirmed phenotypes with either absent/reduced clickbox responses and/or elevated ABR thresholds. These have included early-onset models, late-onset models and models exhibiting progressive hearing loss. Currently, I am investigating two models identified as possessing a late onset auditory phenotype.

1.8.1 Muta-Ped-90

Pedigree muta-ped-90 (MP90) was identified in the Ageing screen at nine months of age as containing seven mice having mildly elevated ABR thresholds at all frequencies tested compared to their littermates **(Figure 1.15)**. In addition, there were no visible behavioural or vestibular phenotypes observed in the affected mice (i.e., head bobbing or circling). Given the phenotyping data and number of affected mice (4/24), this pedigree would appear to be a recessive model of late-onset hearing loss.

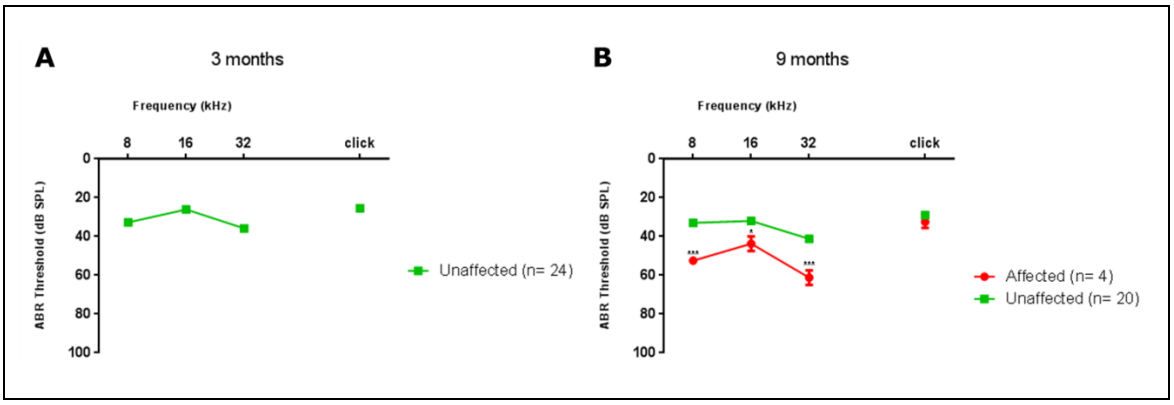

Figure 1.15: ABR thresholds of MP90 mice at three and nine months of age
[A] Average ABR thresholds at three months of age indicate that there were no affected mice (n= 24). [B] At nine months of age four mice exhibit significantly elevated thresholds (*p<0.05, **p<0.01, ***p<0.001) in comparison to littermates (n= 20). Error bars indicate standard error of mean.

1.8.2 Muta-Ped-c3pde-96

Pedigree muta-Ped-c3pde-96 (MPC96) was identified in the Ageing screen at 9 months of age as containing seven mice with significantly elevated ABR thresholds, most pronounced at 8 kHz and 32 kHz, when compared to their littermates **(Figure 1.16)**. In addition, there were no visible behavioural or vestibular phenotypes observed in the affected mice (i.e., head bobbing or circling).

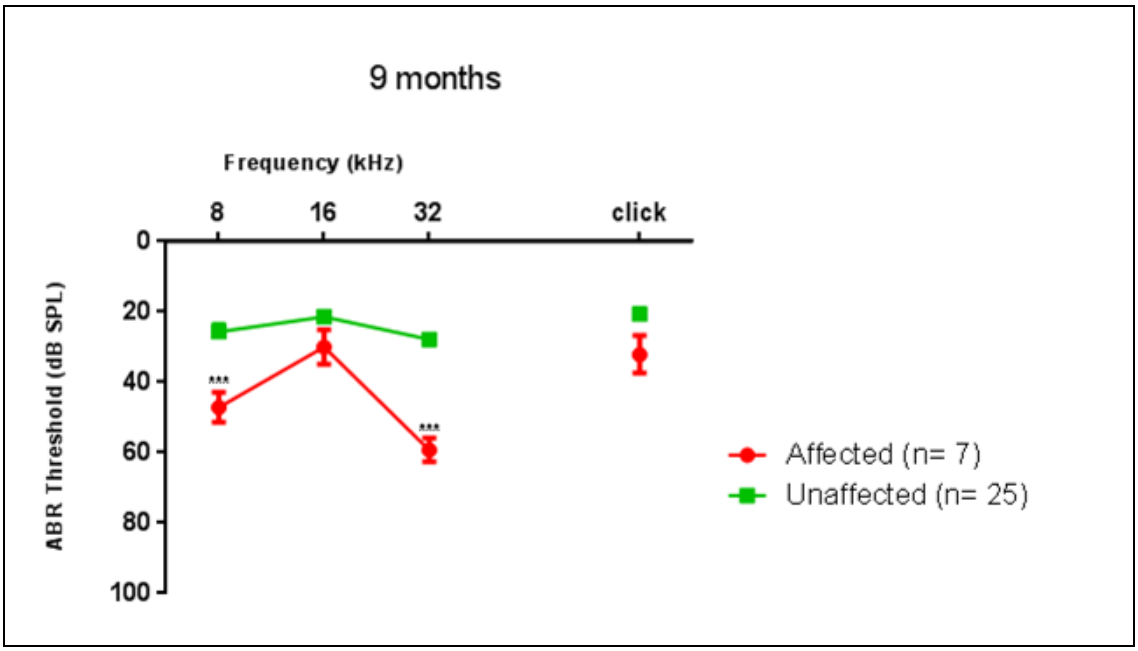

Figure 1.16: ABR thresholds of MPC96 mice at 9 months of age
Average ABR thresholds at 9 months of age indicate that seven mice exhibit significantly elevated thresholds (***p<0.001) in comparison to littermates (n= 25). Error bars indicate standard error of mean.

1.9 Project Aims and Objectives

The aim of my project is to fully characterise these two models of age related hearing loss and clone the underlying genetic lesion causing the phenotype. This will involve the following:

- Longitudinal auditory phenotyping
- Secondary phenotypic characterisation using:
    - Histological studies to examine the morphology of the inner ear
    - Ultrastructural studies using scanning electron microscopy to study the morphology of the inner ear comparing affected mice to their wildtype littermates.
- Gene identification using:
    - Whole genome mapping
    - Next generation sequencing
- Once the gene is identified, perform functional characterisation studies using:
    - *In silico* analysis to assess whether molecular changes caused by ENU-induced lesions would affect the protein structure
    - Immunohistochemistry and immuno-fluorescence employing antibodies specific for the protein products of the genes identified to examine their expression throughout the auditory system and to assess cellular localisation
    - *In vitro* assays : By elucidating the genes responsible for the phenotypes observed in pedigrees MP90 and MPC96, further studies can be undertaken to determine the functional effects of the mutations.

Chapter 2

Materials and Methods

2.1 Animal Care and Husbandry

All of the animals used in the experiments were maintained in accordance with the UK Home Office welfare guidelines (Animals Scientific Procedures Act 1986) and mice chosen for the experiments were euthanized by Home Office Schedule I methods and approved by the Animal Welfare and Ethical Review Board (AWERB) at MRC Harwell. The mice were housed in specific pathogen-free conditions in individually ventilated racks (Techniplast UK Ltd) containing grade 6 sawdust bedding (Datesand Ltd, UK) under a controlled 12 hour light/dark cycle at 21±2°C and 55±10% relative humidity, in the Mary Lyon Centre (MLC), Harwell. The mice were given a commercial irradiated diet (Special Diets Services, UK) and had free access to water (25 ppm chlorine).

All mice were on a mixed C57BL/6J and sighted-C3H (C3H.Pde6b^{+}) (Hoelter et al., 2008) genetic background unless otherwise stated. The *trombone* line was backcrossed to sighted-C3H and offspring were then intercrossed to produce wildtype, heterozygous and homozygous *trombone* mice. Much of

the phenotypic characterisation studies were conducted on ≥backcross 5 mice.

Animal procedures were undertaken under the guidelines of the Home Office Project Licences Nos. 30/2567 (2010-2014), 30/2540(2008-2012), 30/3070 (2014-date), 30/3015 (2013-date) and Personal Licence No. 30/9420.

2.2 ENU Mutagenesis

The Harwell Ageing Screen was set up in 2010 to recover novel mouse models of diseases of aging. Male C57BL/6J mice (G0) at 8-10 weeks of age are injected with 320mg/kg of N-ethyl-N-nitrosurea (ENU) (Acevedo-Arozena et al., 2008) over a three week period. Following a period of sterility, the mice are mated with C3H.Pde6b^{+1} female mice to produce G1 offspring. G1 males, heterozygous for the ENU-induced lesions are then mated with C3H.Pde6b^{+} female mice to produce G2 offspring. The G2 females are then mated to their G1 father to produce G3 offspring that are homozygous, and heterozygous for the ENU-induced lesions **(Figure 2.1)**. The large G3 pedigrees (~100 mice/pedigree) then offspring enter a phenotyping pipeline where they can be screened for dominant and recessive phenotypes.

The use of the two inbred strains (C57BL/6J and C3H.Pde6b^{+}) facilitates the mapping of ENU-induced mutations using SNP (single nucleotide

[1] C3HPde6b mice are susceptible to early onset retinal degeneration because they are homozygous for the *rd1* mutation at the *Pde6b* locus PITTLER, S. J. & BAEHR, W. 1991. Identification of a nonsense mutation in the rod photoreceptor cGMP phosphodiesterase beta-subunit gene of the rd mouse. *Proc Natl Acad Sci U S A,* 88**,** 8322-6.. To prevent this interfering with the Harwell Ageing Screen, a C3Hpde6b sub-strain which has wildtype alleles from the BALB/c strain at the Pde6b locus is used.

polymorphism) markers across the genome that have different alleles between these strains.

2.2.1 Screening for *ahl1*

C57BL/6J mice are predisposed to age-related hearing loss due to the presence of the *ahl1* allele at the *Cadherin23* locus (c.753G>A) (Noben-Trauth et al., 2003, Johnson et al., 1997). This is a synonymous SNP at the last nucleotide of the seventh coding exon of *Cdh23*, where an 'A' (*Cdh23*^{ahl1}*)* is present, in-frame exon skipping occurs, and age-related hearing loss is observed. Normal hearing is associated with a 'G' (*Cdh23*$^{+}$*)* being present at this locus. As such, the G2 females are screened for the *ahl1* allele.

To screen for the *ahl1* allele, a PCR is performed across exon 7 (Section 2.5.1) and then digested with the restriction enzyme *MspI*. The presence of the wildtype 'G' allele will allow for endonuclease digestion of the amplicon, whereas, presence of the *ahl1* 'A' allele does not **(Figure 2.2)**.

In the Harwell Ageing Screen, auditory phenotyping is only undertaken on mice mothered by G2 females which are wildtype for *Cdh23* (*Cdh23*$^{+/+}$). This ensures that there cannot be any homozygous (*Cdh23*$^{ah1/ahl1}$) mice, only *Cdh23*$^{+/+}$ or *Cdh23*$^{+/ahl1}$ mice, in the G3 offspring screened, thus ensuring the auditory phenotyping is not confounded by the recessive *ahl1* allele.

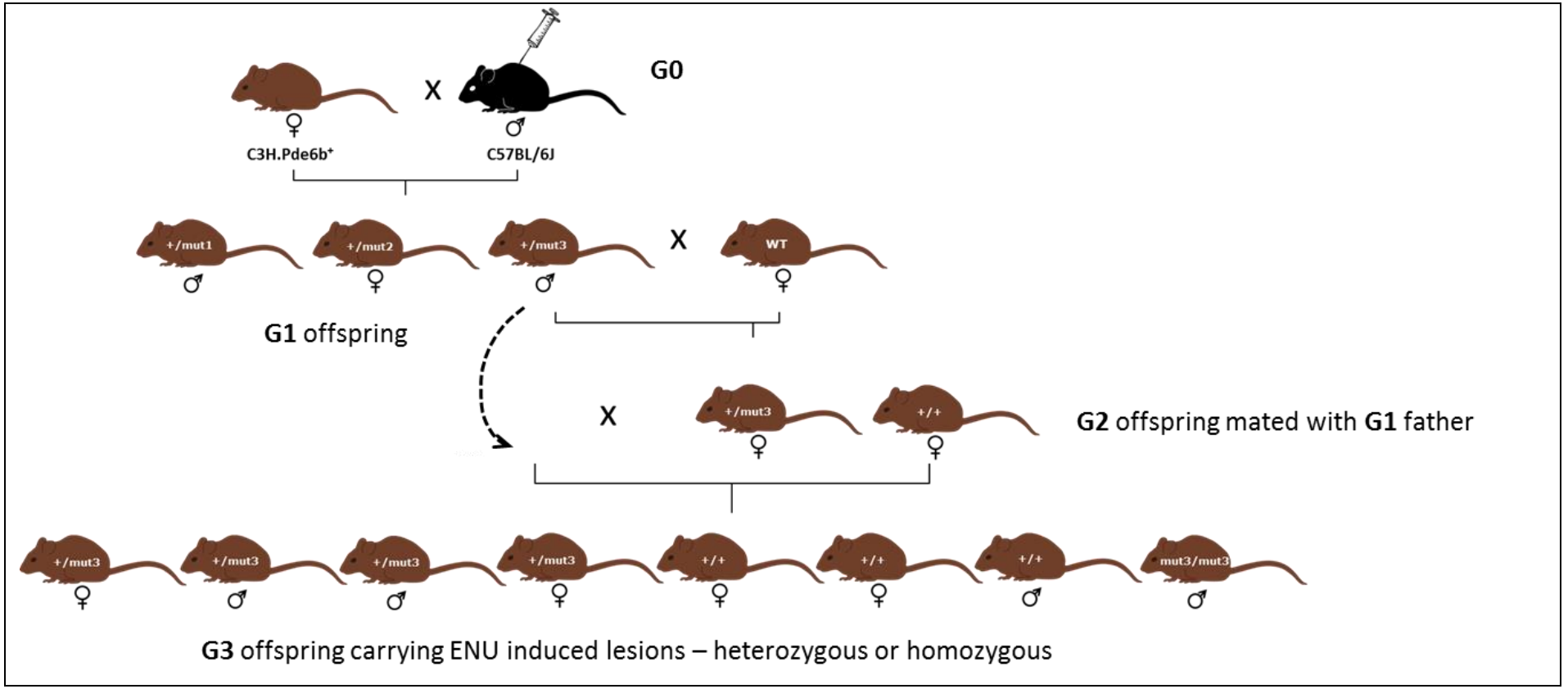

Figure 2.1: Breeding scheme for the Harwell Ageing Screen
Male C57B6/J mice are injected with N-ethyl-N-nitrosourea (ENU) and mated to wildtype sighted C3H females. The resulting G1 male mice are then mated to wildtype C3H.Pde6b^{+} females. Their female (G2) offspring are then mated back to the original G1 in order to homozygose the mutations. The resulting G3 offspring undergo recurrent phenotypic assessments in the Harwell Ageing Screen.

Table 2.1 Primers and PCR conditions used for *ahl1* genotyping

Forward Primer	Reverse Primer	Annealing Temperature (°C)	Cycle Number	Restriction Enzyme
ACCCAGGGTTGTGTGCTCCTGT	AGTCCACAGCCATCCCCAGCAC	60	35	MspI

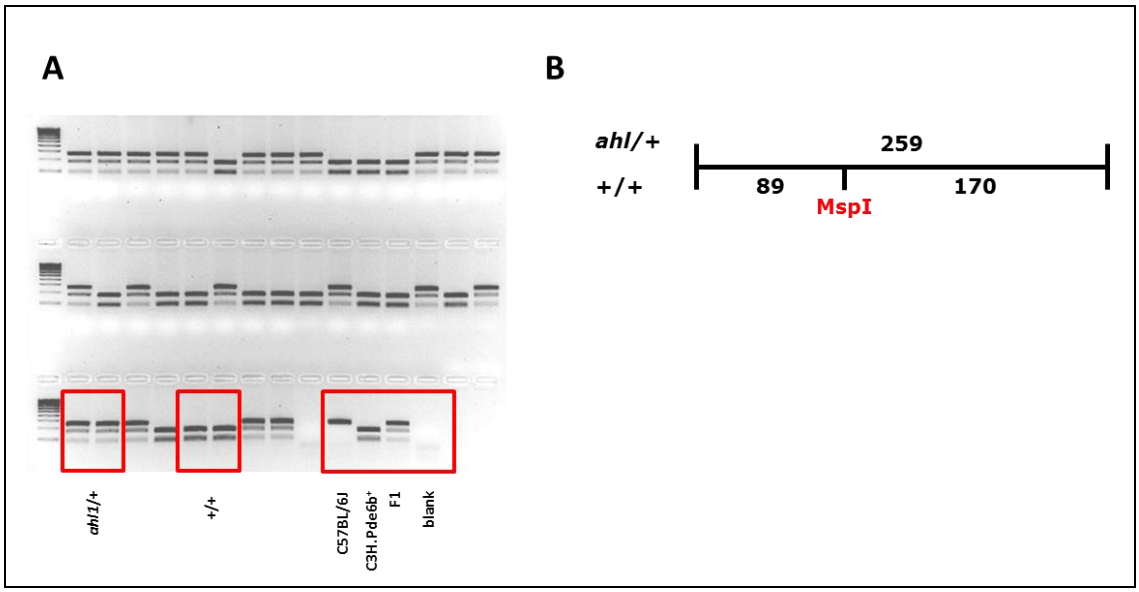

Figure 2.2: Genotyping for the ahl1 allele
All G2 females are screened for the *ahl1* allele at the *Cadherin23* locus. [A] A PCR is performed across exon 7 and then digested with *MspI.* [B] Mice which are heterozygous for *ahl1* will exhibit three bands on the gel, whereas, mice which are wildtype for *ahl1* will exhibit two bands.

2.3 Auditory Assessment

In the Harwell Ageing Screen, auditory phenotyping is undertaken at three, six, nine and twelve months of age. Clickbox tests undertaken at all of the aforementioned time points and auditory-evoked brainstem response (ABR) measurements are conducted at three and nine months, as described in (Hardisty-Hughes et al., 2010).

2.3.1 Click Box

The clickbox test is a simple hearing test which is most useful in detecting profound hearing loss in mice. The clickbox (MRC Institute of Hearing Research, Nottingham) is placed approximately 30cm above the mouse and when activated emits a brief high-frequency (~20 kHz) tone stimulus at a level of 90 dB sound pressure level (dB SPL). In response to this sound, a mouse with normal hearing would normally display the Preyer reflex (movement of one or both pinnae in response to a sudden loud noise), along with a startle response. Mice are graded in relation to their responses to the clickbox: 0 for an absent response, 1 for a reduced/diminished response and 2 for a normal response.

2.3.2 Auditory-evoked Brainstem Response (ABR)

Mice were anesthetised with ketamine (Ketaset®, Fort Dodge Animal Health) and xylasine (Sedaxylan®, Ceva Animal Health) (1ml Ketaset, 0.5ml Sedaxylan in 8.5ml sterile water (Dechra Veterinary products)). This was administered by an intraperitoneal injection at a rate of 0.1ml/10g of body

weight. Mice were kept in a heated cage until fully anaesthetised and Viscotears (Novartis AG) applied to prevent the eyes from drying out. Anesthetised mice are then transferred to a heated mat in a sound-proof booth (IAC 401-A-SE, IAC Acoustics) and three needle electrodes (Grass Telefactor F-E2-12) are positioned subdermally: (1) the ground electrode (below the left pinna), (2) the reference electrode (in the right mastoid) and (3) the active electrode (on top of the head between the two pinnae) **(Figure 2.3)**. A speaker was positioned 1.5cm away from the right pinna, facing directly into the auditory canal.

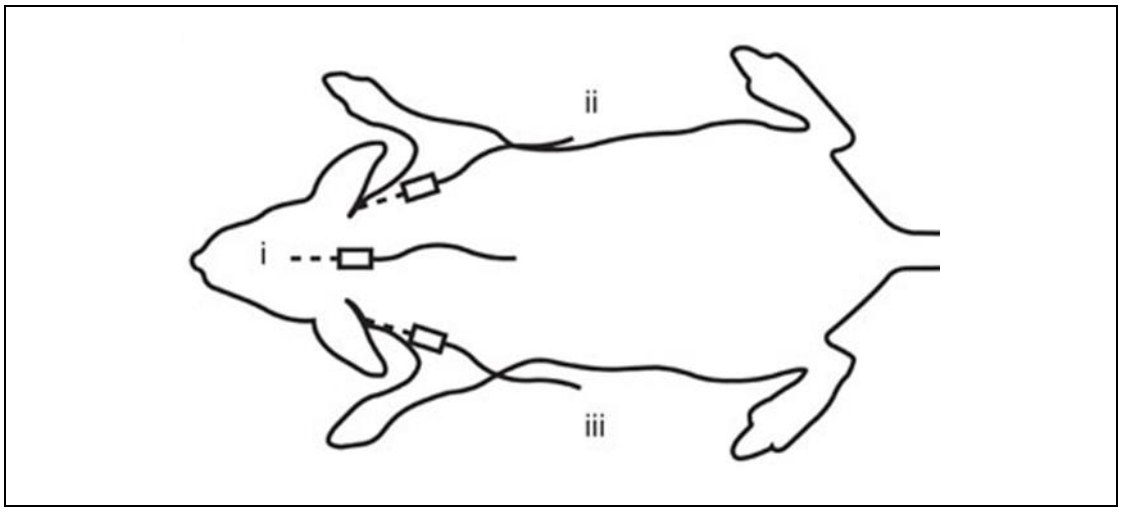

Figure 2.3: Electrode positioning for ABR measurements
The three electrodes, (i) active, (ii) reference and (iii) ground were positioned subdermally into the body.
Adapted from (Hardisty-Hughes et al., 2010)

Auditory stimuli were generated by TDT SigGen RP software (TDT System (systemIII)) and played regularly into the ear. The auditory response files were recorded and analysed in the TDT BioSig RP software (TDT System (system III)) through the generation of a graphical trace containing five

peaks; each peak representing a different part of the neuronal circuit responsible for processing sounds. ABR measurements were collected in response to a short broadband click stimulus in addition to tone burst stimuli (7ms total gated, 1ms rise/fall with Cos^2 filter), at 8, 16 and 32 kHz presented at a rate of 21/sec recordings with 10ms bins averaged between 300-1000 repeats. The stimulus range tested was from 90 dB to 5 dB in 5 dB decrements. As the decibel level is decreased, a hearing threshold can be identified as the point at which no replicable auditory response can be detected.

Mice were allowed to recover in a heated cage after subcutaneous injection of reversal agent containing 0.1ml Atipamezole Hydrochloride (Antisedan®, Pfizer Animal Health) and 9.9ml water (0.1mg/10g body weight). Once fully recovered, mice were returned to their home cage.

In the Harwell Aging Screen, mice which exhibited ABR thresholds greater than or equal to 45 dB across at least two of the frequencies tested were regarded as being affected.

2.4 DNA Extraction

Tissues were collected (ear clips or tail samples) and stored at -20°C until DNA extraction.

2.4.1 DNA Extraction Using Lysis Solution

For "crude" extraction, tissues were lysed in 150µl of lysis solution (1M Tris-HCl pH 8.5, 0.5M EDTA pH8.0, 10% Tween-20 and ddH_2O) with added Proteinasei K (100mg/ml) and incubated for 4 hours at a temperature of 55°C. The samples were placed at 100°C for 12 minutes in order to heat inactivate the Proteinase K. The samples were then centrifuged at 17,000 x g to pellet the undigested tissues. The supernatant containing the relevant lysed material was used in PCR reactions.

2.4.2 Qiagen Extraction

DNA extractions for samples sent for mapping was performed using the DNeasy® Blood and Tissue kit (Qiagen) as per manufacturer's instructions. Tissues were incubated overnight at 55°C with 180µl of Buffer ATL and 20µl Proteinase K (Sigma). The samples were briefly vortexed and 200µl of Buffer AL and 200µl of 100% ethanol were added per sample. After mixing, the samples were passed through a DNeasy mini-spin column at 6000 x g for one minute. The DNA binds to the column at this step. Unbound contaminants were removed by a series of wash steps with Buffers AW1 and AW2. The column was then placed in a fresh 1.5ml microcentrifuge tube and the DNA was eluted with Buffer AE (200µl for tails and 80µl for ears).

2.4.3 Nucleon Extraction

To obtain "high quality" DNA, for next generation sequencing, extractions were performed using the Illustra® Nucleon DNA Extraction Kit (GE Healthcare). 300µl of Reagent B and 20µl of Protinase K (at a concentration of 10mg/µl) was added to the tissues and the solution was incubated at 55°C to lyse the samples. Then, 100 µl of Sodium perchlorate was added to deproteinise the DNA followed by 600µl of chloroform to solubilise the lipids and proteins. 100µl of Nucleon Resin was then added and the samples were centrifuged to separate into an upper aqueous phase (containing the DNA), an interphase (containing the resin) and a lower organic phase (containing chloroform, hair and waste). The upper phase was collected and the DNA was precipitated with 100% ethanol. The DNA was resuspended in 100µl of ddH_2O.

2.4.4 DNA Quantification

After extraction, DNA was quantified using the Epoch Micro-Volume Spectrophotometer System and Take 3 Micro-Volume Plate (BioTek). DNA was then diluted as required.

2.5 PCR (Polymerase Chain Reaction)

The polymerase chain reaction (PCR), originally pioneered by (Saiki et al., 1985), was use to specifically amplify DNA sequences of interest.

A variety of oligonucleotide primers and cycling conditions were used to amplify genomic DNA **(Tables 2.7-2.11).** Primers were designed using an online design tool (Primer 3), produced by Eurofins and diluted to 10μM with ddH_2O. All amplification assays were conducted in 96-well Abgene PCR plates (Thermoscientific). Plates were sealed using peelable heat sealing foil sheets (ThermoScientific) and centrifuged briefly prior to amplification. The reactions were performed on a G-storm thermocyler (GRI) or a Tetrad 2 Peltier thermal cycler (Bio-Rad).

Three different ready-made master mixes were used to perform the PCR reaction.

2.5.1 Reddymix

20μl of x1.1 ReddyMix Mastermix (Thermo Scientific) was combined with 0.75μl of each primer and 2.5μl of DNA (diluted to 5ng/μl) to make a total reaction volume of 24μl.

2.5.2 Amplitaq Gold

A 25μl assay was prepared consisting up 1x buffer (Applied Biosystems), 3mM $MgCl_2$ (Applied Biosystems), 0.15μl of AmpliTaq Gold polymerase (Applied Biosystems), 0,2mM dNTPs (Invitrogen), 1μl of each primer and 3μl

of DNA (at a concentration of 5ng/µl). For sequencing, the reactions were scaled up to give a total volume of 50µl.

2.5.3 Hot Shot

5µl of Hotshot mastermix (Idaho Technology Inc.) was combined with 0.2µl of each primer 2.6µl of ddH_2O and 2µl of DNA (at a concentration of 5ng/µl) to make a total reaction volume of 10µl.

2.6 PCR Purification

PCR products were purified using one of the following methods as per manufacturer's instructions.

2.6.1 QIAquick PCR Purification Kit (Qiagen)

The QIAquick PCR Purification Kit (Qiagen) purifies PCR products between 100 and 10,000bp in size by removing buffer salts and recovering DNA fragments. Five volumes of buffer PB were added to one volume of PCR reaction. The samples were added to a QIAquick column (a silica column which binds DNA in the presence of high salt concentrations) and the samples centrifuged for 30-60 seconds at 17,000x g. A series of washes were then conducted to remove the contaminants (e.g. primers, enzymes and unincorporated nucleotides). 750µl of PE buffer was added to the column and centrifuged for 45 seconds at 17,000x g. The column was further centrifuged for one minute to remove the residual wash buffer. The column was then placed in a clean 1.5ml microcentrifuge tube and the DNA eluted in

25µl of elution buffer. The integrity of the DNA was confirmed through gel electrophoresis on a 1% agarose gel.

2.6.2 GeneClean II (MP Biomedicals)

The GeneClean II kit was used to isolate DNA fragments from TAE agarose gels. The correct sized band was excised from the gel and melted in a three times volume of sodium iodide at 55°C. 5µl of glass milk was added and pelleted at 13,000 rpm for one minute. The pellet was washed several times with New Wash to remove the contaminants left over from PCR and gel electrophoresis. The pellet was then resuspended in 25µl of TE (1x Tris EDTA).

2.6.3 SureClean (Bioline)

The SureClean kit removed primers, dNTPs and restriction enzymes from the PCR reaction. It allows the precipitation of nucleic acids ≥75 bp with 98% recovery of the original sample. Five volumes of SureClean was added to the PCR reaction and incubated at room temperature for ten minutes. The sample was centrifuged at maximum speed (13,000 rpm) for ten minutes and the supernatant aspirated out. A two times volume of the original sample of 70% ethanol was added and vortexed briefly. Following this, the sample was once again centrifuged at maximum speed (13,000 rpm) for ten minutes and the supernatant removed and discarded. The pellet was air-dried and resuspended in 30µl of ddH_2O.

2.7 Agarose Gel Electrophoresis

PCR reaction requiring analysis were studied by gel electrophoresis using 1-2.5% agarose gels (depending on the size of the product). PCR reactions already containing a coloured dye were centrifuged briefly and loaded into the gel. For reactions without a dye, following a brief centrifugation, 3µl of Orange G loading dye was added to the samples prior to loading. The PCR product was separated by gel electrophoreses at 150 volts for 20-30 minutes. PCR product sizes were compared to a 100 base-pair (bp) standard molecular weight marker (New England Biolabs) or Hyperladder® I/IV to determine the product sizes. Gels were imaged using a Ultra-Violet (UV) gel doc system with the Quantity One v7-6.3 software (Bio-Rad).

2.8 Gene Identification

2.8.1 Whole Genome Mapping

DNA was prepared (using the Qiagen kit) and 30µl of DNA at a concentration of 50ng/µl was sent to Tepnel Life Sciences for SNP-based whole genome mapping using a Illumina Golden Gate Mouse Medium Density Linkage Panel. This analyses the different SNPs which are different between the C3H/HeJ and C57BL/6J strains. Allowing regions of C57BL/6J homozygosity to be identified in the affected animals, which are potential regions of interest as the G0 ENU-treated male was a C57BL/6J mouse.

2.8.2 Fine Mapping

The candidate region identified by whole genome mapping was narrowed using strain-specific SNPs which could differentiate between C57BL/6J and C3H/HeJ alleles. SNPs were identified using the Mouse Phenome Database and primers flanking the SNP were designed using the online Primer 3 software. Primers were used to amplify the region containing the change and then digested with an appropriate restriction enzyme **(Table 2.2)** to allow discrimination of the SNP allele.

Table 2.2: Primers used for narrowing the candidate region in the pedigree MPC96

Location on Chr 2 (Ensembl build NCBIM37)	Product Size	Primer Sequence	Restriction enzyme
51428003	250	**F** AACCAGAAAATTCTCAAAAACTTG	*MwoI*
		R TGCAAAAATGTAGATTAAAATGGTC	
53189457	246	**F** TGGATTGGAAGGGACTTGTG	*HaeII*
		R TCCTGATTCTTGTCTCCTCCA	
55238068	214	**F** GCCACGTGAAGGATAGCATAA	*NlaIV*
		R TGATAGGGGAAGACCCACTT	
56388227	271	**F** GGCTCCAGGAAGTGTCTTCCCA	*MfeI*
		R AGCTTTCTAAGCCCCAACCTCCTT	
63384957	242	**F** GGGCACTCGGGTCCTTTA	*MnlI*
		R GGCCATCAAAAGAGTTGCAT	
66805958	577	**F** TTGCCTGTGGTCATGCTTGTGGG	*BstYI*
		R ACTGCACTAACAGCATGCTCCATGA	
69989588	577	**F** TGGCAGGCAATGGTGGTCCT	*NlaVI*
		R CACAGTTGATGCATTCACAGTTGAC	
74004668	240	**F** TGCAGCTTGGCATTATCTTG	*NsiI*
		R TTTCTGTGTGTCTGAAGCGAAT	
78388769	229	**F** GGCATTCCCCTGTACTGAGA	*SacI*
		R AATGGCAACAGGCATGTGTA	
87353090	285	**F** TCCTAGGATGGTCTTGGGACTCA	*BsaJI*
		R TTGGTGTGGTGGGAACCAGC	
92826811	408	**F** GAGGGGAGGTGGGGAGCAACA	*AciI*
		R GGCAAGGCCCATGGTAGGGA	
97160228	224	**F** AATCCATTCGCTTAGTGTCCA	*ScaI*
		R GGTTTCAGGAGCAGGAACTG	
102989561	181	**F** GTCCCGTTGCTGCTATGATT	*PstI*
		R GGGTGAGTAGGAGCTGTGCT	

Table 2.3: Primers used for narrowing the candidate region in the pedigree MP90

Location on Chr 4 (Ensembl build NCBIM37)	Product Size	Primer Sequence	Restriction enzyme
154865395	222	**F** CAGGGCAGGCACTAAGCTAC	*PstI*
		R TATCCCCCAGGCTCAGAAG	
155070695	220	**F** TGCAGGGAGCTTGAGGTACT	*DdeI*
		R CGCGAGTACCTTGGTGTTG	
155556410	248	**F** GAGCCCTTAAACAACGGTGA	*BgIII*
		R TCAGGTGGCAGAGGTACACA	
155628841	228	**F** TAAGGGTGGGGAGACTGTTG	*SphI*
		R TTGGGTCTAAGTGCCAGGTC	
156171976	240	**F** AGCAGCAGTCCCTCTGTCTC	*BbvI*
		R GCTGGCACTGTCTGTGAGAA	

2.8.3 Next Generation Sequencing

DNA from the founder G1 (for MPC96) and an affected G3 mouse (for MP90) were prepared (using the Nucleon extraction method) and sent for Next Generation Sequencing (NGS). 5µg of DNA at a concentration of 50ng/µl was sent to the High-Throughput Genomics Facility at The Wellcome Trust Centre for Human Genetics, Oxford for NGS using the Illumina HiSeq platform. The sequence was aligned to a reference genome by the bioinformatics team at MRC Harwell.

2.8.4 Validating ENU Induced Changes

The NGS data was filtered by the bioinformatics team and all ENU-induced lesions were highlighted. In the case of MP90, DNA from an affected G3 mouse was sent for sequencing and therefore a homozygous change was expected. With MPC96 DNA from the G1 founder was sent for sequencing and therefore heterozygous changes were analysed. In both cases, changes with a quality score of above 100 were validated. There were six homozygous changes identified within the candidate region for MP90 **(Table 2.4)** and only one high confidence ENU-induced change within the candidate region for MPC96 **(Table 2.5)**. If the change introduced or removed a restriction site, the PCR digest method was used for validation. If a restriction site was not altered, the change was amplified, purified using the Geneclean II Kit (MP Biomedicals) (as described in Section 2.6.2) and sent for Sanger sequencing at Source Bioscience, Oxford (as described in Section 2.8.5).

Table 2.4: Primers used to validate the ENU induced changes in pedigree MP90

Location on Chr 4 (Ensembl build NCBIM37)	Gene containing predicted ENU lesion	Primers	Product size (bp)	Digest enzyme
149646844	-	**F** CTGTTAAGGAGGGAAGGCCCGT	287	SspI
		R CGTTTCGGGGAGCTGTGCGAT		
150260319	-	**F** ACCTGGCTAGCTGACCGAGCA	125	BsmAI
		R GGGGGTTTTGCGTTTTCAGCCC		
150281606	*Rere*	**F** CACCAACGCTTGAGATGAGA	227	-
		R CAAACCATTGTGTGCGTGTA		
150431715	*Camta1*	**F** CGCCAAACGCTGGCCTACGA	345	AvaII
		R GGTGGCCGCTGCTTGACACT		
152253061	-	**F** GTGAGCGCTTCTTTTCCCGCTG	195	Tsp45I
		R AGGAGCTGCTAGTGGACGGCT		
154424034	-	**F** CTCCTGCCCAGAGTTTCCCCCT	570	MwoI
		R GACTGCGGGTGTGAGGTAGCA		

Table 2.5: Primers used to validate the ENU induced changes in pedigree MPC96

Location on Chr 2 (Ensembl build NCBIM37)	Gene containing predicted ENU lesion	Primers	Product size (bp)	Digest enzyme
62106906	*Slc4a10*	**F** GCAACACTGTGCATCATCCT	307	SacI
		R GGATCAATTCTAGGCCCACTC		

2.8.5 Sanger Sequencing

Once purified, DNA was quantified and sent to Source Bioscience, Oxford, for sequencing. 5µl of PCR product was sent per reaction at a concentration of 1ng/µl per 100 bp of product. Gene-specific sequencing primers at a concentration of 3.2pmol/µl were also sent. Sequencing results were analysed using the DNAStar SeqMan software.

2.8.6 Gap Analysis

When NGS data fails to align to the reference genome, sequencing gaps are identified. For pedigree MP90, DNA from one affected mouse (MP90/2.5i) was amplified by PCR (using primers designed to amplify these gaps) and sent for Sanger Sequencing **(Table 2.6)**.

2.8.7 *in silico* Analysis

Protein prediction software was used (with the assistance of my supervisor) to investigate whether the molecular changes caused by ENU-induced lesions would affect the protein structure and thus affect its function. This analysis was performed using the software SIFT (Sorting Intolerant from Tolerant), Polyphen-2 and PROVEAN.

Table 2.6: Primers used to sequence the gaps in the pedigree MPC96

Gap	Number of Bases in gap	Primers	Product size (bp)
GAP 1	10	**F** GTTTCGGCGCTTTTGTTTTA	214
		R CTTCAGAGGCCAGGACAAAG	
GAP 2	27	**F** CATTGCTAGCTCATCTTGAATTTT	250
		R GGTTTCATGGTCTGCATTTTT	
GAP 3	20	**F** TCCTGTGGCTGGAGAATCTT	231
		R TCAGTGCCCATTCAACTGAG	
GAP 4	74	**F** CCGTTCCCATCCCGGTG	347
		R CACCCGAGCACGGTTCC	
GAP 5	97	**F** TTGATTCCAGGCCAATCACTTTA	319
		R TTGATTCCAGGCCAATCACTTTA	
GAP 6	47	**F** CACTGAGCTGCCCAAGACTA	491
		R CATCTCCTCCGCGAACAG	
GAP 7	662	**F** GCGCTTCTGGAGGCAGAC	149
		R GCGCACAGCGAGTCAGAG	
GAP 8	500	**F** AAAGACGTGGGCAAGTGCTA	33
		R ACCCGTGGATTCCTCTGC	
GAP 9	392	**F** CAGCAGATGTGGGACAGAAA	31
		R GAGCAACATGGCAGCTCATA	
GAP 10	397	**F** CCGCCTGTGCTAGGTAGACT	47
		R CCTCGGACAGCACCTTGTAG	
GAP 11	594	**F** AGACAGCGCTCGGAGAGAC	124
		R TGAGCACGTTCTTGAAGTCG	
GAP 12	229	**F** CCTCAAACTGAAACTTCTCTGC	1
		R CCAACCTGAGACACCATGAG	

2.9 Genotyping

Several platforms were used to genotype the lines of interest. To begin with, all genotyping was conducted using a restriction digest method. However, some assays were migrated onto the pyrosequencing platform. The GEMS (Genotyping and Mutation detection Screens) core facility at MRC Harwell has recently taken over the genotyping tasks and employ the Lightscanner to genotype, where possible.

2.9.1 Restriction Digest

The Slc4a10 change introduced a restriction site and could therefore be genotyped by PCR and restriction digest **(Figure 2.4)**. Following PCR **(Tables 2.10 and 2.11)** 10µl of the PCR product was digested in a reaction containing 2µl of 10X buffer, 2µl 10X BSA and 5.5µl of dH_2O. The reaction was incubated at the appropriate temperature on a thermal cycler (Tetrad2 Peltier) 3 hours (1 hour for high fidelity enzymes) with the enzyme *SacI*. The reaction was then run on a 2.5% TAE gel.

2.9.2 Pyrosequencing

Pyrosequencing is a DNA sequencing technique that relies on detection of pyrophosphate release upon nucleotide incorporation (Ronaghi, 2001). This technique was used to genotype the *trombone* line. A PCR was set us using the Hot Shot Mix (Section 2.5.3). The GEMS core facility at MRC Harwell conducted the pyrosequencing using The Qiagen PSQ HS 96 instrument. The PCR is performed using one biotinylated and one normal primer. The PCR

products are then separated using the vacuum prep station and a sequencing primer annealed to the biotinylated PCR template strand.

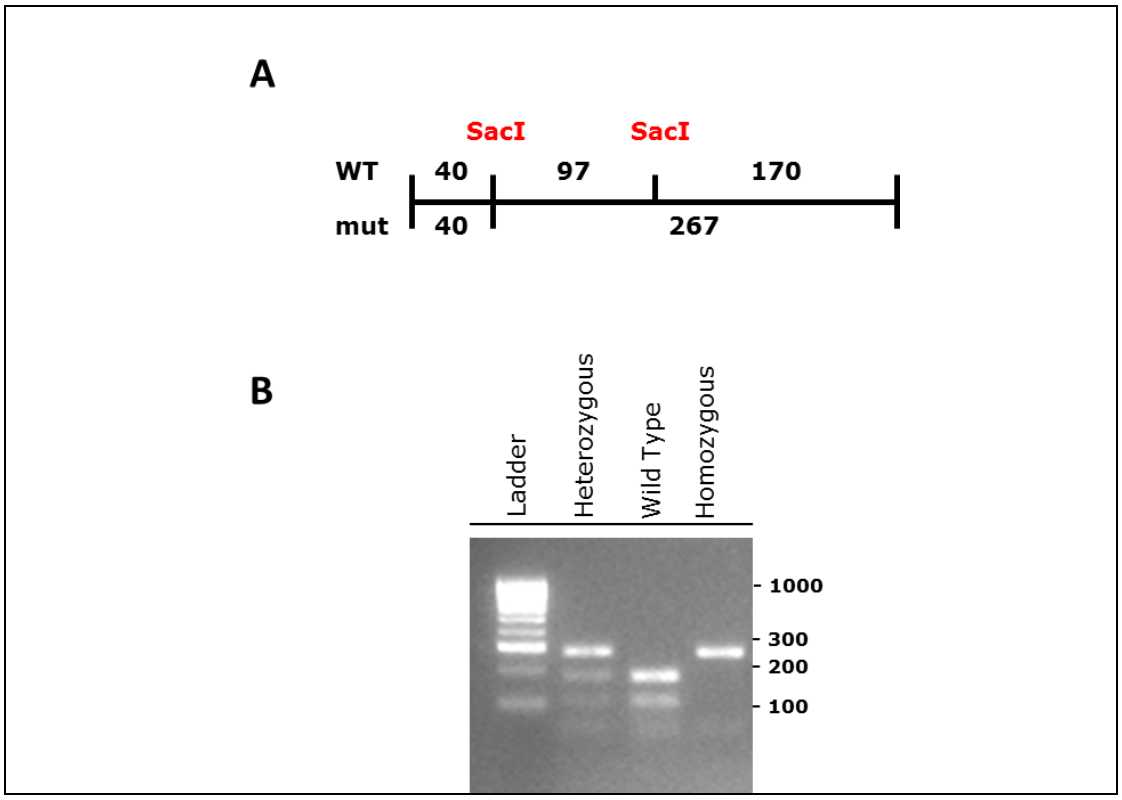

Figure 2.4: Restriction digest of *Slc4a10*^{trmb}
[A] The predicted PCR product with SacI restriction sites. The restriction enzyme SacI cuts the wild type PCR product at two sites resulting in three bands of 40, 97 and 170 bp. The T>C change in Slc4a10 removes one of these restriction sites resulting in only 2 bands of 40 and 267 bp. [B] Result of PCR and digest. The wild type shows three bands of 40, 97 and 170 bp. The homozygous mutant shows two bands of 40 and 267 bp. The heterozygous animal has all 4 bands of 40, 97, 170 and 267 bp.

The instrument adds enzymes, DNA polymerase, ATP sulfurylase, luciferase and apyrase as well as substrates, adenosine 5' and phosphosulfate (APS) and luciferin. DNTPs are added one by one and as the dNTPs are incorporated into the template strand, there is a release of pyrophosphate equal to the number of nucleotides incorporated. The chemical reaction causes bioluminescence which is seen as a peak on the instrument display **(Figure 2.5)**.

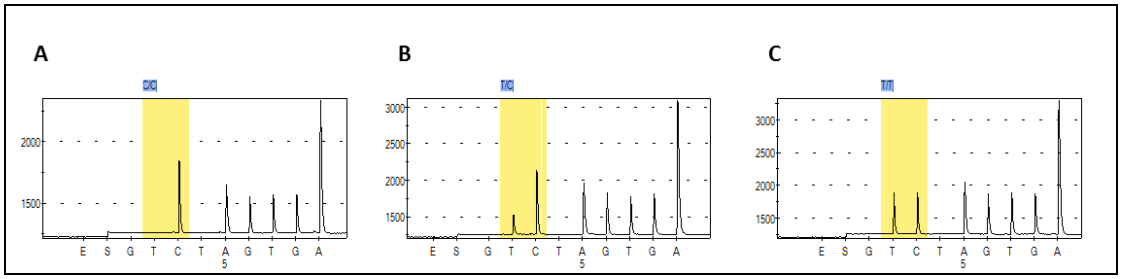

Figure 2.5: Genotyping *trombone* using the pyrosequencing
An example of the pyrosequencing output for the *trombone* genotyping [A] Homozygous [B] Heterozygous [C] Wildtype

2.9.3 LightScanner

The GEMS core facility at MRC Harwell recently took over the genotyping of the *trombone* using unlabelled probe genotyping.

The Idaho Technology LightScanner is a system used to perform high throughput DNA melting analysis. PCR is performed in the presence of the double-stranded DNA binding dye LCGreen. The PCR samples are then heated on the LightScanner and the fluorescence emitted by bound LCGreen is monitored (Wittwer et al., 2003). As the DNA melts, the LCGreen is released and the fluorescence decreases until all the DNA has melted and all of the LCGreen is unbound. Unlabelled probe genotyping is used to distinguish between different homozygote samples at a given SNP where scanning analysis may not have enough sensitivity. Here a 3' blocked oligonucleotide (LunaProbe) is designed that sits directly over the SNP. Asymmetric exhaustive PCR is performed using five times the amount of probe and opposite primer. This creates two products, one is the full PCR product between the normal primers and the other is the probe that is bound

to the opposite strand. The melting profiles of homozygous, heterozygous and wildtype mice are shown in **(Figure 2.6)**.

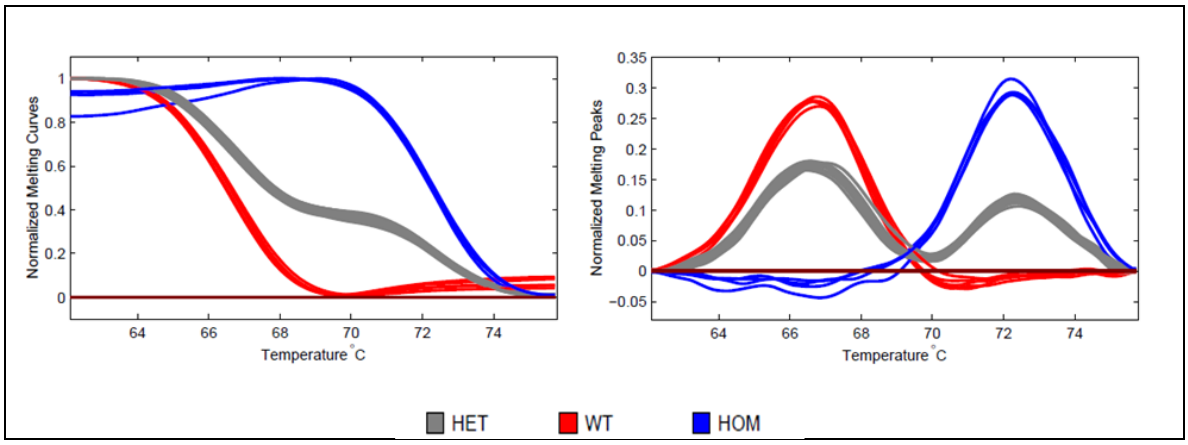

Figure 2.6: Genotyping *trombone* using the LightScanner
An example of the LightScanner output for the *trombone* genotyping

Table 2.7: Primer sequences and enzyme used for agarose gel based PCR assays and restriction digests

Assay	Primer type	Primer Sequences 5'-3'	Product Size	Restriction Enzyme
Slc4a10 – Restriction Digest	Forward	GCAACACTGTGCATCATCCT	307	*SacI*
	Reverse	GGATCAATTCTAGGCCCACTC		

Table 2.8: Primer sequences used for pyrosequencing based PCR assays trombone

Assay	Primer type	Primer Sequences 5'-3'
Slc4a10 - Pyrosequencing	Forward	ATGAAGCCCTGGAGAAGTTGT
	Reverse	TGTGTCAGCAGTTCCAAATCAT
	Sequencing Primer	GGAGAAGTTGTTTGAGC

Table 2.9: Primer sequences used for LightScanner-based PCR assays

Assay	Primer type	Primer Sequences 5'-3'
Slc4a10 - Lightscanner	Forward	CTCGTCTGCTACATCACCC
	Reverse	CGAGTATTGTGTCAGCAGTTC
	Probe	GAAGTTGTTTGAGCCCAGTGAAACCTA

Table 2.10: PCR mix details for agarose gel based, pyrosequencing and LightScanner-based genotyping assays

Assay	Reagent	Volume (µl)	Total volume (µl)
Slc4a10 – Restriction Digest	Reddy Mix	20	24
	Forward Primer (10µM)	0.75	
	Reverse Primer (10µM)	0.75	
	DNA	2.5	
Slc4a10 - Pyrosequencing	HotShot	5	10
	Forward Primer (10µM)	0.2	
	Reverse Primer (10µM)	0.2	
	DNA	2	
	ddH_2O	2.6	
Slc4a10 - Lightscanner	HotShot master mix	5	10
	LC Green	1	
	Forward Primer (20ng/µl)	0.1	
	Reverse Primer (20ng/µl)	0.5	
	Probe	0.5	
	DNA	2	
	ddH_2O	0.9	

Table 2.11: PCR cycling conditions for (A) Reddy mix standard PCR cycling conditions, (B) pyrosequencing PCR cycling conditions and (C) LightScanner PCR cycling conditions.

	A		B		C	
Step	**Temperature**	**Time**	**Temperature**	**Time**	**Temperature**	**Time**
1	**95 °C**	**3 mins**	**95 °C**	**3 mins**	**95 °C**	**2 mins**
2	**95 °C**	**30 secs**	**95 °C**	**30 secs**	**95 °C**	**30 secs**
3	**52 °C** **X 35**	**30 secs**	**60 °C** **X 44**	**30 secs**	**60 °C** **X 55**	**30 secs**
4	**72 °C**	**30 secs**	**72 °C**	**30 secs**	**72 °C**	**30 secs**
5	**72 °C**	**4 mins**	**72 °C**	**4 mins**	**95 °C**	**30 secs**
6	**16 °C**	**hold**	**16 °C**	**hold**	**25 °C**	**30 secs**
7					**15 °C**	**30 secs**

2.10 Scanning Electron Microscopy (SEM)

2.10.1 Tissue Collection

Mice were sacrificed through cervical dislocation and decapitated. The head was then skinned and bisected down the midline. The brain and extraneous tissue from around the ear was removed to expose the inner ear. The inner ear was then dissected out and the bulla lifted away to expose the round and oval windows, which were cleared using fine watchmakers forceps. A small hole was made in the apex of the cochlea by gently scratching away at the shell to allow for complete penetration of the fixative. The inner ears were then fixed overnight in glass specimen jars containing 5ml of 2.5% gluteraldehyde in 0.1M phosphate buffer (Sigma-Aldrich). The ears were then washed at room temperature three times (five minutes per wash) with 0.1M phosphate buffer and decalcified at 4°C for 48 hours in 4.3% EDTA in 0.1M phosphate buffer (Sigma-Aldrich). The ears were once again washed three times for 15 minutes in 0.1M phosphate buffer and stored at 4°C until fine dissection.

2.10.2 Fine Dissection of the Inner Ear

Fine dissections were performed using a Zeiss Discovery v.20 stereomicroscope (Zeiss, Jenna). Inner ears were pinned to a Sylguard filled petri dish using a 30G needle. The ears were covered with 0.1M phosphate buffer to prevent them from drying out. The bony shell of the inner ear was then removed to reveal the cochlear duct. Fine watchmaker forceps were used to remove the stria vascularis, to reveal the hair cell rows beneath. The inner ears where then placed back into the glass pots containing 0.1M

phosphate buffer until Osmium-Thicarbohydozide-Osmium-Thicarbohydozide-Osmium (OTOTO) processing.

2.10.3 OTOTO Processing

OTOTO processing is a post-fixative procedure which prepares the samples for ultrastructural analysis (Hunter-Duvar, 1978). Dissected inner ears were placed in a specimen holder and incubated in 1% osmium tetroxide (O_sO_4) (Agar Scientific) in 0.1M phosphate buffer for one hour at room temperature. The samples were then washed six times in distilled water, with each wash lasting three minutes. Following this, the samples were immersed in 1% Thiocarbohydrazide (Sigma Aldrich) for 30 minutes. The samples were again washed six times with distilled water, as before. The ears were fixed in osmium tetroxide solution and thiocarbohydrazide solution alternatively resulting in a total of three osmium tetroxide fixation steps and two thicarbohydrazide immersion steps, with washes between each incubation.

The samples were then dehydrated, in the glass jars, in increasing strengths of ethanol (Fisher Scientific) for 45 minutes each (25%, 40%, 60%, 80%, 95%, and 100%) at 4°C. Following ethanol dehydration, the samples were stored in 100% acetone until further processing.

2.10.4 Critical Point Drying and Mounting

The samples were critical point dried using an Emitech K850 (EM Technologies Ltd.) as per the manufacturer's instruction, with two soak and purge steps. Critical point drying uses liquid carbon dioxide to replace

solvents. The carbon dioxide is then removed in a supercritical state to remove the liquid present in the sample (Hall et al., 1978).

The dried specimens were then mounted on 12.5mm stubs (Agar Scientific) using 12mm adhesive tabs (Agar Scientific) and silver paint (Agar Scientific). The inner ears were mounted with the cochlea facing upwards.

2.10.5 Sputter Coating

The mounted samples were sputter coated twice with platinum in an argon atmosphere using an automated routine on a Quorum Q150T sputter coater (Quorum Technologies). Sputter-coating ensures that the samples are conductive and can therefore be imaged using a scanning electron microscope (SEM).

2.10.6 Imaging

The processed and prepared cochleae were visualised using a JEOL LSM-6010-LV (Jeol Ltd) scanning electron microscope. All images were taken at an accelerating voltage of 10kV. To assess the gross morphology of the cochlea, a spot size of 50 and magnification 100x was used. To study the hair cells in detail, a spot size of 30 and magnification 2,000x was used.

2.10.7 Hair Cell Counts

Hair cells counts were performed by manually quantifying the number of outer hair cells and inner hair cells adjacent to ten pillar cells. For further analyses, the cochlea was split into three sections (apex, mid and base). SEM

images were obtained and hair cell counts were performed at the three regions independently.

2.11 Histology and Morphological Analysis

The processing steps for decalcification, embedding and sectioning for histological analysis were conducted by the histology team at MRC Harwell. The haematoxylin and eosin (H&E) staining was also carried out by the histology team.

2.11.1 Tissue Collection

Animals were sacrificed; the heads were removed, skinned, bisected along the midline and fixed in 10% neutral buffered formaldehyde (Surgipath Europe).

2.11.2 Decalcification, Embedding and Sectioning

The heads were fixed for 24 hours and then decalcified in D.F.B decalcifying agent (Kristenson; Pioneer Research Chemicals) for 48 hours. Samples were then rinsed with water and placed in an automated ThermoShandon Pathcentre machine (Thermoscientific) to dehydrate samples by immersion in a series of graded industrial methylated spirits (70, 90 and 100%) (Chemix). The specimens were then cleared with a xylene substitute clearing agent: Sub-X (Surgipath Europe). The samples were coated with paraffin wax (Surgipath Europe) and then embedded in a fresh paraffin wax block. The samples were left to solidify and 5µm sagittal sections were cut on a

microtome (Finesse ME; ThermoShandon) using a S35 feather disposable microtome blade (Surgipath Europe). The sections were floated into clean distilled water at 50°C to remove creases and transferred to electrostatically-charged slides (Surgipath Europe).

Alternate sections were stained with H&E whilst the remaining slides were left unstained on charged slides.

2.11.3 H&E Staining

Alternate paraffin wax embedded sections were stained with haematoxylin and eosin using a Shandon Varistain 24 (Thermoscientic) machine which automates solution changes **(Table 2.12).**

Table 2.12: Staining procedure using Shandon Varistain 24

Solution	Time
Sub-X	15 minutes
Sub-X	4 minutes
Sub-X	2 minutes
Alcohol (IMS or IPA)	2 minutes
Alcohol (100%)	1 minute
Alcohol (100%)	90 seconds
Alcohol (70%)	90 seconds
Running water	90 seconds
Gill 3 haematoxylin	6 minutes
Running water	1 minute
1% acid/ alcohol	15 seconds
Running water	1 minute
1% Lithium carbonate	30 seconds
Running water	1 minute
Eosin	90 seconds
Running water	10 seconds
IPA	10 seconds
IPA	1 minute
IPA	1 minute
IPA	2 minutes
IPA	2 minutes
IPA	1 minute
IPA	1 minute
IPA	30 seconds

(*IPA = Immunoperoxidase)

The paraffin was removed from the slides by submerging the samples first in SubX clearing agent (a xylene substitute). The samples were then rehydrated through a graded series of isopropanol and running water. The slides were then incubated in Haematoxylin (Shandon Gill 3, Thermoscientific) for 6 minutes to stain for the basophilic structures and then rinsed in running water. The slides were then immersed in 1% acid alcohol to remove any background staining. The slides were then washed with running water and immersed in 1% lithium carbonate (Fisher Scientific) which gives the nuclei a blue colour. The slides were then washed in running water and stained with eosin to counterstain the eosinophilic structures pink. The slides were then washed and dehydrated with isopropanol changes. Sections were then mounted with Clearium (Surgithpath Europe) and a 24 x 50mm coverslip slides (Fisher Scientific).

The H&E slides were analysed on a Zeiss Axiostar plus microscope, set up for Köhler illumination, with a 10x/NA 0.25 CP-Achromat and/or a 40x/NA 0.65 CP-Achromat objective in brightfield mode. Images were captured with an Altra-20 CCD camera (SIS systems) running under Cell B imaging software version 2.0 (Build 1187).

2.11.4 Spiral Ligament Analysis

The H&E stained sections were analysed using the Nanozoom digital pathology software version 1.1.27 (Hamamatsu). The cross-sectional surface area of the spiral ligament and strial thickness was measured using the

ImageJ software (version 1.46r) (National Institute of Health) (Schneider et al., 2012).

2.11.5 Nuclei Counts and Spiral Ganglion Neuron Count

Paraffin wax embedded sections were counterstained with Gill 3 haematoxylin and then immersed in 1% lithium carbonate to stain the cell nuclei blue. The slides were then, rinsed, dehydrated and mounted as with Section 2.11.3. The ImageJ software was used to count the nuclei in the stria vascularis and the spiral ligament. The ImageJ software was also used to count the number of spiral ganglion neurons.

2.12 Immunohistochemistry

Immunohistochemistry was used to study the expression of *Slc4a10* in the cochlea. For immunohistochemistry, 5µm paraffin wax sections mounted on charged slides were used (Section 2.11.2).

Primary antibody: Goat anti-NCBE (sc-161917, Santa Cruz Biotechnology)

Secondary antibody: Biotinylated rabbit anti-goat (DAKO)

Tertiary antibody: Streptavidin-peroxidase complex (VECTASTAIN elite ABC kit, Vector laboratories)

2.12.1 Dewaxing

The slides were dewaxed with three changes of Sub-X (xylene substitute) clearing medium (Leica Microsystems). The dewaxing solution was removed through a graded series of alcohol washes **(Table 2.7)** followed by a final wash with ddH_2O.

2.12.2 Blocking

The slides were incubated in a Coplin jar at room temperature for 30 minutes with 3% hydrogen peroxide (VWR) in 2-propanol to block the endogenous peroxidase activity. The samples were then washed twice with ddH_2O followed by a PBS wash. If required, antigen retrieval was performed at this stage (Section 2.13.3). If not, the slides were then incubated with the desired antibody (ies) (Section 2.13.4).

2.12.3 Antigen Retrieval

After dewaxing and rehydrating the tissue sections, antigen retrieval was performed where required. Slides were placed in a ChemMate chamber (DAKO), filled with 10mM citrate buffer. Empty slides were used to fill in the unused slide slots in order to ensure uniformed heat distribution. The slides were then heated twice in the microwave for seven minutes each. Between each microwaving step, the chamber was topped-up with distilled water, to ensure that the samples would not dry out. Slides were left to cool at room temperature and then washed once with PBS.

2.12.4 Antibodies

Either after the blocking or antigen retrieval step (when required), sections were outlined with a hydrophobic marker pen. The slides were then incubated with 10% rabbit blocking serum for 30 minutes. The blocking serum used depends on which species the secondary antibody was raised.

The sections were incubated with 1:200 primary antibody (diluted in normal blocking serum) for one hour at 4°C, inside a humidified chamber. Negative control sections received no primary antibody. In a test slide, the specificity of the primary antibody was analysed by pre-blocking the primary antibody (1:200) with the immunising peptide.

The sections were then rinsed twice with PBS and incubated at room temperature for 30 minutes with 1:400 secondary antibody (DAKO). As the primary antibody was raised in goat, a biotinylated rabbit anti-goat secondary antibody was used. Sections were then washed twice with PBS

and incubated with VECTASTAIN *Elite* ABC Reagent (Vector) for 30 minutes. Following this, the sections were once again washed with PBS.

2.12.5 Detection and Analysis

A peroxide-based immunohistochemical method utilising diaminobenzidine (DAB) was used to detect staining. The DAB solution (DAKO) was made as per the manufacturer's instructions and added to the sections. Once the brown stable became visible (approximately 2 minutes), the slides were washed with PBS.

The slides were then counterstained with haematoxylin, cleared and mounted by the histology team at MRC Harwell (Section 2.11.3). Sections were imaged using a Zeiss Axiostar Plus bright-field microscope and the Cell^B software (Olympus) was used to capture the images.

2.13 Immunofluorescence

Immunofluorescence was performed on wax sections to study the different cell types present in the lateral wall of the cochlea.

2.13.1 Dewaxing

Paraffin wax sections were dewaxed by the histology team at MRC Harwell as was described in Section 2.13.1.

2.13.2 Permeabilisation and Blocking

The sections were permeabilised with 0.1% Tween in PBS (PBST) for ten minutes and washed with PBS. The sections were then outlined with a hydrophobic marker pen and blocked with 10% donkey serum (diluted in PBS) for 30 minutes at room temperature. The blocking serum used depended on which species the secondary antibody was made.

2.13.3 Antibodies

The sections were then incubated with primary antibodies **(Table 2.13)** (diluted in 10% donkey serum) for one hour at room temperature. Following incubation, the slides were rinsed once with PBST followed by three further five minute washes with PBS. The samples were then re-blocked with 10% donkey serum for 30 minutes after which they were incubated with secondary antibody for one hour at room temperature **(Table 2.14)**. The slides were rinsed once with PBST followed by three further five minute washes with PBS.

Table 2.13: Primary antibodies used for immunolabelling

Primary Antibody	Target	Manufacturer	Species	Primary Concentration
Glut1	basal cells and stria blood vessels	15309	Rabbit	1:200
Kir4.1	Intermediate Cells	APC-035	Rabbit	1:400
Acetylated Tubulin	microtubules in marginal cells, basal cells, organ of Corti	T6793	Mouse	1:1000

Table 2.14: Secondary antibodies used for immunolabelling

Secondary Antibody	Manufacturer	Primary Concentration
Alexafluor donkey α rabbit IgG 647	Invitrogen	1:200
Alexafluor donkey α mouse IgG 488	Invitrogen	1:200

2.13.4 Mounting and Imaging

The sections were stained with NucBlue Fixed Cell DAPI stain (Part No.= R-37606) (Life Technologies, Paisley UK) for five minutes to stain the nuclei and washed with PBS. The slides were mounted using Slowfade mounting agent (Life Technologies, Paisley UK) and a 20x22mm Menzel Glaser coverslip (Thermoscientific).

Images were captured using a Zeiss 1.4 megapixel AxioCam HRc 14-bit CCD camera (1388x1040 1.4 Megapixel) connected to a Zeiss Axio-Observer Z1 microscope (Zeiss, Jena) using a 40x/ NA 0.75 EC-plan Neofluor objective running under Zen Blue (2012) version 1.1.1.0.

2.14 Endocochlear Potential

Endocochlear potential measurements were undertaken as stated (Teubner et al., 2003). This experiment was conducted at the Pasteur Institute in Paris with assistance from Vincent Michel.

Mice were intraperitonealy anesthetized with 0.1 mg/g thiobutabarbital sodium (Inactin, Sigma, Deisenhofen, Germany). Anaesthesia was confirmed by checking for the pedal reflex. The mouse was then mounted on a stand and secured so that the measurements could be conducted without any hindrance. The cochlea was exposed by a ventral approach. Access to the endolymphatic compartment (scala media) of the basal turn was gained by thinning the bone over the spiral ligament and making a small opening with a small pick. Borosilicate capillaries were used to create double-barrelled glass electrodes and the inner surface of one of the barrels was siliconised by exposure to dimethyldichlorosilane vapour for 1 min followed by baking for 2 h at 200°C. The tip of the siliconised electrode was filled with potassium ion-exchange (World Precision Instruments, Berlin, Germany) and 0.5M NaCl. The second barrel (non-siliconised) was filled with 0.5M NaCl. Electrodes were connected to a FD223 (World Precision Instruments) differential electrometer which was used to measure the endocochlear potential. The electrodes were calibrated before every measurement in KCl standards over a range of 0-150mM. K+ concentrations were calculated from the respective voltages using an algebraic rearrangement of the Nicolski equation: $V=Vi+S\times\log([K+]+A\times[Na+])$, where Vi is an offset term, S is slope, and A is selectivity (Teubner et al., 2003).

2.15 Statistical Analysis

All statistical analyses and graphs were generated using Microsoft Excel and GraphPad Prism version 6. The data was first analysed to establish Normal distribution. When the data was normally distributed, a Student's *t*-test was used. If the data was not normally distributed, a Kruskal-Wallis or Mann-Whitney *U* test was used to establish if the results were significant. The data is presented as the mean ± standard error of mean (SEM). Difference of $p<0.05$ are considered statistically significant.

2.16 Online Tools

Mouse Phenome Database: http://phenome.jax.org

Ensemble: http://ensemble.org/

Primer3web: http://primer3.ut.ee/

Sorting Intolerant from Tolerant (SIFT): http://sift.jcvi.org/

Polymorphism Phenotyping (PolyPhen):

http://genetics.bwh.harvard.edu/pph2/

Mutation Taster: http://www.mutationtaster.org/

Webcutter 2.0: ma.lundberg.gu.se/cutter2/

2.17 Stock Solutions

All solutions were prepared as per the Molecular Cloning: Laboratory Manual (Sambrook et al., 1989). The ddH_20 water used was deionised RNAse-free water from Mill-Q.

Phosphate buffered saline (PBS): 137nM NaCl, 2.7mM KCl, 10mM Na_2HPO_4, and 2mM KH_2PO_4

0.1M Phosphate buffer: 4.44g sodium phosphate monobasic, 17.04g sodium phosphate dibasic, 789ml ddH_2O

Fixative for cochlear: 2.5% glutaraldehyde in 0.1M phosphate buffer

Decalcification for cochlea: 4.3% EDTA in 0.1M phosphate buffer

1% Thiocarbohydrazide: 0.3g Thiocarbohydrazide in 30ml distilled water

1% Osmium tetroxide: 2 x 5ml OsO4 ampoules in 30ml sodium cacodylate

0.2M sodium cacodylate: Sodium cacodylate in 900ml distilled water calibrated to pH 7.2 using 1M hydrochloric acid made up to one litre with distilled water

PBST: Phosphate buffered saline with 0.05% Tween 20

PFA: 4% paraformaldehyde in 0.1MPBS

Orange G: 110ml glycerol, 90ml TE pH8.0, Orange G powder

Ethidium bromide: 10mg Ethidium bromide in 1ml ddH_2O

1M Citrate buffer: 210g citric acid in 1000ml distilled water, calibrated to pH 6 using NaOH

Chapter 3

Muta-Ped-90

3.1 Auditory Phenotyping

Muta-Ped-90 (MP90) underwent initial auditory screening as part of the Harwell Ageing Screen (Section 1.8.1). At nine months of age, four animals exhibited elevated ABR thresholds when compared to littermate controls. Recurrent auditory screening of this pedigree at 14 months of age showed that the affected mice still had elevated ABR thresholds. However, there had not been any progression in the hearing loss **(Figure 3.1)**.

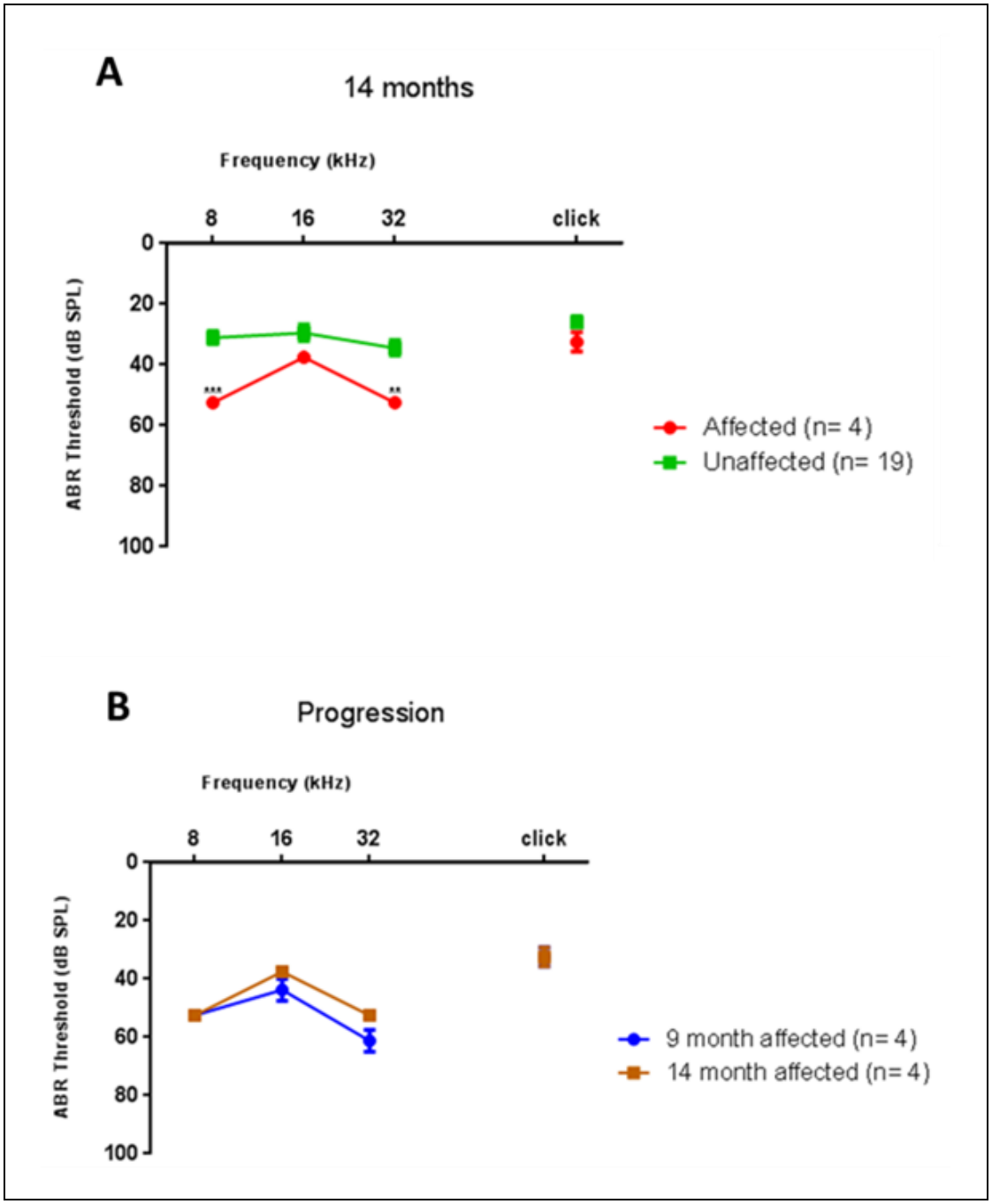

Figure 3.1: ABR thresholds of MP90 mice at 14 months of age and the progression of hearing loss between nine and 14 months of age
[A] Average ABR thresholds at 14 months of age indicate that four mice exhibit significantly elevated thresholds (**p<0.01, ***p<0.001) in comparison to littermates (n=19). [B] Comparison of the affected mice at 9 months of age and 14 months of age showed that there was no progression of the hearing loss observed. Error bars indicate standard error of mean, SEM.

3.2 Identifying the causative mutation in Muta-Ped-90

3.2.1 Mapping

To elucidate the location of the underlying genetic lesion responsible for the phenotype observed in MP90, DNA from affected (n=3) and unaffected animals (n=5) were sent to Tepnel Life Sciences for whole genome single nucleotide polymorphism (SNP) mapping. Initial results obtained identified three potential intervals of interest, on chromosomes 4, 13 and 19. Further mapping using additional affected and unaffected animals confirmed a region of interest on chromosome 4: 145785696-tel containing 174 genes (NCBIM37). Additional SNPs informative for the parental strains (B6 and C3H) were identified and used to try and narrow the candidate region, but this did not narrow the region any further.

The critical interval does not contain any known deafness genes, and there are too many genes in the region to undertake prioritised candidate gene sequencing. Therefore, whole genome sequencing was undertaken.

3.2.2 Next Generation Sequencing

DNA from one affected G3 animal (MP90/2.5i) was prepared and sent to the High Throughput Genomics Facility at the Wellcome Trust Centre for Human Genetics, Oxford, for whole genome sequencing using the Illumina Hi Seq platform. The NGS results indicated the presence of five high confidence homozygous changes within the candidate region of interest. However, all these changes were within intronic or intergenic regions. In addition, the candidate region contained 11 sequencing gaps.

3.2.3 Validating the ENU lesions

PCR followed by Sanger-sequencing were employed in order to validate the presence of the NGS-identified ENU-induced lesions. DNA from an affected mouse (MP90/2.5i) was used as a template **(Table 3.1)**. This indicated that all of the high confidence homozygous ENU-induced lesions identified by NGS are present in the affected MP90 mouse. However, one heterozygous lesion identified by NGS was found not to be present.

Table 3.1: ENU-induced lesions identified by NGS

Location on Chr 4 (Ensembl build NCBIM37)	Reference	Change	Hom/ Het	Quality Score	Result
149646844	A	G	Hom	65	Present
150260319	T	A	Hom	108	Present
150281606	T	A	Hom	210	Present
150431715	T	G	Het	40	Not Present
152253061	A	T	Hom	86.1	Present
154424034	T	C	Hom	106	Present

NGS results indicated the presence of five high confidence homozygous changes in the candidate region. These were validated using DNA from one affected mouse. Results indicated that all of the homozygous changes were present. In addition, one heterozygous change was predicted by NGS, but when tested, this change was not present (Ensembl build NCBIM37).

3.2.4 Gap Analysis

The NGS alignment had several sequence gaps (i.e. regions where reads did not align) in several places across the region of interest. This may have been due to erroneous reads or possibly sequence regions that were different in the sample tested. Of these, only the 12 gaps near, or encompassing coding sequences were interrogated **(Table 3.2)**. Two of the 'gaps' fall over protein coding sequence. Using PCR and Sanger sequencing, eleven of these gaps

have now been amplified and sequenced using DNA from an affected mouse (MP90/2.5i) as a template. No mutations have been identified in these gap sequences. The remaining gap, gap 5 encompasses a coding sequence; however, it was proved impossible to Sanger sequence, most likely due to the high complexity of the sequence and the number of small repeats.

Table 3.2: Sequencing gaps within NGS data

Gap	Gap Start	Gap End	Number of Bases	Gene Name	Biotype (Ensemble)	Sanger Sequenced?
GAP 1	148045492	148045502	10	*Gm572*	3' UTR	Yes
GAP 2	148328670	148328697	27	*Casz1*	3' UTR	Yes
GAP 3	148870731	148870750	19	*Lzic*	3' UTR	Yes
GAP 4	148960742	148960816	74	*Clstn1*	Coding (Exon 1)	Yes
GAP 5	151235729	151235826	97	*Camta1*	Coding (Exon 1)	No
GAP 6	151712839	151712872	33	*Chd5*	5' UTR	Yes
GAP 7	152856338	152856486	148	*Ajap1*	5' UTR	Yes
GAP 8	153690946	153690978	32	*Prdm16*	3' UTR	Yes
GAP 9	154995537	154995568	31	*Slc35e2*	3' UTR	Yes
GAP 10	155068537	155068583	46	*B930041F 14Rik*	Pseudogene	Yes
GAP 11	155221610	155221733	123	*Dvl1*	5' UTR	Yes
GAP 12	155488074	155488075	1	*9430015 G10Rik*	5' UTR	Yes

The MP90 NGS data failed to align to the reference genome (C57BL/6J) at 12 positions within the candidate interval. The position and size of these gaps on chromosome 4 are given (NCBIM37). Two gaps encompass coding sequences (red text).

3.3 Phenotypic Characterisation

3.3.1 Histological Studies

To assess for gross pathological changes in the inner ear, mid-modiolar histological sections from affected mice (n=3) were compared to those from unaffected mice (n=2) **(Figure 3.2)**. Results showed no gross dysmorphology of the inner ear. The organ of Corti and the hair cells appeared normal. The stria vascularis, Reissner's membrane and spiral ganglion neurons also appeared normal.

3.3.2 Ultrastructural Studies

To assess the ultrastructure of the stereocilia, scanning electron microscopy of the cochlear sensory epithelium of affected animals (n=3) and of unaffected littermates (n=2) was undertaken. The comparison revealed that although the stereocilia were present in both affected and unaffected mice, there was a difference seen in the appearance of the stereocilia **(Figure 3.3)**. The inner and outer hair cell stereocilia of affected mice appear shorter and have deposits on them compared to those of unaffected littermates. This is intriguing, but due to the small number of samples available for analysis conclusive assumptions cannot be drawn from these observations.

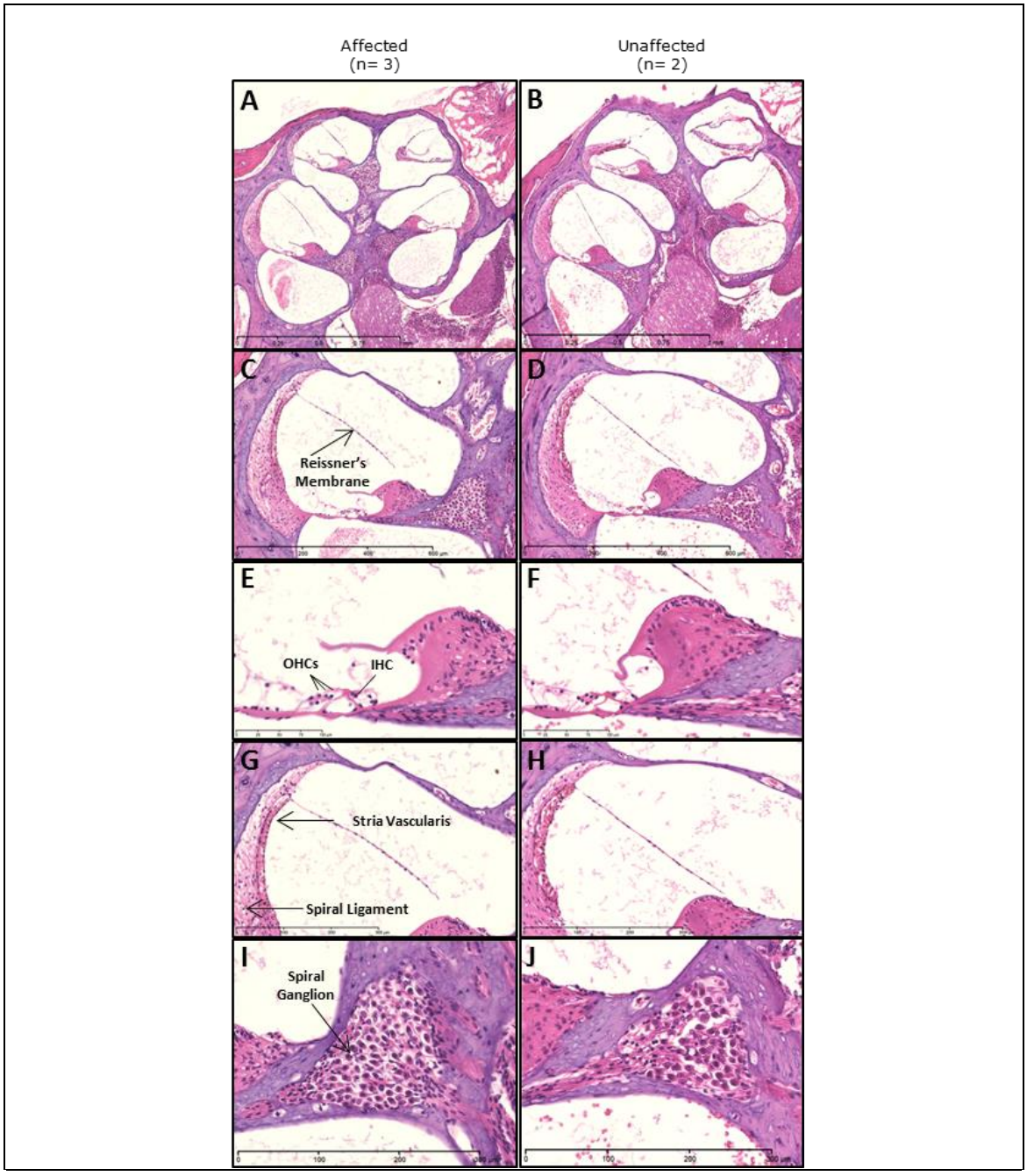

Figure 3.2: Histological analyses of the inner ear from affected (n=3) and unaffected (n=2) animals.
There were no gross morphological changes observed in the inner ear of affected [A] and unaffected animals [B]. Histological analysis of the basal turn also showed no dysmorphology of the inner ear of affected [D] and unaffected [D] animals. The gross morphology of the key structures in the inner ear that are important for auditory transduction also appeared to be normal. In particular, there are no differences in the morphology of the Reissner's membrane [C, D], organ of Corti [E, F], stria vascularis [G, H] and the spiral ganglion [I, J] of affected animals when compared with unaffected animals.
Scale bars represent 1mm (A and B), 600μm (C and D), 100μm (E and F) and 300μm (G-J).

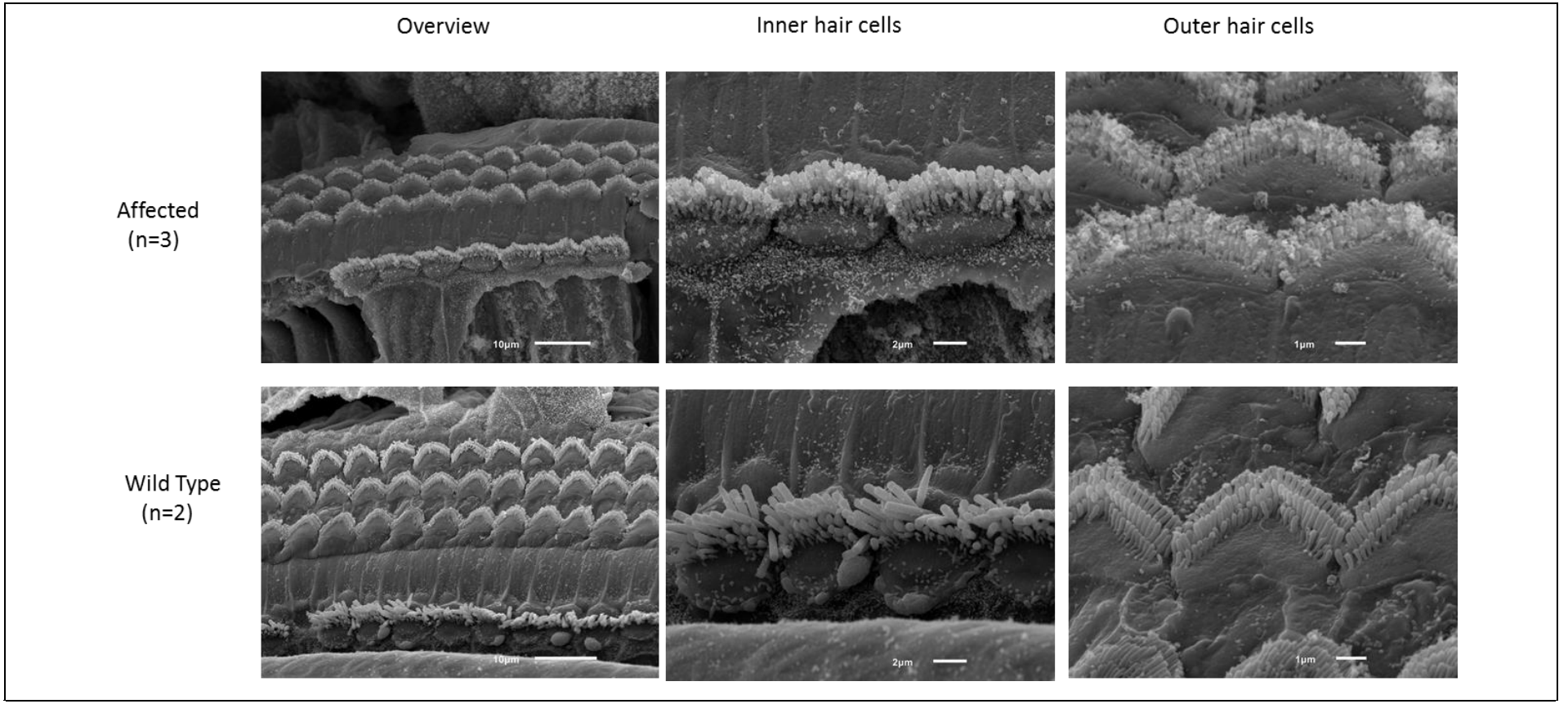

Figure 3.3: Scanning electron micrographs of hair cells from affected (n=3) and unaffected (n=2) MP90 animals
The gross overview of the hair cells shows no loss or gain of stereocilia in the affected animals when compared to the unaffected animals. Closer analysis of the inner and outer hair cells of affected animals show the presence of deposits which is not seen in the unaffected animals. In addition, the stereocilia of the affected animals appear to be shorter than that of the unaffected animals. However, owing to the number of animals analysed, this result should be viewed with caution.
Scale bars represent 10µm, 2µm and 1µm.

3.4 Discussion and Conclusion

MP90 was identified at nine months of age as a model of late onset hearing loss. Whole genome mapping and next generation sequencing were employed and six ENU-induced changes were found in the region of interest. Validation of these changes indicated that all five of the homozygous ENU-induced lesions identified by NGS were present; however, they are all outside of coding regions. The sequencing gaps have also been investigated, but so far no lesions have been identified. Importantly one of the sequencing gaps, yet to be successfully investigated, encompasses coding sequence and may prove to harbour the causative lesion.

Once this remaining coding gap is sequenced, if it does not contain the causative lesion, further study of the validated intronic and intergenic lesions will need to be undertaken. The intronic lesions should be assessed to see if they generate cryptic splice sites and both intronic and intergenic lesions should also be assessed to investigate if they lie in non-coding conserved regions, which could represent regulatory sequences.

MP90 is an interesting pedigree and in order to help with cloning of the underlying genetic lesion, the line would need to be rederived and additional mice bred to allow further phenotyping and mapping studies.

However, owing to the late-onset phenotype and the time constraints associated with mouse production, it was not feasible to continue with this project during my PhD. Sperm from the mice have been frozen and archived. It is hoped that MP90 will be interrogated in the further by myself or other

members of the team in order to elucidate the gene responsible for the phenotype observed.

For my PhD, I have concentrated my efforts entirely on the second pedigree of age-related hearing loss identified from the Harwell Ageing Screen: Muta-Ped-C3pde-96 (*trombone).*

Chapter 4

Identifying the Causative Mutation in Muta-Ped-C3Pde-96

4.1 Auditory phenotyping

Muta-Ped-C3Pde-96 (MPC96) underwent initial auditory screening as part of the Harwell Ageing Screen (Section 1.8.2). At nine months of age, seven mice were identified with significantly elevated ABR thresholds, most pronounced at 8 kHz and 32 KHz, when compared with wildtype littermates. Recurrent screening of this pedigree at 12 months of age indicated that the affected mice exhibit severe hearing loss and that the severity of hearing loss had progressed significantly from the thresholds observed at nine months of age **(Figure 4.1)**. In addition, there were still no apparent behavioural or vestibular phenotypes observed in the affected mice (i.e., head bobbing or circling). The ratio of impaired hearing to hearing animals was 7:25, which suggested that the phenotype was caused by a recessive mutation.

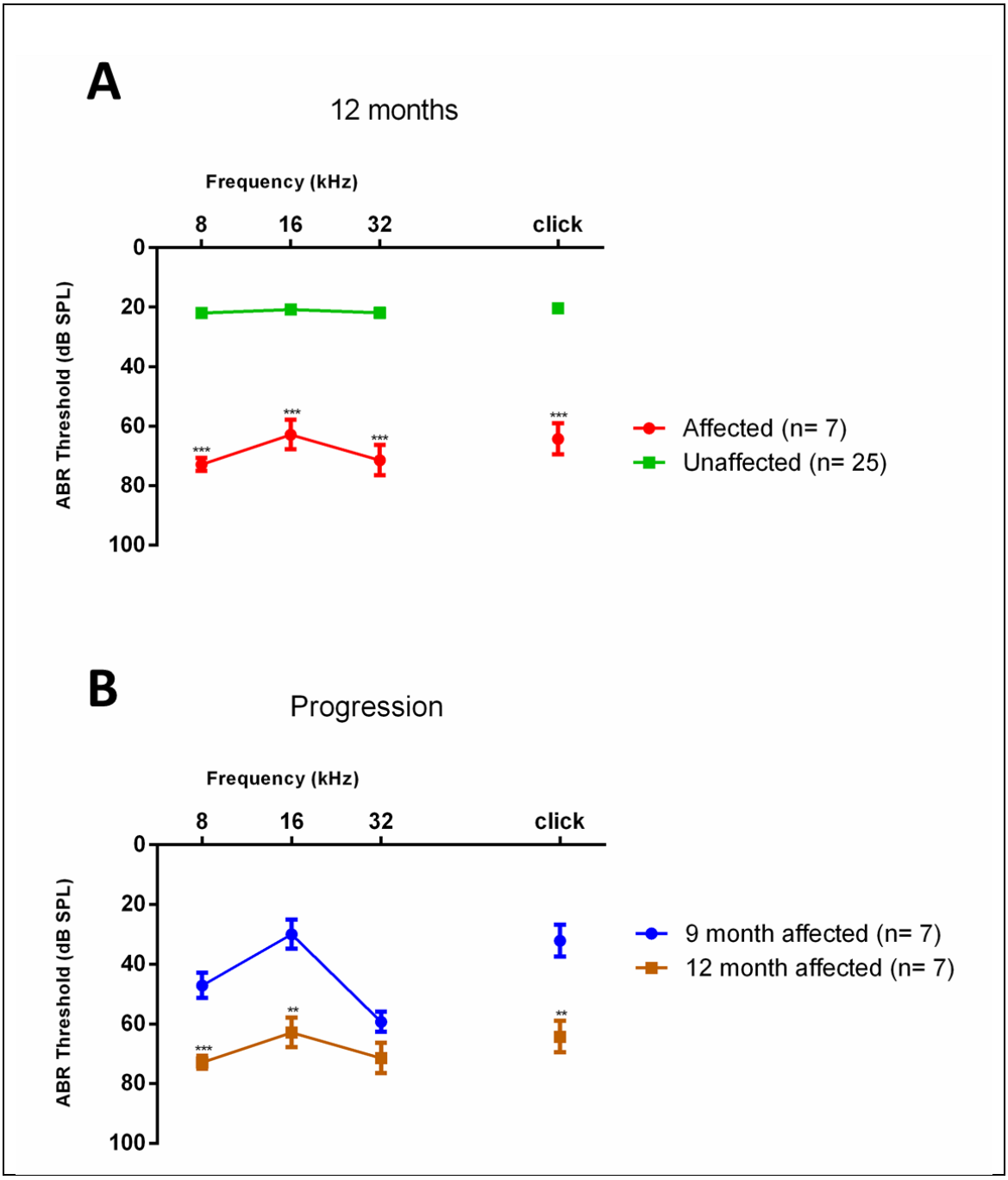

Figure 4.1: ABR thresholds of MPC96 mice at 12 months of age and the progression of hearing loss
[A] Average ABR thresholds at 12 months of age indicate that seven mice exhibit significantly elevated thresholds (**p<0.01, ***p<0.001) when compared to littermates (n= 25). [B] Comparison of the auditory threshold estimations obtained from affected mice at 9 months and 12 months of age. This shows significant progression of the hearing loss. Error bars indicate standard error of mean.

4.2 Identifying the Causative Mutation in MPC96

4.2.1 Mapping

To elucidate the location of the underlying genetic lesion responsible for the phenotype observed in MPC96, DNA from affected (n=7) and unaffected animals (n=3) were sent to Tepnel Life Sciences for whole genome single nucleotide polymorphism (SNP) mapping. This highlighted a region of interest on chromosome 2: 51321215- 114205619 (NCBIM37). This region of 63 megabases (Mb) contains 936 genes.

Known SNP markers informative for the parental strains (B6J and C3H.pde6b^{+}) were identified and used to narrow down the candidate interval to approximately 12.5 megabases, 2: 51428003-63920418 **(Figure 4.2 and Figure 4.3)**.

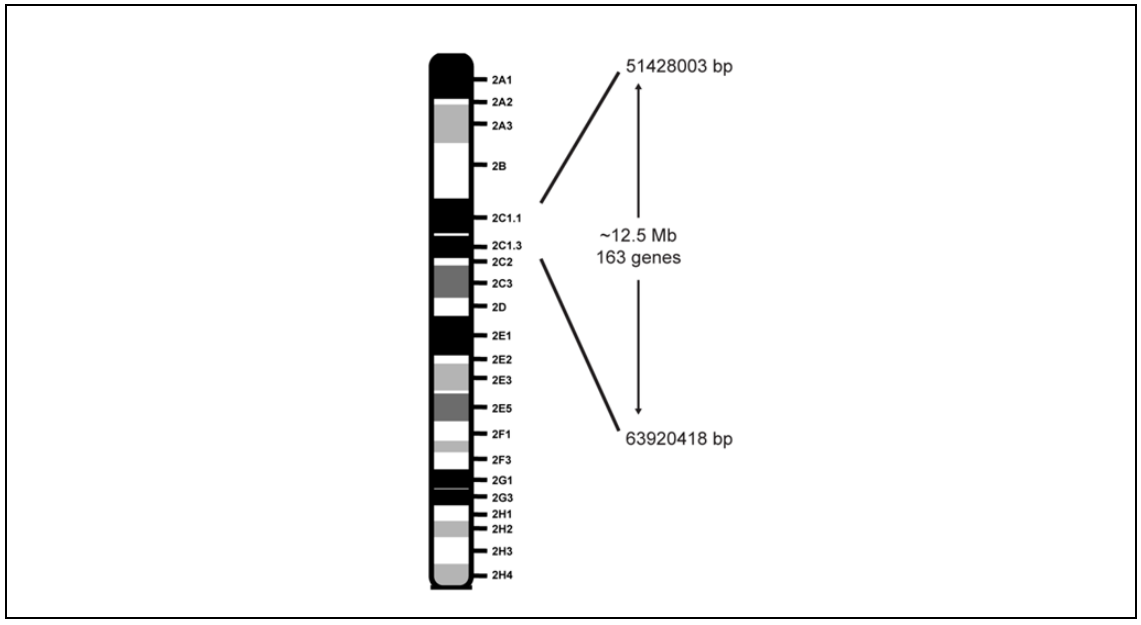

Figure 4.2: Critical region of interest of chromosome two
Whole genome mapping and subsequent fine mapping using SNPs polymorphic between the two parental lines identified a region of interest on chromosome 2 (51428003bp-63920418bp), containing 163 genes.

4.2.2 Next Generation Sequencing

The narrowed interval contains 163 genes, and so in order to identify the underlying genetic lesion, Next Generation Sequencing was undertaken. DNA from the founder G1 male animal was prepared and sent to the High Throughput Genomics Facility at the Wellcome Trust Centre for Human Genetics, Oxford, for whole genome sequencing using the Illumina Hi Seq platform. Analysis of the NGS data identified 16 ENU-induced nucleotide changes in the region of interest (2:51428003-63920418). In addition, the candidate region contained seven sequencing gaps in total.

	Chromosome 2					
Mouse ID	**51428003**	**53189457**	**55238068**	**56388227 (rs3718711)**	**62106906 *(Slc4a10)***	**63920418**
2.3e	B6	B6	B6	B6	C/C	B6
2.3i	B6	B6	B6	B6	C/C	B6
2.5a	B6	B6	B6	B6	C/C	B6
2.2e	Het	B6	B6	B6	C/C	B6
2.2f	Het	B6	B6	B6	C/C	B6
2.2g	Het	B6	B6	B6	C/C	B6
5.5c	Het	B6	B6	B6	C/C	Het
2.2c	C3	Het	Het	Het	T/C	Het
2.3h	C3	C3	C3	C3	T/T	C3
2.3c	C3	C3	C3	C3	T/T	C3

Figure 4.3: The narrowed MPC96 candidate interval contains one high confidence NGS identified ENU-induced lesion
The smallest region of C57BL/6J homozygosity (B6) common to all affected animals (red text) was observed between SNPs 51428003 and 63920418. All affected mice are homozygous for the c.1940T>C ENU-induced lesion within the *Slc4a10* gene (ENMUST00000102735). Conversely, the unaffected mice (black text) were either heterozygous or wildtype for the ENU induced lesion within the *Slc4a10* gene.

4.2.3 Validating the ENU Lesions

Of the 16 NGS-identified ENU-induced changes, one attained a high quality score **(Table 4.1)**. A higher 'read depth' or 'coverage' and a change in sequence that is observed in a number of reads, will obtain a higher quality score, whereas a variant that is only observed in one read will gain a low quality score and likely represents a sequencing error rather than a true sequence change.

The high quality score identified was a non-synonymous coding change within the mapped interval, consisting of a T-to-C transition at nucleotide 1940 of the *Solute carrier family 4, sodium bicarbonate cotransporter-like, member 10* gene (*Slc4a10* - ENSMUST00000112480) causing a leucine-to-proline substitution at residue 647 of the encoded protein. The presence of this lesion was confirmed using Sanger sequencing **(Figure 4.4)**.

Table 4.1: High confidence ENU-induced lesion identified by NGS

Location on Chr 2 (Ensembl build NCBIM37)	Reference	Change	Quality Score	Gene	Amino Acid Change
62106906	T	C	426.96	*Slc4a10*	L647P

The NGS results highlighted one high confidence ENU-induced nucleotide change, causing a T>C change in *Slc4a10*, within the candidate interval.

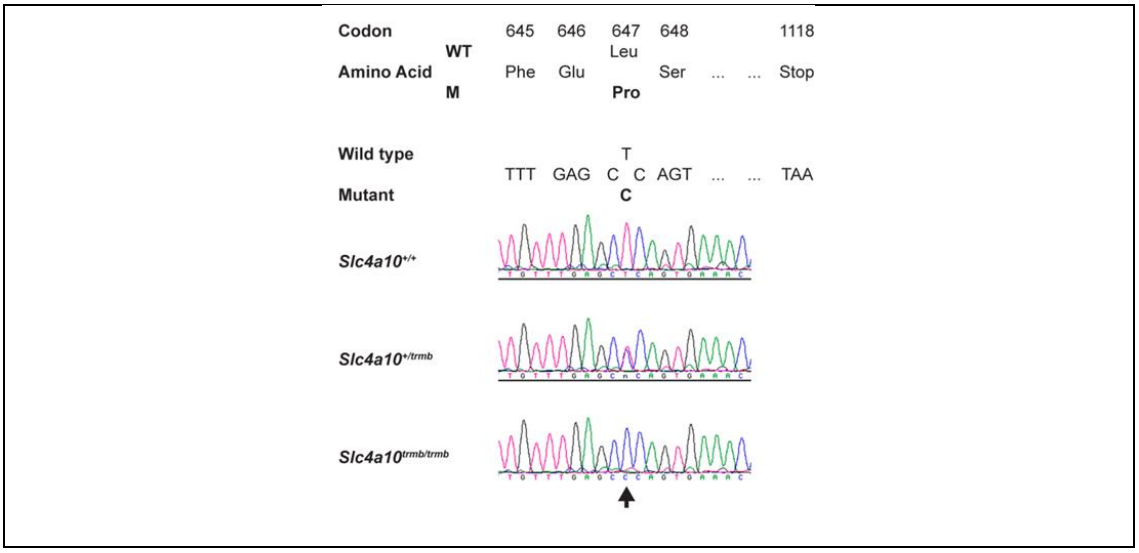

Figure 4.4: Confirmation of the presence of an ENU-induced lesion in *Slc4a10*
Whole-genome sequencing identified a T>C changing at nucleotide 1940 of the gene *Slc4a10*. The presence of this change was confirmed using Sanger sequencing.

The L647 residue is within the transmembrane helices coding domain of the protein, and although not within a helix motif it is conserved across species **(Figure 4.5)**. The human orthologue of mouse Slc4a10 is highly conserved at 98% identity.

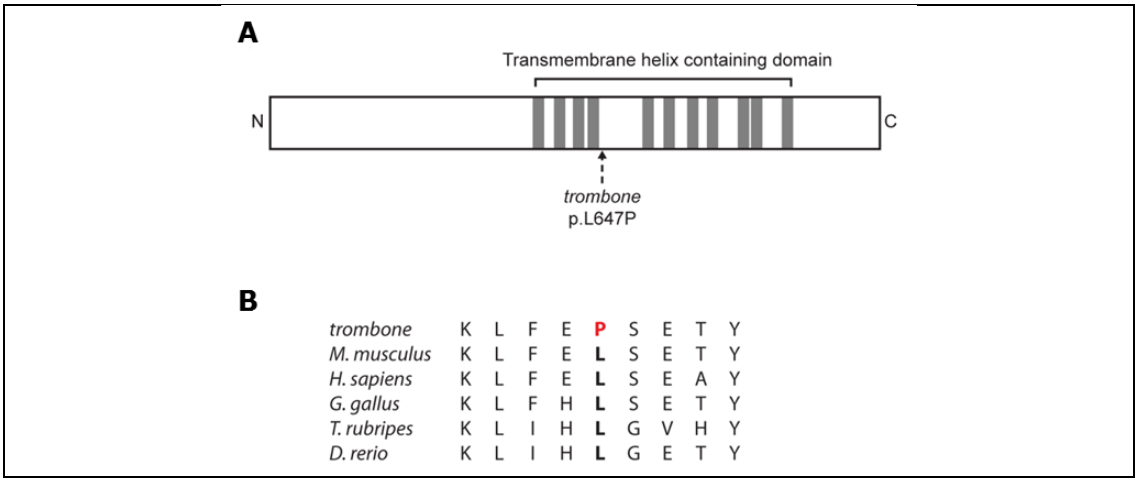

Figure 4.5: Location of the L647 residue and its conservation across species
[A] The L647 residue identified in MPC96 was within the transmembrane domain of the Slc4a10 protein. [B] Comparison of the region around the mutation shows high sequence conservation across species.

4.2.4 *in silico* analysis

In order to assess the effect of the amino acid substitution, resulting from the ENU-induced change, within the Slc4a10 protein, web-based protein prediction software was used - SIFT (Sorting Intolerant from Tolerant), Polyphen-2 and PROVEAN. The software predicted that the Slc4a10 mutation would affect protein function **(Table 4.2).**

Table 4.2: Protein prediction of the Slc4a10 mutation

	SIFT		Polyphen-2		PROVEAN	
	Score	**Prediction**	**Score**	**Prediction**	**Score**	**Prediction**
Slc4a10 (L647P)	0.01	Affect protein function	1.00	Probably Damaging	-4.709	Damaging

Web based protein prediction software (SIFT, Polyphen-2 and PROVEAN) predicted that the *Slc4a10* nucleotide change was likely to affect protein function.

4.3 Analysis of Terminal Tissues

The MPC96 pedigree was also recurrently phenotyped by other groups as part of the Harwell Ageing Screen and therefore, tissues could not be harvested at different time points. However, tissues were collected at 12 months of age for analysis. This mouse line was subsequently renamed as *trombone (trmb)*.

4.3.1 Expression on Slc4a10 in the inner ear

In order to determine the expression of Slc4a10 within the inner ear, immunolabelling of mid-modiolar sections of the cochlea was undertaken. Sections prepared from homozygous, heterozygous and wildtype mice were used to analyse the expression pattern of Slc4a10 **(Figure 4.6)**. Wildtype (n=1) and heterozygous (n=2) animals showed expression of Slc4a10 in the spiral ligament with increased expression in the type II and type V fibrocytes. However, homozygous (n=5) animals showed no immunoreactivity. In addition, there was no Slc4a10 expression observed in the organ of Corti, Reissner's membrane or the stria vascularis across all three genotypes.

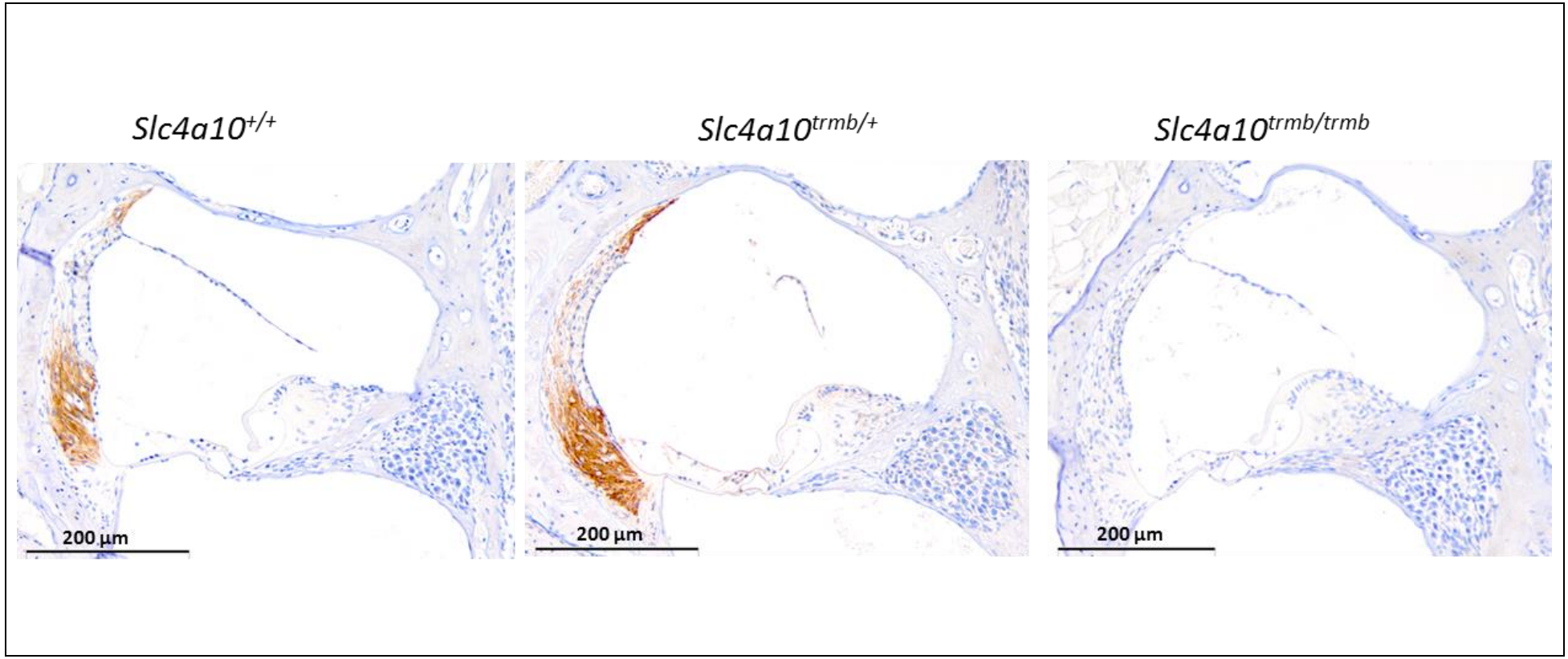

Figure 4.6: Immunolabelling with an anti-Slc4a10 antibody
At 12 months of age, the distribution of the Slc4a10 gene product in wildtype, (*Slc4a10*$^{+/+}$) and heterozygotes *(Slc4a10*$^{trmb/+}$) animals appears to be localised to the type II and V fibrocytes of the spiral ligament. In homozygous (*Slc4a10*$^{trmb/trmb}$) animals, no Slc4a10 expression was observed. Magnification x20.

4.3.2 SEM Analysis of the Hair Cells

To assess the ultrastructure of the cochlear sensory epithelium, scanning electron microscopy of the inner ear was undertaken. This showed that wildtype (n=4) and heterozygous (n=11) mice exhibited no dysmorphology (**Figure 4.4** and data not shown) of the hair cells throughout all turns of the cochlea. However, animals which were homozygous for the *Slc4a10* mutation (n=9) showed significant loss of hair cells (outer and inner), which was most pronounced in the basal and apical regions of the cochlea **(Figure 4.7)**.

4.3.3 Gross Histological Analysis

To assess for gross morphological changes within the inner ear, histological mid-modiolar sections were prepared. Sections from mice homozygous for the *Slc4a10* mutation (n=5) were compared to those from wildtype (n=1) and heterozygous (n=2) mice **(Figure 4.8)**. Results showed no gross dysmorphology of the inner ear. The organ of Corti and the hair cells also appeared normal. The Reissner's membrane and spiral ganglion neurons also appeared normal. However, mice homozygous for the *Slc4a10* mutation appeared to have a thinner stria vascularis.

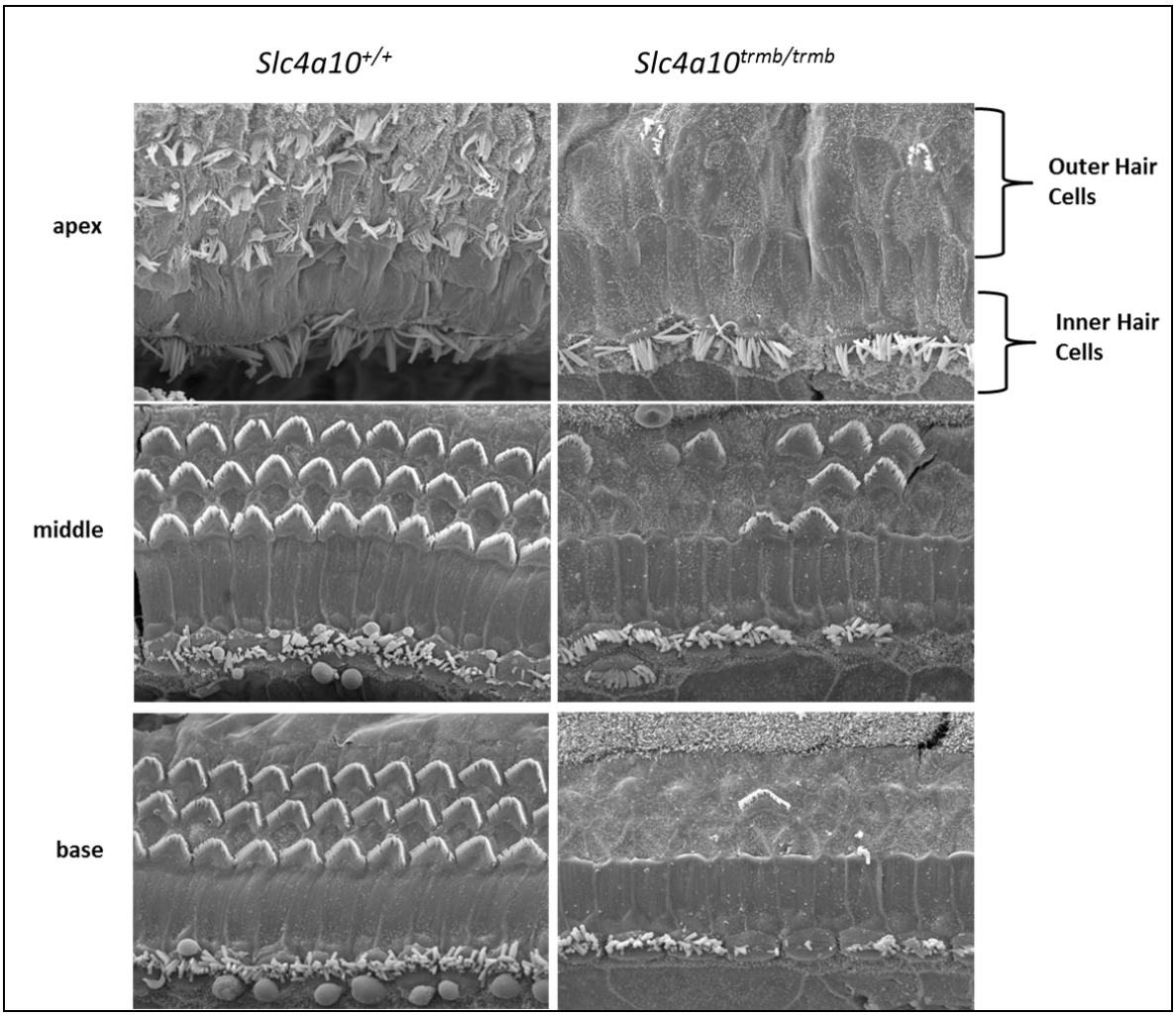

Figure 4.7: Scanning electron micrograph of *Slc4a10*$^{+/+}$ and *Slc4a10*$^{trmb/trmb}$ hair cells
At 12 months of age, *Slc4a10*$^{trmb/trmb}$ animals (n=9) exhibited significant hair cell loss throughout the cochlea in comparison to *Slc4a10*$^{+/+}$ (n=4) animals, with the greatest loss observed in the apical and basal regions of the cochlea. Magnification x 2500.

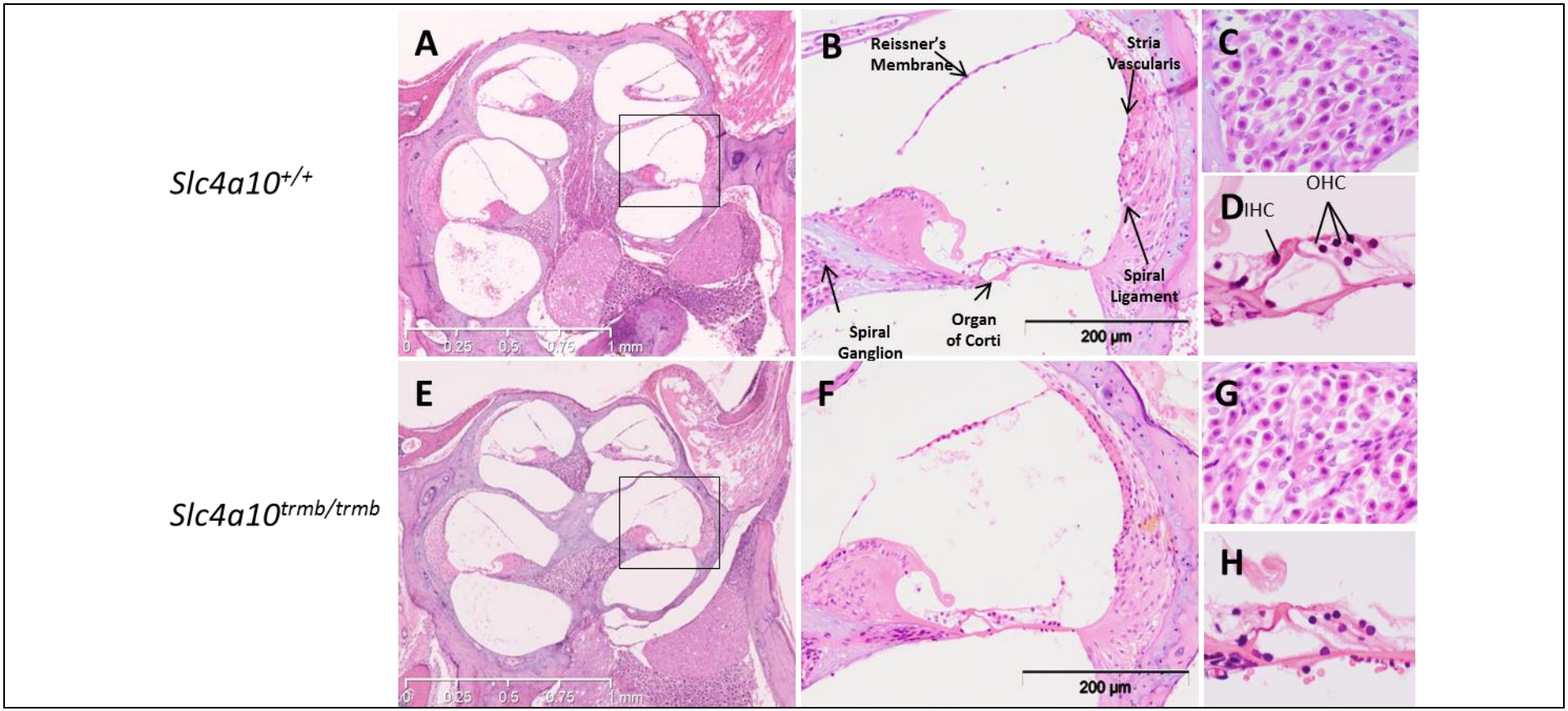

Figure 4.8: Gross morphology of 12 month old *trombone mice*
The gross morphology of the inner ear of *Slc4a10*$^{trmb/trmb}$ animals (E) appear to be normal when compared with *Slc4a10*$^{+/+}$ animals (A). The organ of Corti and Reissner's membrane did not exhibit any dysmorphology (B and F). The neurons present in the spiral ganglion also appeared normal and similar density (C and G). The hair cells within the organ of Corti did not show any signs of dysmorphology (D and H). However, the stria vascularis of *Slc4a10*$^{trmb/trmb}$ animals did appear to be thinner than that of *Slc4a10*$^{+/+}$ animals. Magnifications: A and E x2.5; B and F x20; C, D, G and H x100

4.4 Discussion and Conclusion

MPC96 (*trombone*) has been identified as a model for presbycusis. It was identified at nine months of age exhibiting elevated auditory thresholds across all frequencies tested, with the severity of the hearing loss progressing with age.

Ultrastructural studies have shown significant hair cell loss, which was most pronounced in the basal and apical regions of the cochlea, corresponding to the regions that detect sound of high and low frequency, respectively. These data are consistent with the auditory threshold data, with high and low frequencies being the most affected, compared to the mid frequency, which is detected by the mid-cochlear hair cells.

As the study undertaken was a phenotype driven screen, the main aim was to elucidate the gene responsible for the observed auditory phenotype. Whole genome mapping and next generation sequencing identified one coding mutation within the candidate gene *Slc4a10*. *In silico* studies indicates that the resulting amino acid substitution in the Slc4a10 protein is likely to affect function.

4.4.1 *Slc4a10*

Slc4a10 is a member of the solute carrier 4 (SLC4) group of membrane transporter proteins which play an important role in maintaining intracellular pH. The regulation of cellular pH is attributed to the balance of acid loaders and acid extruders which controls the direction of bicarbonate (HCO_3^-) transport. In total, there are ten such transporters including, five Na^+

coupled HCO_3^- transporters (NCBTs) **(Figure 4.9)** and three Na^+ independent $Cl^-HCO_3^-$ exchangers (Boron et al., 2009) .

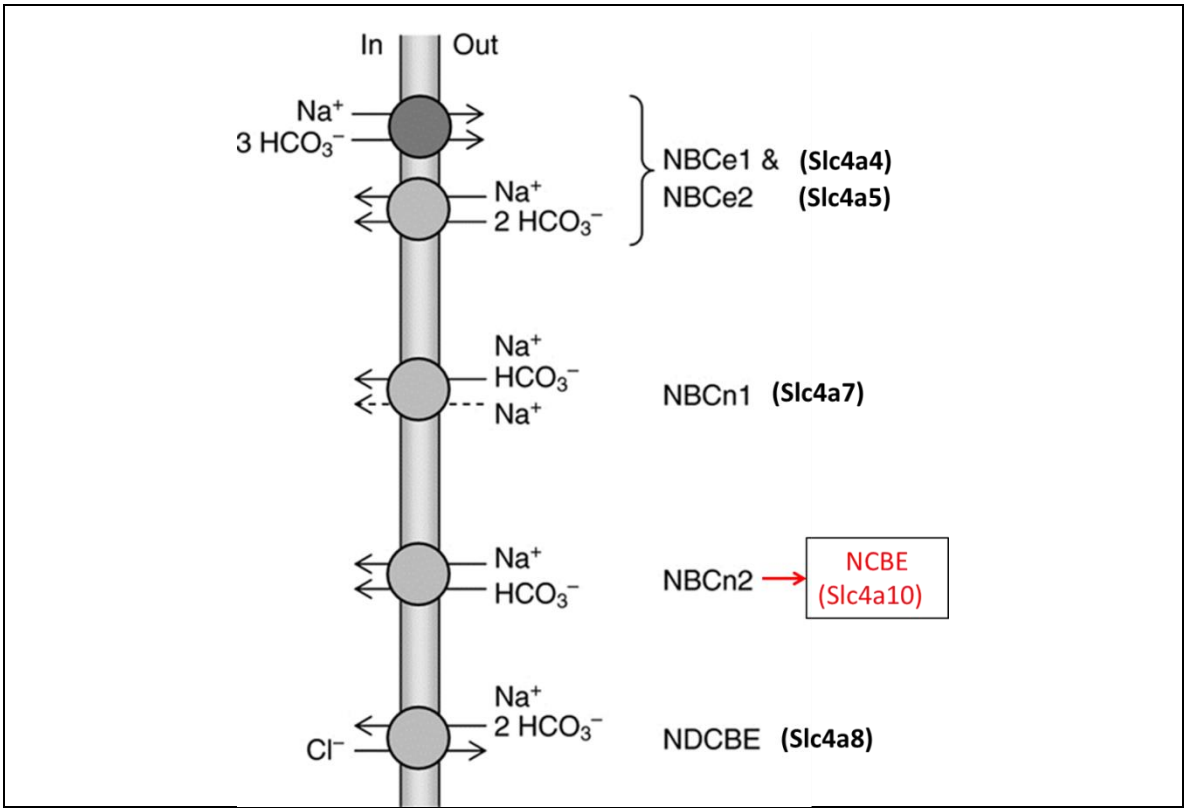

Figure 4.9: There are five Na^+ coupled HCO_3^- transporters in the Slc4 family. There are five NCBTs in the Slc4 family. Slc4a10 is also known as NBCn2 or NCBE. *Adapted from* (Boron et al., 2009)

One of the five NCBTs in the Slc4 family is Slc4a10. Slc4a10 functions by transporting bicarbonate into the cell and was originally classed as a Na^+ driven Cl^-/HCO_3^- exchanger and referred to as NCBE (Na-driven chloride/bicarbonate exchanger) (Wang et al., 2000). However, further studies showed that the intracellular pH is not attributable to the bicarbonate transport alone but to the transport of Na^+, HCO_3^- and Cl^- ions. It was later proposed that the mechanism of Slc4a10 was to function as a Na^+/HCO_3^- co-transporter which is not dependant of Cl^- (Giffard et al., 2003). Therefore,

the protein was classed as an NBCn2 (Na-bicarbonate co-transporter, electroneutral 2). However, more recently, studies have confirmed that *Slc4a10* functions as a Na^+ dependant Cl^-/HCO_3^- exchanger and should therefore remain classed as a NCBE (Damkier et al., 2010). NCBEs in general function by the co-transport of Na^+ with HCO_3^- in exchange for Cl-. This net transport is therefore electroneutral (Parker et al., 2008).

The *Slc4a10* gene produces four splice variants (NBCn2-A to –D) **(Figure 4.10)**. The mutation identified in Slc4a10 is a leucine to proline change which is located between transmembrane domains 4 and 5. This region is common to all four splice variants, and therefore the mutation will be present in all isoforms.

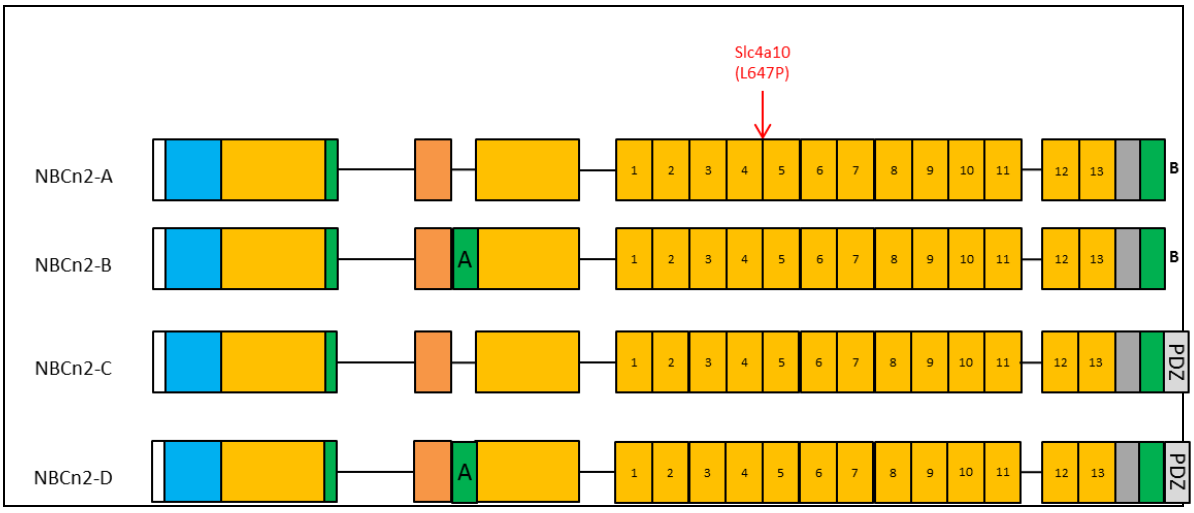

Figure 4.10: Splice variants of Slc4a10. There are four different splice variants of *Slc4a10* (NBCn2 A to D). Variants A and B contain the splice cassette B, whereas variants C and D contain the PDZ-binding motifs (PDZ) instead of this cassette. Variant B and D in addition contain the splice cassette A. *Adapted fr*om (Boron et al., 2009).

To-date research has shown that *Slc4a10* is widely expressed throughout the brain and the choroid plexus (Giffard et al., 2003, Liu et al., 2011, Jacobs et al., 2008, Chen et al., 2008, Praetorius et al., 2004, Hubner et al., 2004, Chen et al., 2007). More recent studies have also shown strong expression in both plexiform layers of the retina (Hilgen et al., 2012). However, the expression of *Slc4a10* in the inner ear has not been studied and hence has not been associated with deafness. Neurological studies conducted on *Slc4a10* knockout mice have not included any complex auditory phenotyping methods.

4.4.2 Role of the Spiral Ligament in the Inner Ear

The fibrocytes are components of the spiral ligament which is pivotal in generating the endocochlear potential. This is achieved by controlling the levels of $[K^+]$ in the endolymph. The influx of $[K^+]$ into the endolymph generates the endocochlear potential (EP) which is crucial for the transduction of sound (Hudspeth, 1997). Absence or disruption of the fibrocytes will therefore lead to poor sound transduction and thus, hearing loss.

It is known that the type II and IV fibrocytes in the spiral ligament express two K^+-uptake transporters: Na^+,K^+-ATPase and $Na^+,K^+,2Cl^-$ -cotranporter (NKCC1). Studies have shown that both transporters contribute to the EP by transporting K^+ from the perilymph into the fibrocytes across their membrane (Hibino et al., 2010). The K^+ is then taken up by the fibrocytes and moves through the gap junctions of the basal and intermediate cells to the apical surface of the stria vascularis. Disruption of these K^+ transporters

have been shown to drastically suppress the EP, leading to hearing impairment (Hibino et al., 2010).

Results obtained show that *Slc4a10* is expressed in the type II and type V fibrocytes of heterozygous and wildtype animals. There was no expression observed in the homozygous mice, which is slightly surprising as the *trombone* mutation is a missense mutation and therefore would have expected to observe production of a full-length mutant protein. Endocochlear potential measurements in *trombone* mice will help to assess the consequence of the $Slc4a10^{trmb}$ allele on cochlear fibrocyte function.

4.4.3 Future Work and Conclusion

trombone is a model of presbycusis, investigation of which has identified *Slc4a10* as a novel deafness gene. Given the expression of *Slc4a10* in the lateral wall of the cochlea, it is possible that *trombone* is a model of strial presbycusis. There are currently no mouse models for strial presbycusis. To fully elucidate the requirement of this protein within the ageing auditory apparatus, further functional characterisation studies need to be undertaken. In addition, a longitudinal study needs to be conducted across several time points in order to identify the onset of the phenotypes established.

Chapter 5

Phenotypic Characterisation of *trombone*

The *trombone* model was identified from the Harwell Ageing Screen as exhibiting elevated ABR thresholds at nine months of age, which progressed with age. The underlying genetic lesion was mapped and next generation sequencing identified a coding change in the gene *Slc4a10*. At twelve months of age initial SEM analysis showed degeneration of cochlea hair cells, whilst expression studies showed a uniform pattern of expression of Slc4a10 in the cochlear lateral wall of heterozygous and wildtype mice. However, there was no immunoreactivity observed in homozygous mice.

These initial experiments were conducted on mice involved in the Harwell Ageing Screen and therefore were limited in terms of when the experiments could be conducted and when the tissues could be harvested. To allow a full phenotypic characterisation of the *trombone* model, additional mice were bred and longitudinal studies undertaken.

5.1 Longitudinal Studies

Studies were undertaken to fully explore the phenotypes observed in the initial studies. Importantly, I wanted to establish the onset and progression of the identified phenotypes.

5.1.1 Onset and Progression of Hearing Loss

The *trombone* model was first identified in the Harwell Ageing Screen at 9 months of age with seven out of 32 animals exhibiting elevated ABR thresholds. In order to obtain a complete picture of auditory decline in the *trombone* mice, a longitudinal auditory assessment was undertaken at two, six, nine and twelve months of age. Results obtained show that at two and six months of age, the homozygous mice have very similar ABR thresholds to that of wildtype and heterozygous littermate mice (between the ranges of 20-40 dB) with only a slight elevation of 5 dB seen in homozygous mice **(Figure 5.1 A-B)**. However, at nine months of age, homozygous mice display a 15-20 dB elevation in ABR thresholds across all frequencies tested. This increase progresses further by 12 months of age with homozygous mice exhibiting a 30 dB elevation in ABR thresholds at all frequencies tested in comparison to wildtype and heterozygous littermate mice **(Figure 5.1 C-D)**.

The heterozygous and wildtype mice display very similar ABR thresholds (between the ranges of 20-45 dB) at all ages tested. There was no auditory deficit observed in the heterozygous mice demonstrating that the *trombone* hearing loss phenotype is recessively inherited.

The progression of hearing loss in *Slc4a10*$^{trmb/trmb}$ mice was analysed and showed that for the majority of frequencies tested, the ABR thresholds at two and six months of age fall within the running mean for ABR thresholds, calculated from all mice tested in the Harwell Ageing Screen. However, mice homozygous for the *Slc4a10*^{trmb} allele begin to lose hearing between six and nine months of age and this decline continues between nine and 12 months of age **(Figure 5.2)**.

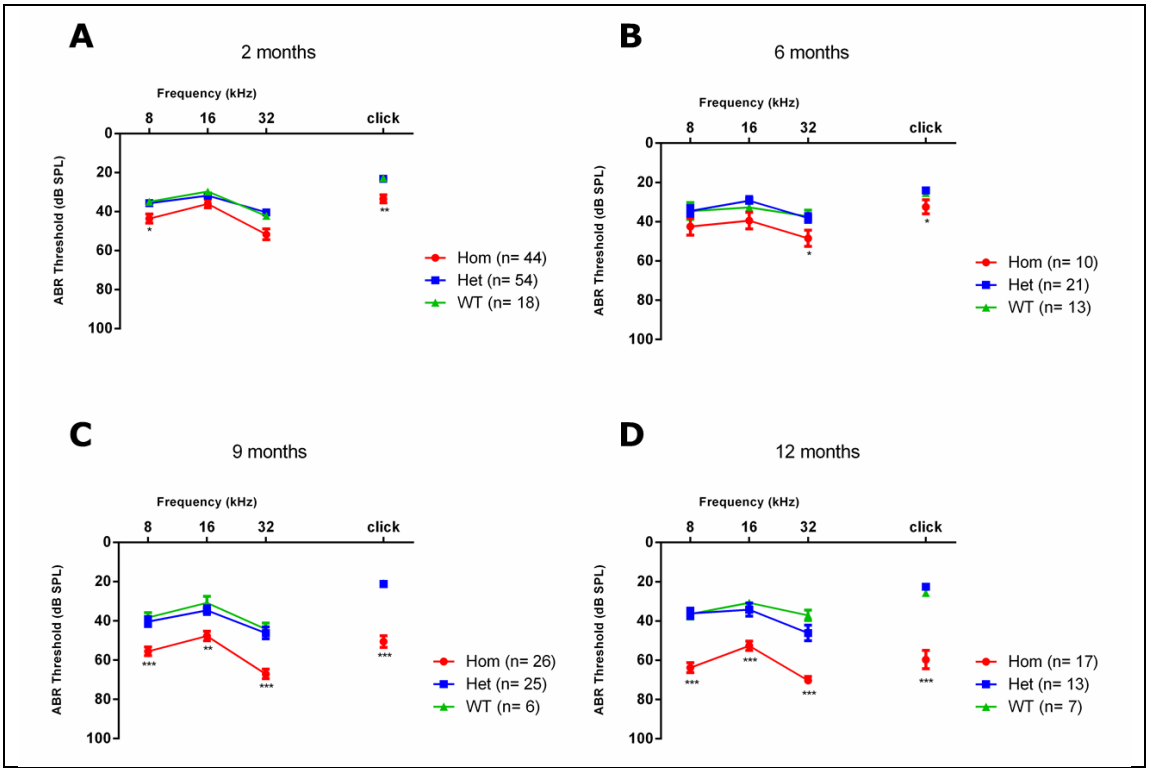

Figure 5.1: Longitudinal ABR assessment of *trombone* mice at two, six, nine and 12 months of age. [A] Results show that at 2 months of age, homozygous mice (n=44) only show a subtle elevation in ABR thresholds in comparison to heterozygous (n=54) and wildtype (n=18) littermates. [B] By 6 months of age, the ABR thresholds of the homozygous animals (n=10) are still mildly elevated in comparison to heterozygous (n= 21) and wildtype (n= 13) littermates but as with the 2 month data, the auditory phenotype is very subtle. [C] However, at 9 months of age, the homozygous animals (n= 33) show significantly elevated ABR thresholds at each frequency tested in comparison to heterozygous (n=44) and wildtype (n=15) littermates. [D] A significant elevation in ABR thresholds at each frequency tested is also observed at 12 month of age. (*p<0.05, **p<0.01, ***p<0.001). Error bars indicate standard error of mean.

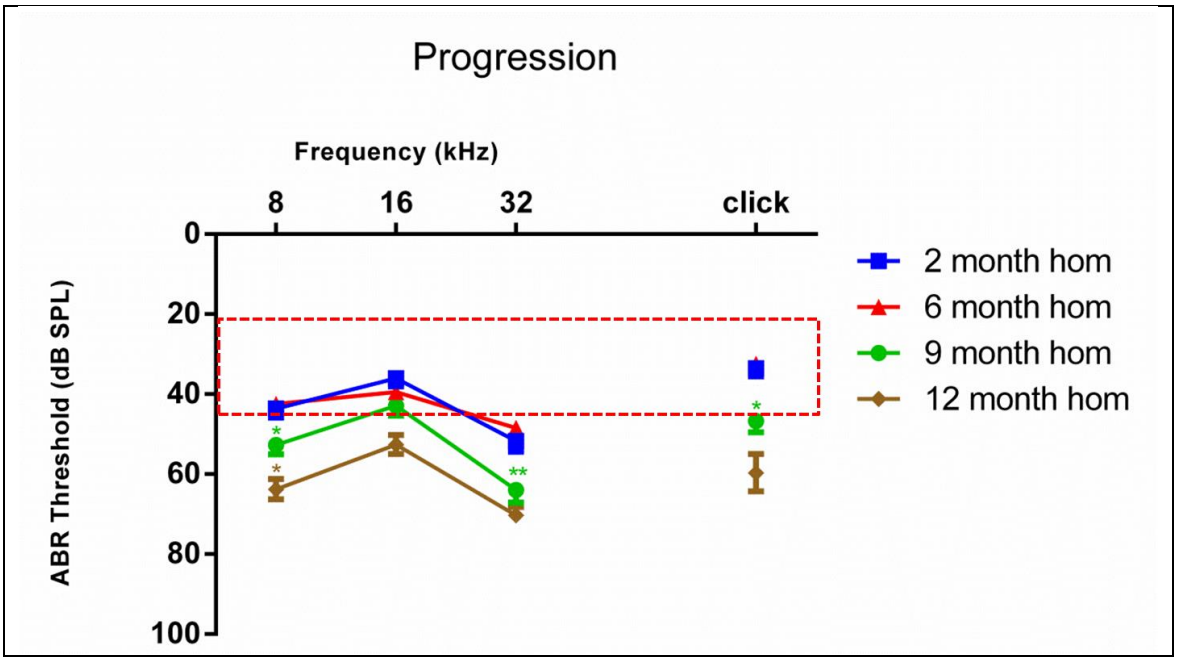

Figure 5.2: The progression of hearing loss in *Slc4a10*$^{trmb/trmb}$ mice. Results indicate that only a subtle auditory phenotype was observed at two months of age (n=44). The ABR thresholds do not increase significantly between two and six months (n=10) of age. However, the ABR thresholds significantly increase between six and nine months (n=26) of age and continue to increase between nine and 12 months (n=17) of age. N.B. Red dotted bar indicates normal hearing threshold of mice in the Harwell Ageing Screen. (*p<0.05, **p<0.01). Error bars indicate standard error of mean.

5.1.2 Ultrastructural Studies

Initial ultrastructural studies at 12 months of age showed dysmorphology of the hair cells. To understand the fate of the sensory hair cells in the cochlea as a result of the *trombone* mutation in *Slc4a10*, a longitudinal study was undertaken at two, six, nine and 12 months of age.

5.1.2.1 SEM Analysis of Hair Cells

Scanning electron microscopy was used to study the morphology of the stereocilia across all turns of the cochlear spiral (apex, mid and base) **(Figure 5.3)**. The results obtained followed the same trend as was seen with the ABR data. At two and six months of age, the outer and inner hair cells of homozygous mice are intact and look very similar to that of heterozygous and wildtype littermates **(Figure 5.3 A-B)**. There are three rows of outer hair cells and one row of inner hair cells. The outer hair cell stereocilia are arranged in "V" shaped bundles with several rows of stereocilia arranged in increasing height, forming the expected "staircase" pattern.

However, at nine months of age, there is significant degeneration of hair cells (both outer and inner) throughout all the turns of the cochlea in homozygous mice **(Figure 5.3C)**. No cell loss is identified in wildtype and heterozygous littermates **(Figure 5.3C)**. The degeneration appears to progress by twelve months of age, with further cell loss apparent in the homozygous mice **(Figure 5.3D)**. This loss of outer hair cells was not restricted to one particular cochlear turn and affected all three rows of outer hair cells.

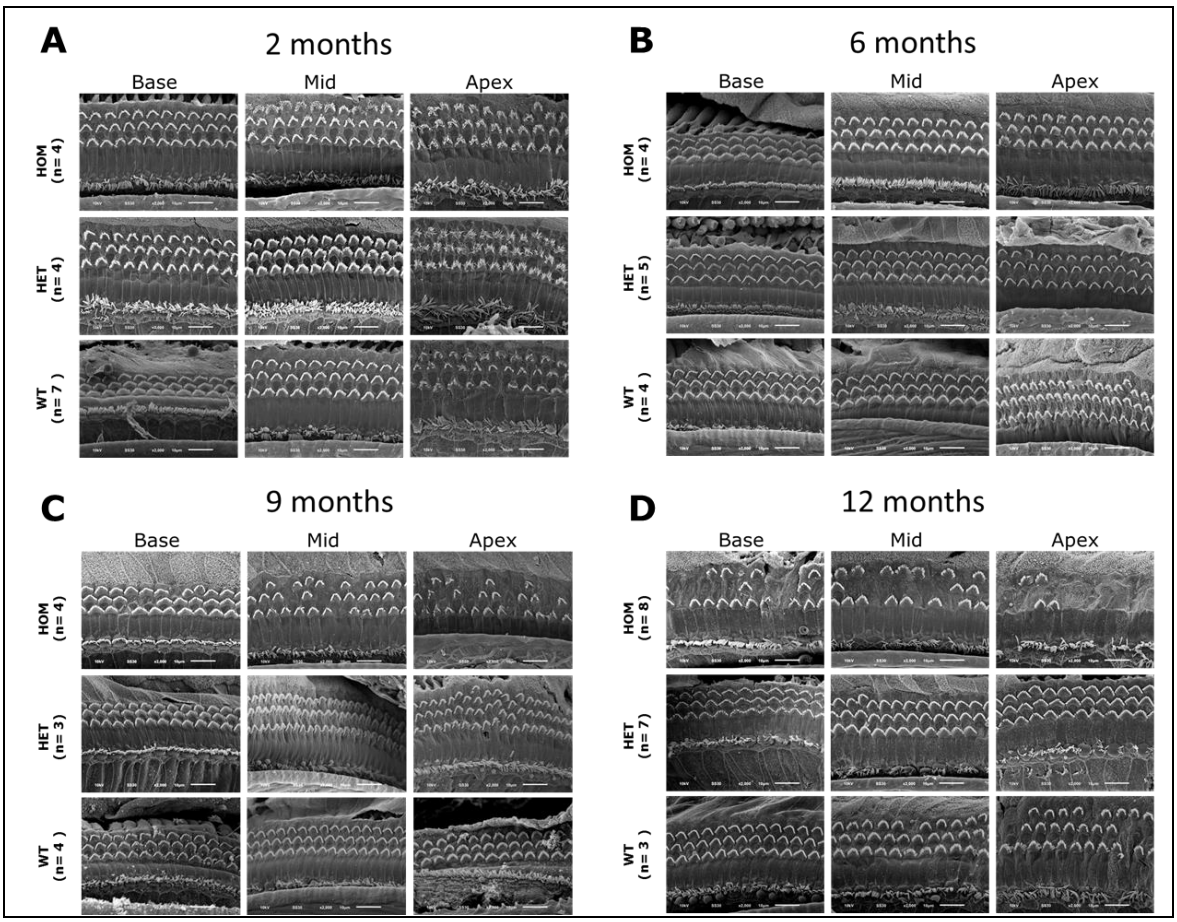

Figure 5.3: Longitudinal ultrastructural studies of the hair cells. [A] At two months of age, the hair cells of *Slc4a10*$^{trmb/trmb}$ animals (n= 4) showed no dysmorphology in comparison to heterozygous (n= 4) and wildtype (n= 7) animals. [B] This trend is further seen at six month of age were homozygous mice (n= 4) have a similarly morphology of hair cells to heterozygous (n= 5) and wildtype (n=4) mice. [C] At nine months of age however, homozygous mice (n= 4) show loss of outer hair cells whereas the hair cells of heterozygous (n= 3) and wildtype (n= 4) mice remain intact. [D] This phenotype is further exacerbated at 12 months of age where there is significant hair cell loss seen in *Slc4a10*$^{trmb/trmb}$ animals (n= 3) animals. The hair cell of heterozygous (n= 7) and wildtype (n= 3) mice at this age remained intact. Magnification x2000. Scale bar = 10μm

5.1.2.2 Hair Cell Counts

Quantification of hair cell number, by counting outer hair cells adjacent to 10 pillar cells, was used to assess the scanning electron micrographs from the ultrastructural studies. At two and six months of age, the *trombone* mice do not show loss of cochlear sensory hair cells **(Figure 5.4 A-B)**. However by nine months of age, there is a 25-50% reduction in the number of outer hair cells in homozygous mice when compared to their wildtype and heterozygous littermates **(Figure 5.4C)**. By 12 months of age, there appears to be further degeneration, with a 50-75% reduction in the number of outer hair cells in homozygous mice **(Figure 5.4 D)**. The loss of hair cells is most pronounced at the apical region of the cochlea, however there is loss seen throughout all turns of the cochlea.

The progressive loss of outer hair cells in the *Slc4a10*$^{trmb/trmb}$ mice is contemporaneous with the elevated ABR thresholds observed in *Slc4a10*$^{trmb/trmb}$ mice. In the *Slc4a10*$^{trmb/trmb}$ animals **(Figure 5.5A)** there is no difference in the number of hair cells between two and six months of age. However there is a 40% reduction in the number of outer hair cells between six and nine months and a further 60% reduction between nine and 12 months of age. This is observed throughout all turns of the cochlea. Conversely, there was no change in the total number of hair cells in heterozygous **(Figure 5.5B)** and wildtype **(Figure 5.5B)** mice at any age and throughout the cochlea.

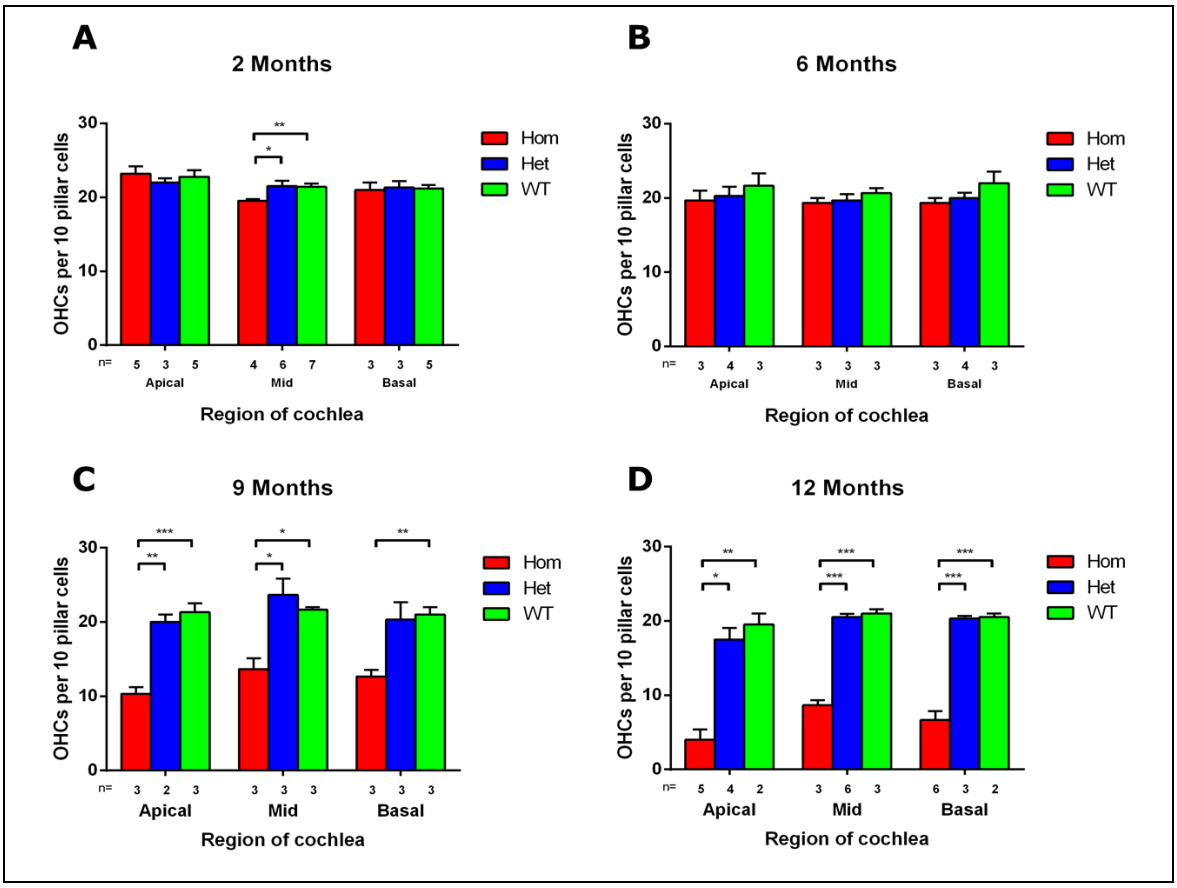

Figure 5.4: Quantification of outer hair cells throughout the cochlear. Quantification of the outer hair cells at two [A] and six months of age did not show a gross difference in the number of hair cells between the different genotypes. Examination at nine months of age [C] however showed significant degeneration in the number of outer hair cells in homozygous mice when compared to wildtype and heterozygous littermates. This degeneration also appears to progress further at 12 months of age [D] with homozygous mice exhibiting a significant reduction in the number of outer hair cells when compared to wildtype and heterozygous littermates throughout all turns of the cochlear. (*p<0.05, **p<0.01, ***p<0.001) Error bars indicate standard error of mean.

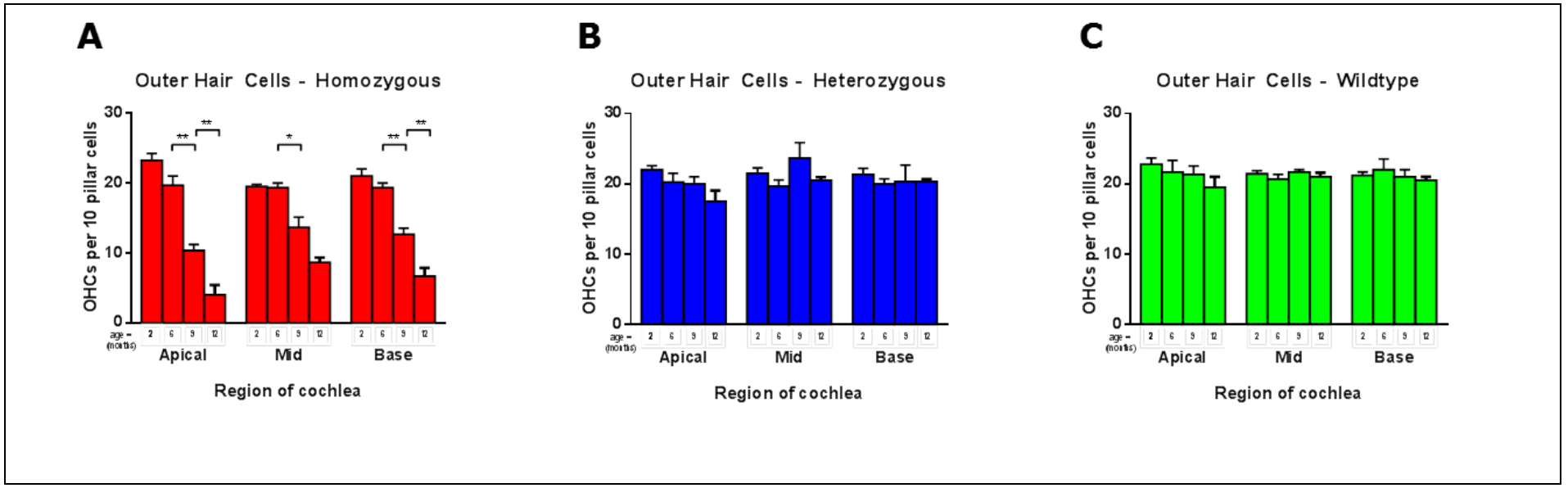

Figure 5.5: Comparison of outer hair cell loss across the genotypes. [A] Analysis of the outer hair cell counts of homozygous mice showed no significant decline in the number if hair cells between two and six months of age. However, between six and nine months of age and further between nine and 12 months of age, there was a significant deterioration in the number of hair cells in homozygous mice. Analysis of heterozygous [B] and wildtype [C] mice however showed no difference in the number of hair cells across the cochlear, over time. (*$p<0.05$ and **$p<0.01$) Error bars indicate standard error of mean.

5.1.3 Expression studies

Initial analysis showed that *Slc4a10* is expressed in the type II and type V fibrocytes of the spiral ligament of heterozygous and wildtype mice at 12 months of age. However, no immunoreactivity was seen in *Slc4a10*$^{trmb/trmb}$ mice. To examine if this loss of expression in the homozygous mice is age dependant, a longitudinal study was undertaken at two, six, nine and 12 months of age **(Figure 5.6)**.

Studies show that *Slc4a10* is expressed in the type II and type V fibrocytes of the lateral wall in heterozygous and wildtype mice. There is a uniformed pattern of expression in these fibrocytes seen throughout all the time points examined. The lack of immunoreactivity observed in homozygous mice during the initial studies at 12 months of age was also mirrored at the earlier time points of two, six and nine months of age.

There was no expression of Slc4a10 observed in any other region of the cochlea, e.g. organ of Corti, Reissner's membrane or stria vascularis for any genotype at any time point tested.

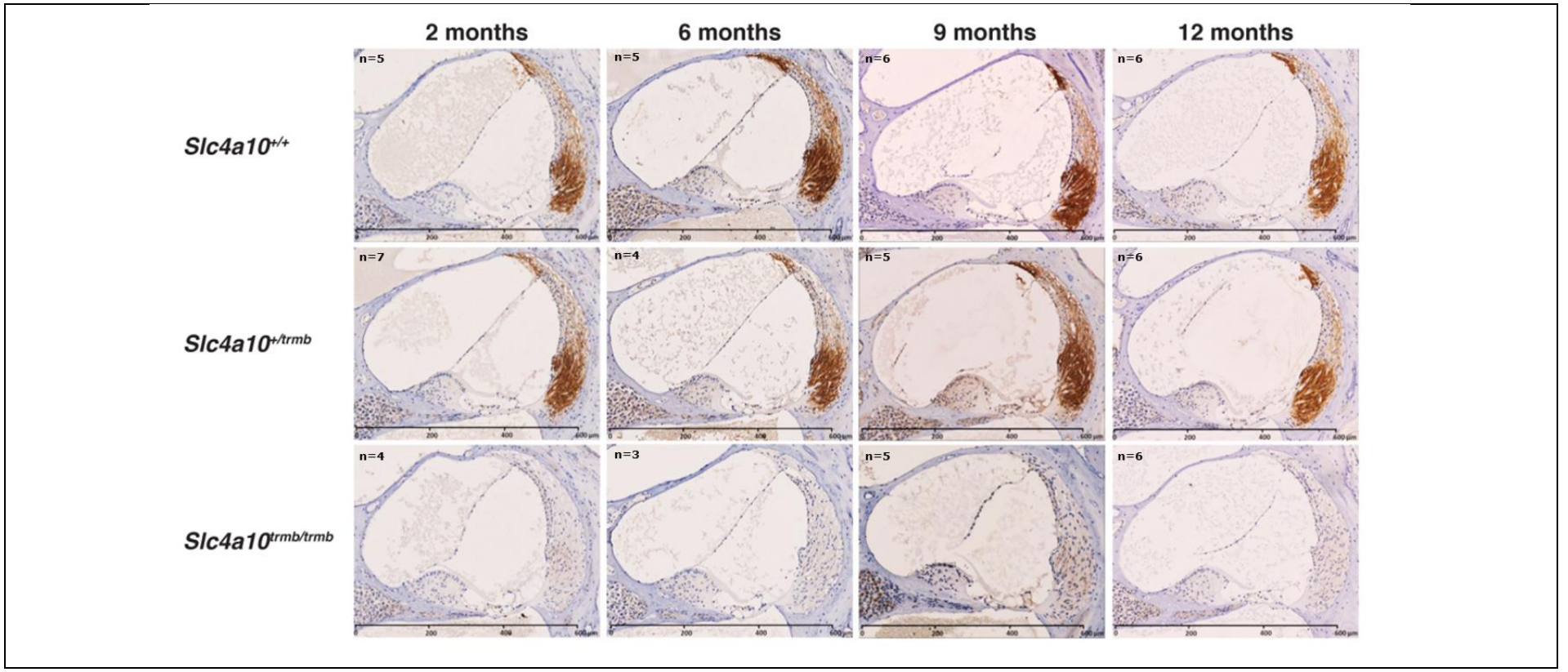

Figure 5.6: Immunolabelling of Slc4a10 in *trombone* mice. Immunolabelling studies showed that Slc4a10 was expressed in the type II and type V fibrocytes of the spiral ligament. This uniformed pattern of expression was seen across all of the ages tested in heterozygous and wildtype mice. However, there was no immunoreactivity observed in homozygous mice, at all the time points analysed.

5.2 Strial Analysis

Owing to the expression of Slc4a10 in the cochlear lateral wall, closer examination of the spiral ligament and stria vascularis was conducted.

5.2.1 Strial Surface Area

Initial histological analysis showed a possible thinning of the stria vascularis at 12 months of age in homozygous mice when compared to wildtype mice **(Figure 5.7)**.

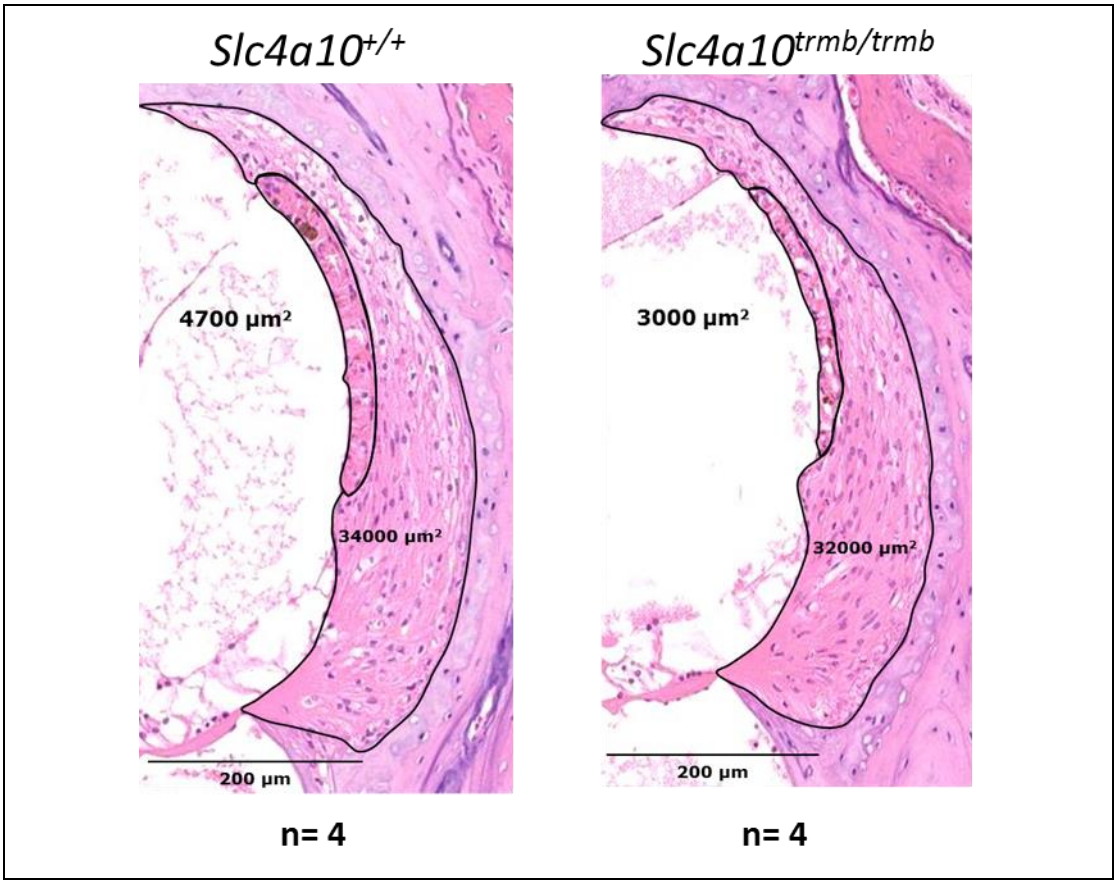

Figure 5.7: Strial vascularis morphometric analysis of Slc4a10$^{+/+}$ and Slc4a10$^{trmb/trmb}$ mice. *Slc4a10*$^{trmb/trmb}$ animals (n=4) exhibited significantly reduced strial surface area throughout the cochlea in comparison to *Slc4a10*$^{+/+}$ (n= 4) animals. Magnification x20.

To analyse this further, the cross-sectional surface area of the spiral ligament **(Figure 5.8)** and the stria vascularis **(Figure 5.9)** from mid-modiolar sections, were measured in *trombone* mice from two months of age. All measurements were conducted on the basal turn on the cochlear. Results obtained show that the cross-sectional surface area of the spiral ligament in homozygous mice is very similar to that of heterozygous and wildtype mice. The area remained unchanged at all ages analysed (two, six, nine and 12 months) and across all the genotypes (*Slc4a10*$^{+/+}$, *Slc4a10*$^{trmb/+}$ and *Slc4a10*$^{trmb/trmb}$). In contrast the cross-sectional surface area of the stria vascularis in homozygous mice is significantly smaller than that of wildtype and heterozygous mice. This reduction in strial surface area is observed from two months of age and is constant at the later time points i.e. no progressive change in strial cross-sectional surface area is observed.

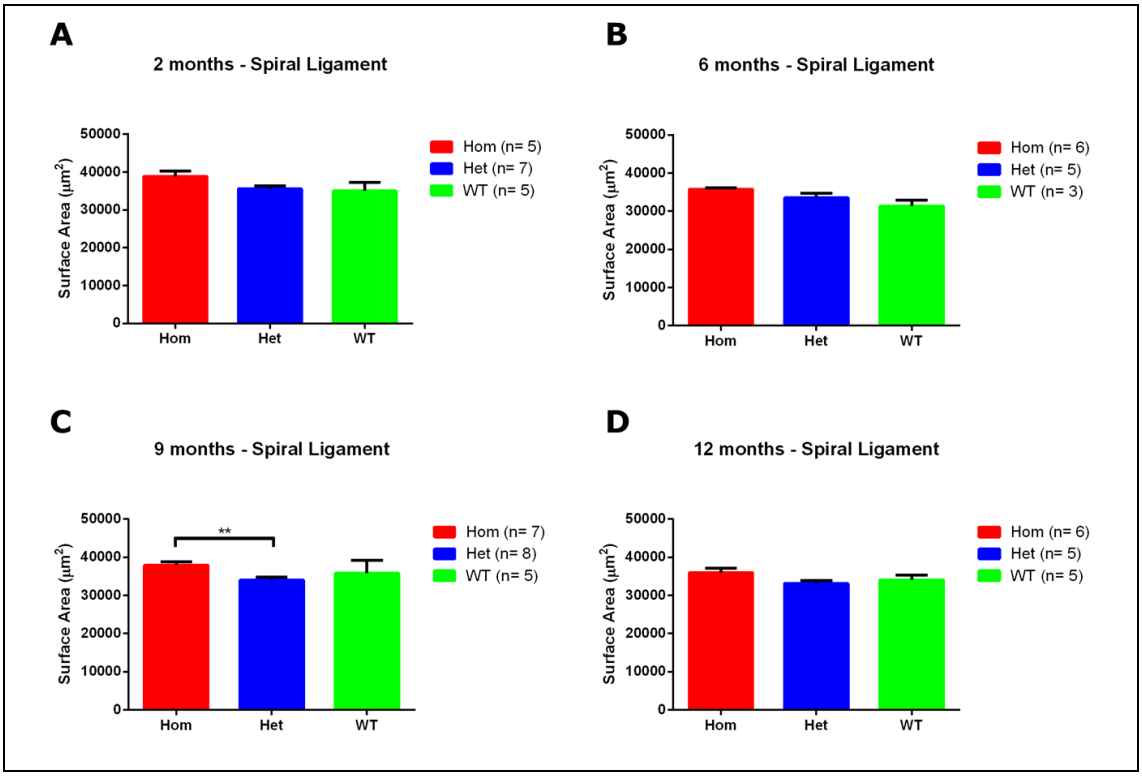

Figure 5.8: Analysis of Spiral Ligament Surface Area in *trombone* Mice.
Analysis of the cross sectional surface area of the spiral ligament in *trombone* mice at two months of age [A] showed no significant difference in the surface area of homozygous mice (n=5) when compared to heterozygous (n=7) and wildtype (n=5) littermates. This was also seen at six months of age [B], where there were no significant differences in the surface area of the spiral ligament in homozygous mice (n=6) when compared to wildtype (n=3) and heterozygous (n=5) littermates. At nine months of age [C], a difference was observed between the surface area of homozygous (n=7) and heterozygous (n=8) mice but no significant changes were seen in relation to wildtype (n=5) mice. As seen at two and six months of age, at 12 months of age [D] there was no difference in surface area of the spiral ligament in homozygous mice (n=6) when compared to wildtype (n=5) and heterozygous (n=5) littermates. (**p<0.01) Error bars indicate standard error of mean.

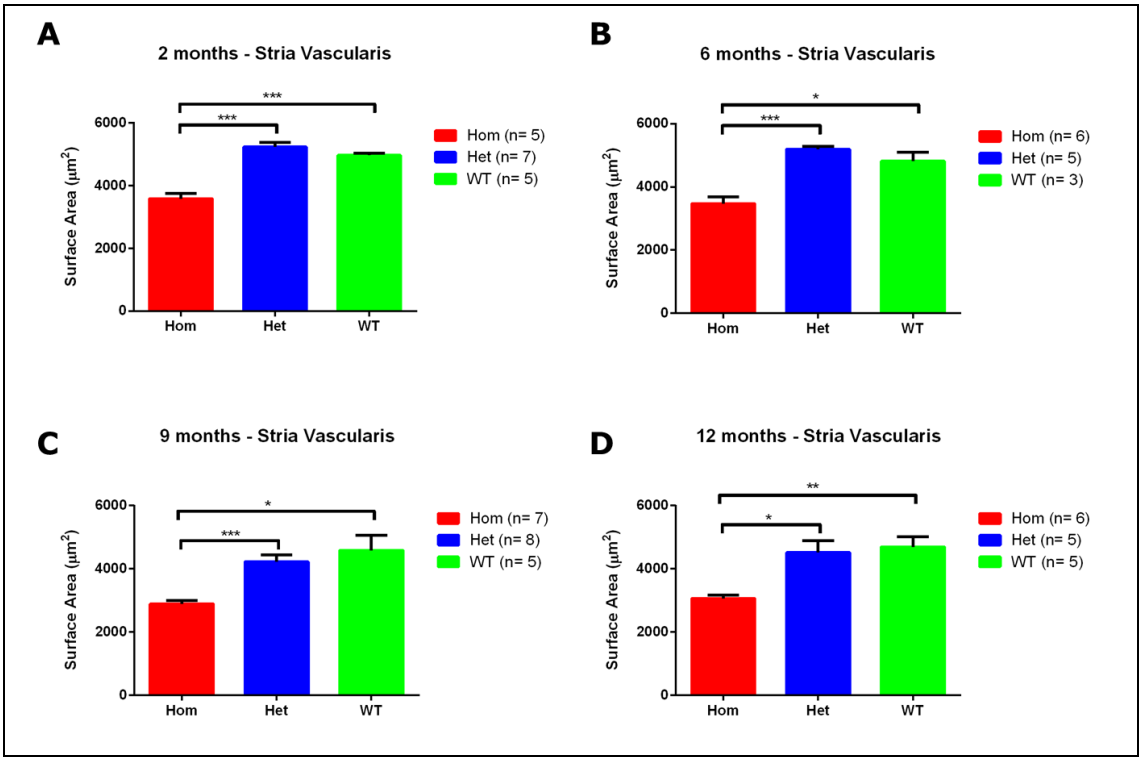

Figure 5.9: Analysis of Stria Vascularis Surface Area in *trombone* Mice.
Analysis of the cross sectional surface of the stria vascularis in *trombone* mice at two months of age [A] showed a significant reduction in homozygous mice (n=5) when compared to wildtype (n=5) and heterozygous (n=7) littermates. This trend was further seen at six months of [B] and nine months of age [C] where the surface of the stria vascularis in homozygous was significantly reduced when compared to wildtype and heterozygous littermates. This reduction in the surface area of the stria vascularis was also seen at twelve months of age [D] where the strial surface area of homozygous mice (n=6) was significantly reduced when compared to wildtype (n=5) and heterozygous (n=5) littermates. (*p<0.05, **p<0.01, ***p<0.001) Error bars indicate standard error of mean.

5.2.2 Nuclei Counts

The stria vascularis is a structure made up of three distinct cell types; marginal cells, intermediate cells and basal cells (Section 1.1.5). The observed reduction in strial surface area may be due to loss of cells across the stria or a compaction of the three layers. In order to elucidate the reason for the strial surface area reduction, nuclei counts were undertaken **(Figure 5.10)**. This would determine if loss of cells in the stria vascularis is the cause of the reduced strial surface area.

My immunohistochemical studies (section 5.1.3) demonstrate that Slc4a10 is expressed by type II and V fibrocytes in heterozygous and wildtype *trombone* mice, but not in homozygous mice. In order to ascertain whether lack of expression is due to a loss of fibrocytes, nuclei counts of the entire spiral ligament was conducted **(Figure 5.11)**. Due to the complex compartmentalisation of the spiral ligament fibrocytes, each type of fibrocyte was not counted separately.

The results obtained show that across all the ages analysed, there is no loss of cells seen in the spiral ligament or the stria vascularis of homozygous mice. This indicates that the reduction in surface area of the stria vascularis observed previously is not due to lack of cells, but more likely a result of compaction of the three cell layers making up the stria vascularis.

Although nuclei counts were not performed for each individual type of fibrocyte, analysis of haemotoxylin stained sections shows that the density of type II and of type V fibrocytes in the spiral ligament appears normal in homozygous mice. In particular, the type V fibrocytes are clearly visible in the suprastrial region of the spiral ligament. Therefore, the lack of Slc4a10 immunoreactivity seen in the spiral ligament of the homozygous mice is not due to the absence of the fibrocytes, but there is complete absence of Slc4a10 protein in these fibrocytes. Thus, the *trombone* mutation likely affects protein stability or processing, and is likely degraded. Another explanation could be that the *trombone* mutation causes misfolding of the protein leading to the anti-Slc4a10 antibody not recognizing the epitope. However, the epitope for the antibody is within the C-terminal region of the Slc4a10 protein, which is a long way from the site of the mutation. Hence, I am of the opinion that the protein is most likely degraded.

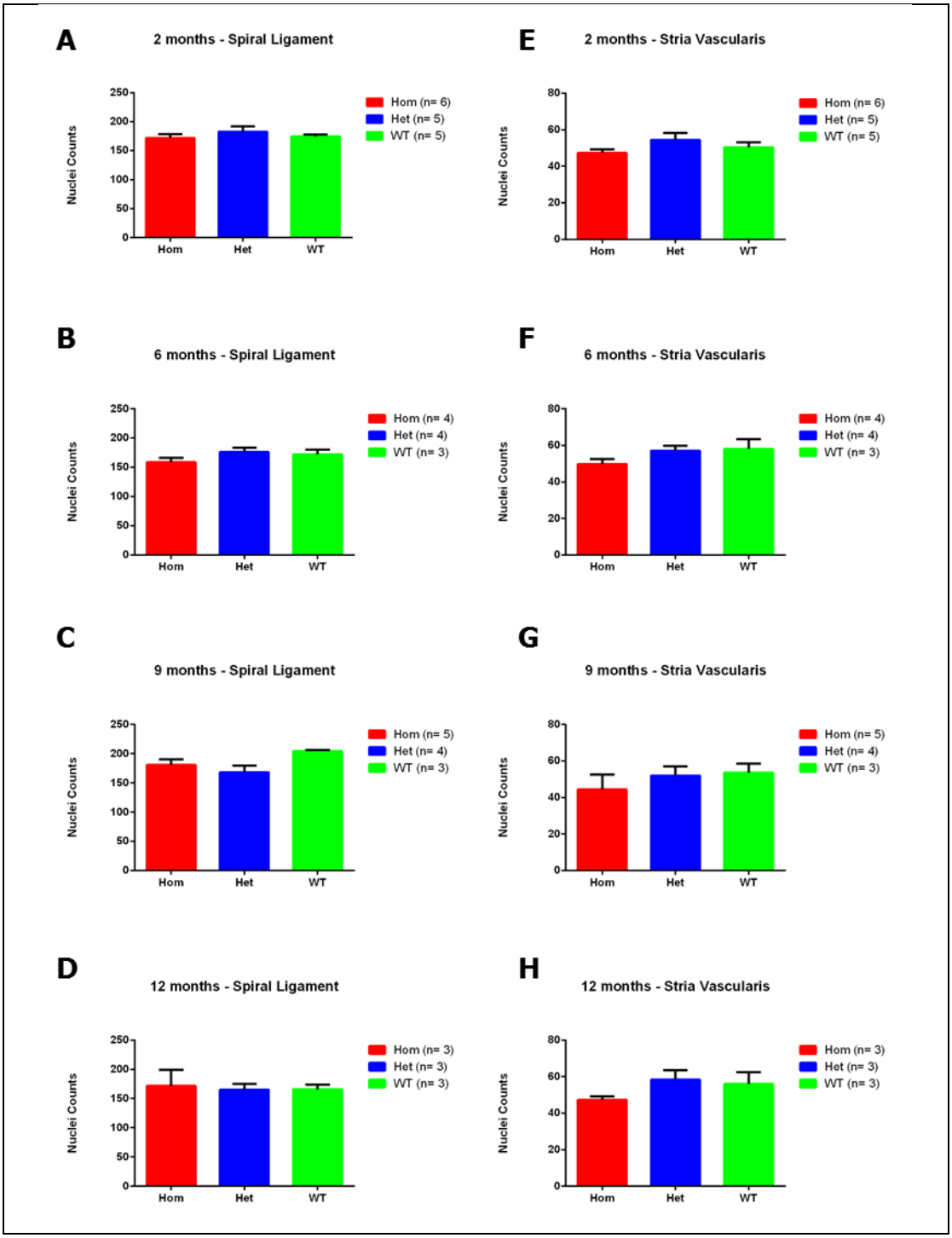

Figure 5.10: Nuclei Counts to Determine the Number of Cells in the Spiral Ligament [A-D] and the Stria Vascularis [E-H] of *trombone* mice. Nuclei counts of the spiral ligament conducted at two [A], six [B], nine [C] and twelve [D] months of age showed no difference in the number of cells present in the spiral ligament of homozygous mice when compared to wildtype and heterozygous littermates. Similarly, analysis of the stria vascularis at two [E], six [F], nine [G] and twelve [H] months of age also showed no difference in the number of cells present in the stria vascularis of homozygous mice when compared to wildtype and heterozygous littermates. Error bars indicate standard error of mean.

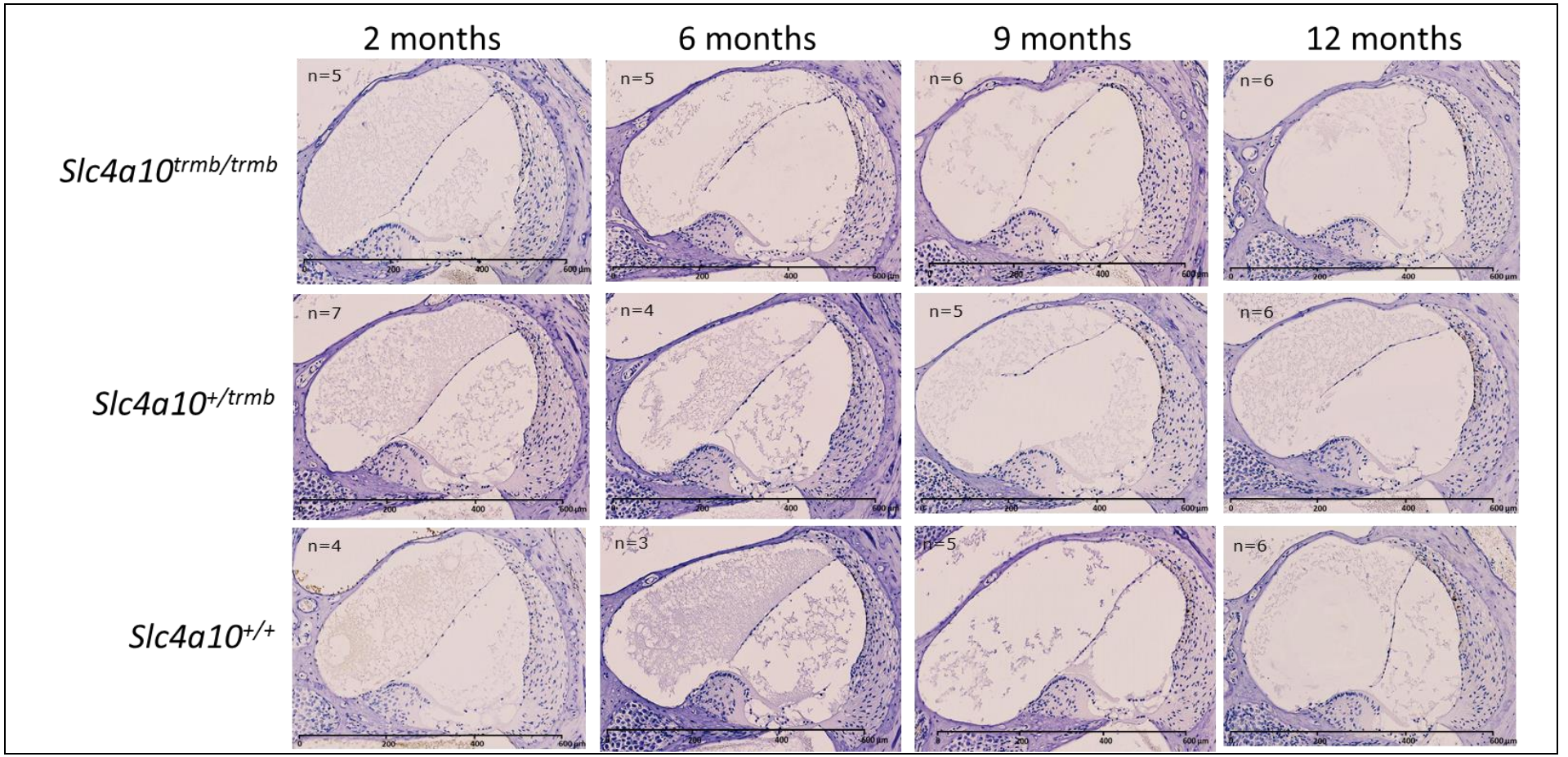

Figure 5.11: Analysis of fibrocytes density in the spiral ligament of *trombone* mice. Analysis of sections stained with haemotoxlyin showed that for any genotypes, at all ages tested, the density of the fibrocytes appears normal. There does not appear to be any loss of fibrocytes seen. In particular, the type V fibrocytes in the suprastrial region are present in in the homozygous mice at all of the time points tested. This shows that the loss of immunoreactivuty seen previously is not due to the lack of fibrocytes number.

5.2.3 Analysis of the Different Layers of the Stria Vascularis

The results obtained in sections 5.2.1 and 5.2.2 show that although there is a reduction in the stria surface area of *Slc4a10*$^{trmb/trmb}$ mice, this reduction is not attributable to a loss in the number of cells. To ascertain the morphology of this strial surface area reduction, the stria vascularis was analysed more closely using markers specific for each of the three cell layers that comprise the stria vascularis.

Immunofluorescence studies using Glut1, a glucose transporter expressed in apical and basolateral membranes of the strial basal cells and vascular pericytes was used to immunolabel strial sections of *trombone* mice at two and twelve months of age **(Figure 5.12)**. Results obtained show that in heterozygous (n=3) and wildtype (n=3) mice at two months of age the strial basal cells appear normal and intact, as do the blood vessels. By twelve months of age in heterozygous (n=3) and wildtype (n=3) mice the basal cells and vessels still appear to be present. However, the fluorescence signal is not as intense as seen at two months of age. In homozygous mice at two months of age (n=3), the basal cell layer and blood vessels appear to be present. However, the labelling is much less intense compared to wildtype and heterozygous littermates. By twelve months of age homozygous mice (n=3) show a similar level of expression of Glut1 as seen at two months of age.

The intermediate cells were analysed using an antibody to the ATP-dependent inwardly-rectifying potassium channel, Kir4.1 **(Figure 5.13)**. Results obtained show that at two months of age, the intermediate cells are

present in the homozygous (n=3), heterozygous (n=3) and wildtype (n=3) mice. By twelve months of age, the expression levels of Kir4.1 do not appear to have changed in heterozygous (n=3) and wildtype (n=3) mice. However, in homozygous (n=3) mice, there appears to be an age-related reduction in the expression of Kir4.1.

The marginal cells were studied using acetylated tubulin as a marker **(Figure 5.14)**. Results obtained show that at two months of age, homozygous (n=3), heterozygous (n=3) and wildtype (n=3) mice show a uniformed pattern of expression of acetylated tubulin, suggesting the presence of intact marginal cells. A similar pattern of expression was also observed at twelve months of age advocating that there are no age-related morphological changes observed in the marginal cells of *trombone* mice.

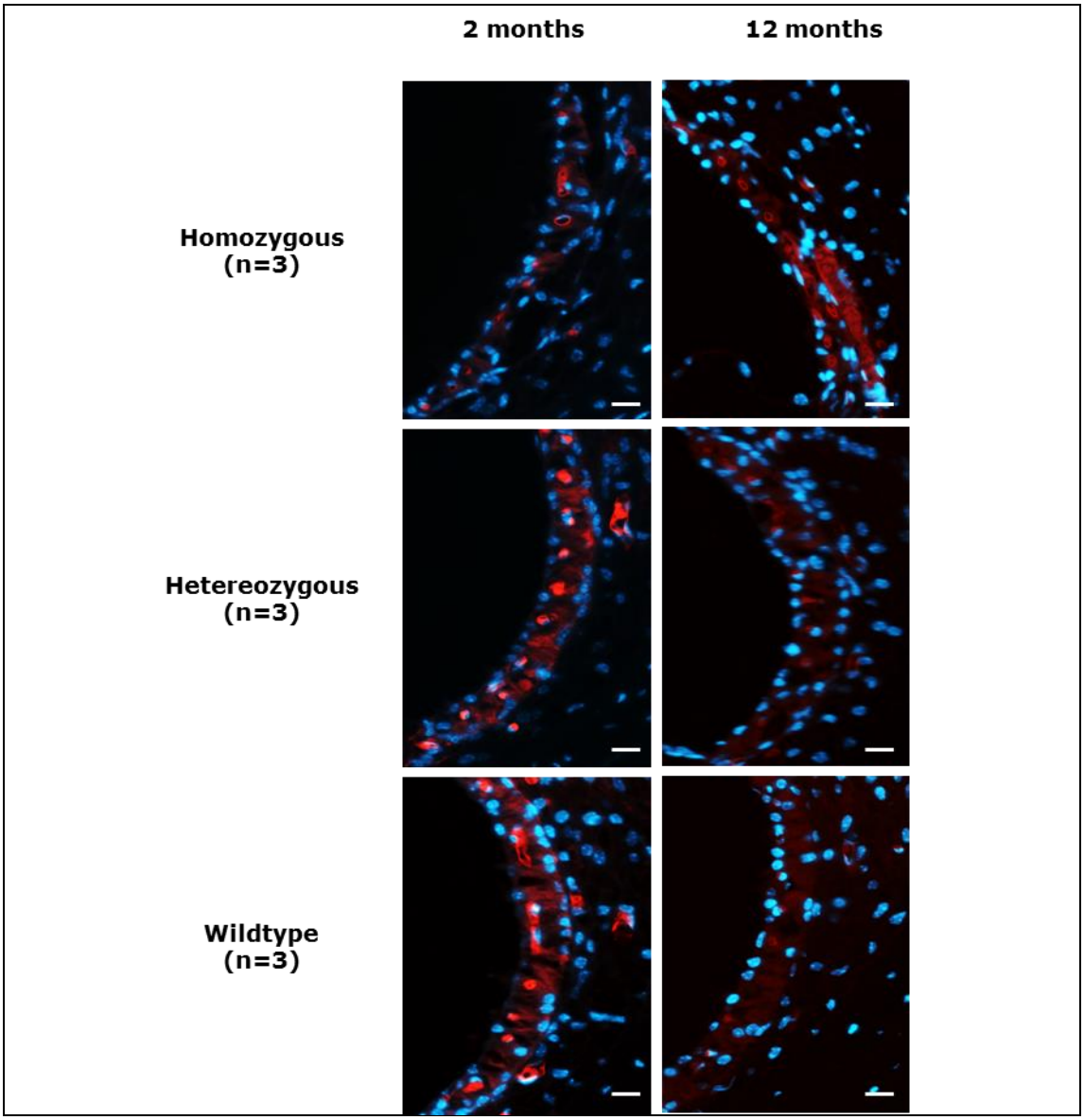

Figure 5.12: Immunofluorescence Analysis of the Strial Basal Cells and vasculature in *trombone* Mice using Glut1 as a marker. Analysis of the cross sectional surface of the stria vascularis in *trombone* mice at two months of age showed that the Glut1 labelling is evident in heterozygous (n=3) and wildtype (n=3) mice with the level expression of Glut1 diminishing a twelve months of age. In homozygous mice however, there is a reduced level of expression from two months of age (n=3) with no progression seen in this reduced expression levels at twelve months of age.
Sections were labelled with Glut1 (red) and DAPI (blue) was used as a counterstain to label the nuclei. Scale bars indicate 20μm.

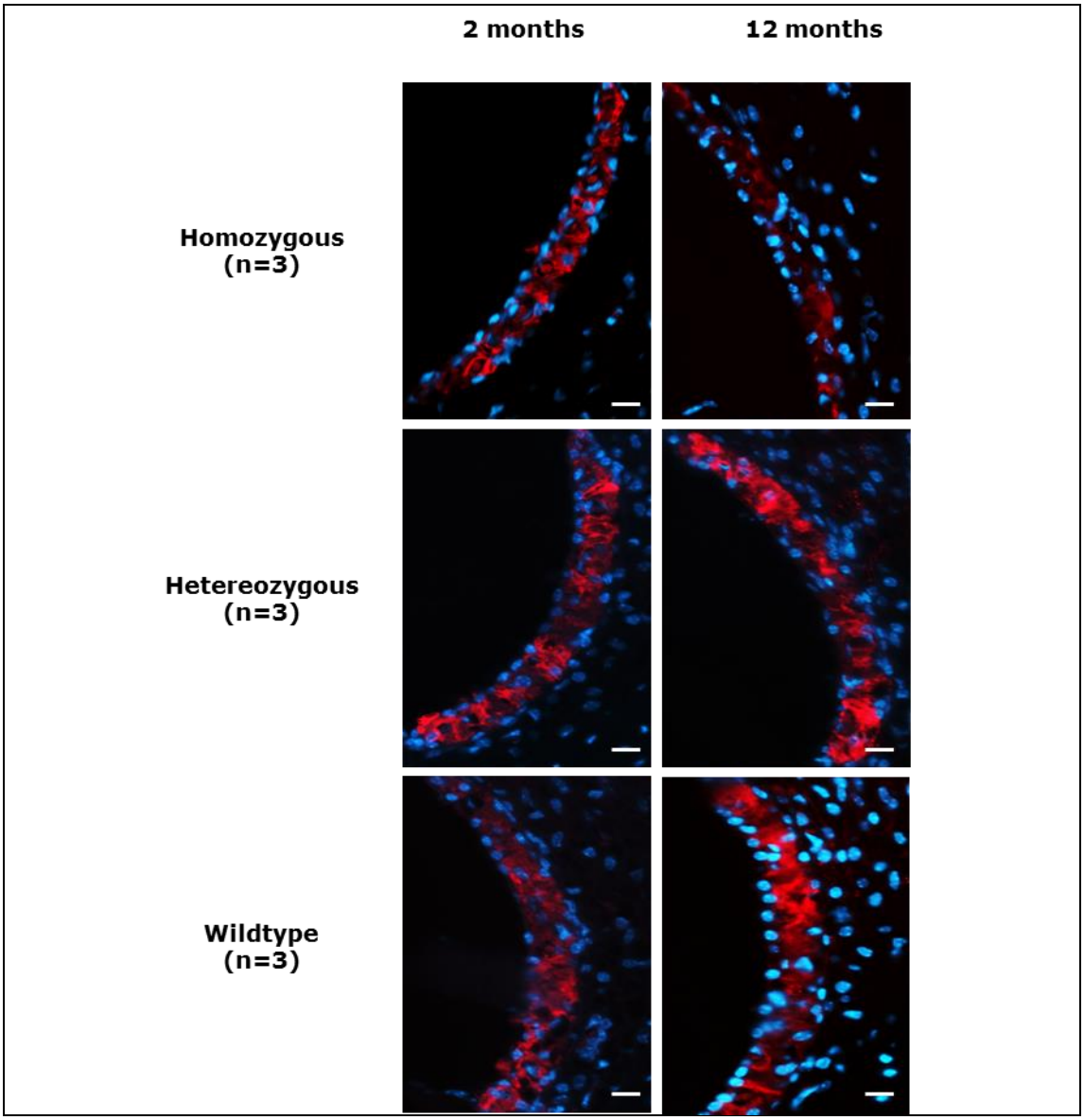

Figure 5.13: Immunofluorescence Analysis of the Intermediate Cells in *trombone* Mice using Kir4.1 as a marker. Analysis of the cross sectional surface of the stria vascularis in *trombone* mice at two months of age showed that the presence of the Kir4.1 clearly in homozygous (n=3), heterozygous (n=3) and wildtype mice, with no dysmorphology observed. At twelve months of age, this similar pattern of expression on Kir4.1 is detectable in heterozygous (n=3) and wildtype (n=3) mice. In homozygous mice (n=3) however, at twelve months of age, there appears to be a reduction in the expression of Kir4.1 suggesting a possible degradation of the marginal cells with age.
Sections were labelled with Kir4.1 (red) and DAPI (blue) was used as a counterstain to label the nuclei. Scale bars indicate 20μm.

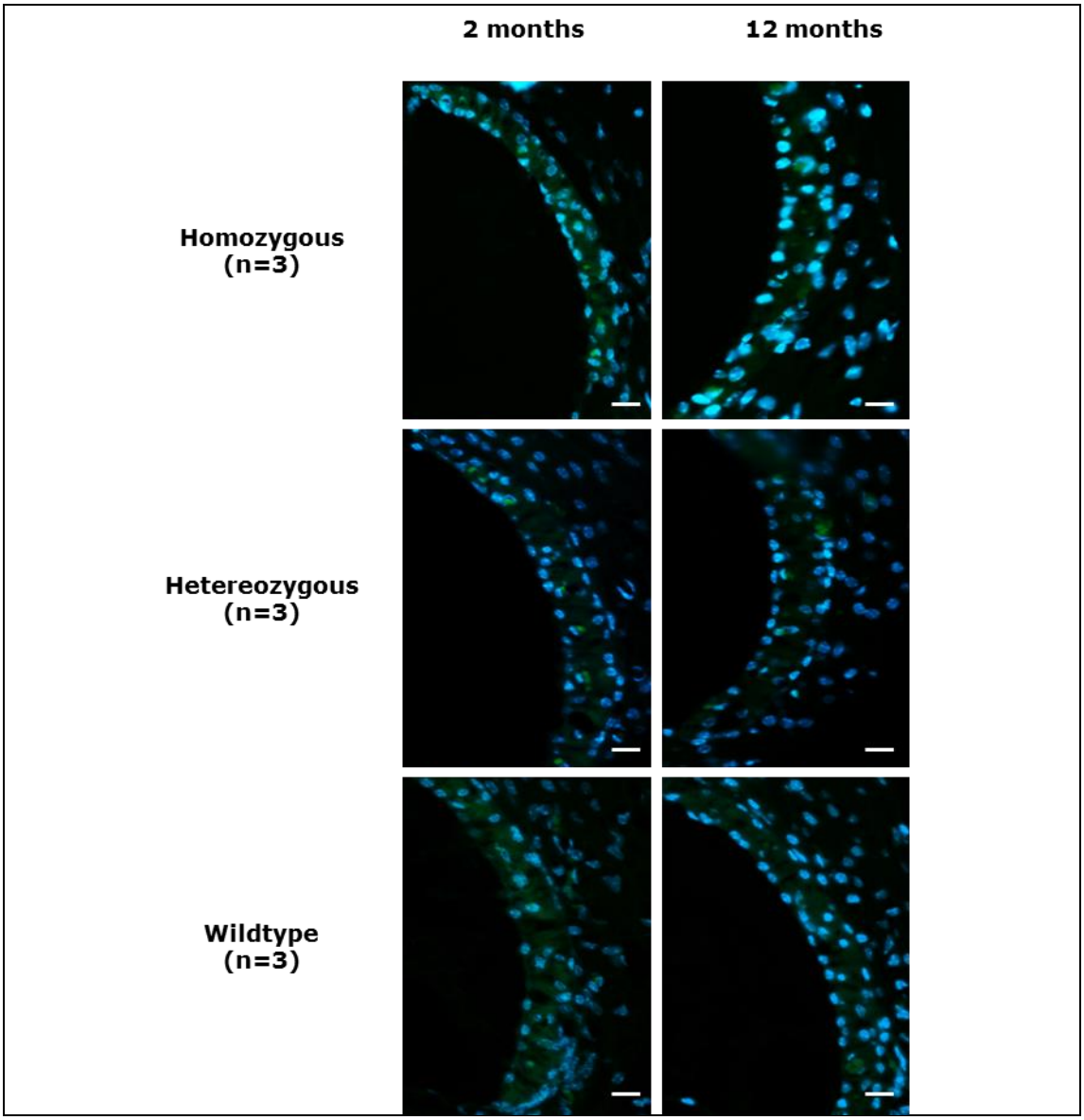

Figure 5.14: Immunofluorescence Analysis of the Marginal Cells in *trombone* Mice using Acetylated Tubulin as a marker. Analysis of the cross sectional surface of the stria vascularis in *trombone* mice at two months of age showed a uniformed expression pattern of acetylated tubulin in homozygous (n=3), heterozygous (n=3) and wildtype (n=3) mice suggesting the presence of intact marginal cells. This pattern of expression is further seen at twelve months on age with homozygous (n=3), heterozygous (n=3) and wildtype (n=3) mice display displaying similar expression levels of acetylated tubulin as seen at two months of age.
Sections were labelled with acetylated tubulin (green) and DAPI (blue) was used as a counterstain to label the nuclei. Scale bars indicate 20μm.

5.3 Endocochlear Potential

The potential of the endolymph, relative to that of the perilymph is known as the endocochlear potential (EP). An EP of +80 mV is thought to be essential for auditory transduction. The stria vascularis is important for generating the endocochlear potential and given the observed strial phenotypes and the pattern of expression of *Slc4a10* in *trombone* mice, the endocochlear potential was measured **(Figure 5.15)**. This work was done in collaboration with the Christine Petit Lab at the Pasteur Institute.

Endocochlear potential measurements were conducted at two, nine and twelve months. This identified that at two months of age, homozygous mice (n=8) mice have a two-fold reduction in the endocochlear potential compared to their wildtype (n=6) and heterozygous (n=10) littermates. This is also observed at nine months of age where homozygous mice (n=6) exhibit a 25-40mV reduction in the endocochlear potential measurements when compared to heterozygous (n=12) and wildtype (n=6) littermates. At nine months, the endocochlear potential of heterozygous mice also appear to be significantly reduced (by 15mV) when compared to wildtype mice. The results obtained at twelve months of age mirror that of the two month data. The endocochlear potential measurements of homozygous mice (n=9) were 35mV lower than that of heterozygous (n=11) and wildtype (n=8) littermates.

Analysis of the EP values obtained from homozygous mice shows no significant progression over the ages tested. There appears to be a significant reduction of the EP in heterozygous mice between two and nine

months of age, but no further reduction by twelve months of age. In the wildtype mice, as with the homozygous mice, no progressive decline is observed.

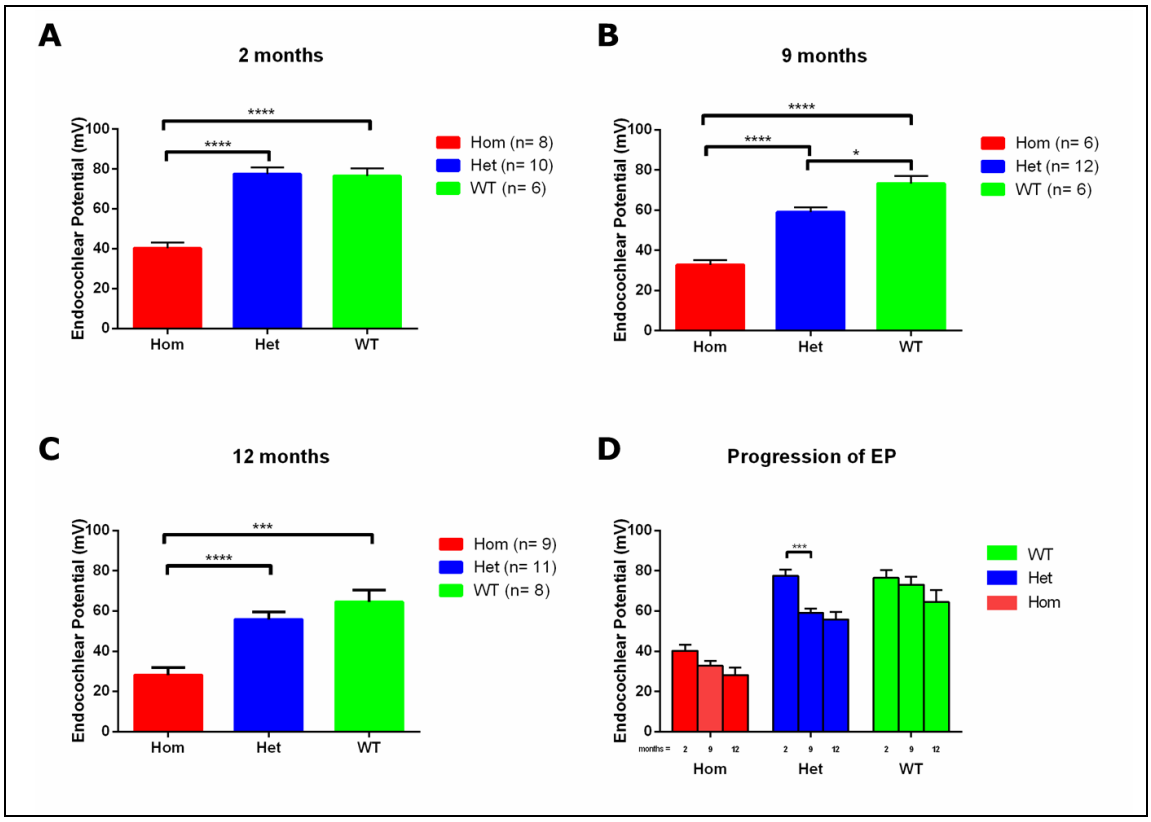

Figure 5.15: Endocochlear Potential Measurements of *trombone* Mice.
Endocochlear potential measurements conducted at two months of age [A] showed that homozygous mice (n=8) exhibited chronically reduced EP measurements when compared to wildtype (n=6) and heterozygous (n=10) littermates. This was also seen at nine months of age [B] with homozygous mice (n=6) displaying reduced EP measurements when compared to wildtype (n=6) and heterozygous (n=12) littermates. In addition however, there was also a significant reduction in the EP measurements of heterozygous mice when compared to wildtype littermates. At twelve months of age [C] the results follow a similar trend to that observed at two months on age. The homozygous mice (n=9) demonstrated significantly reduced EP measurements when compared to wildtype (n=8) and heterozygous (n=11) littermates. Additional analysis showed that the EP did not seem to decline with age in homozygous or wildtype mice. There was a significant difference observed in the EP of heterozygous mice between two and nine months of age, however, no difference was observed between nine and twelve months of age. (*p<0.05, **p<0.01, ***p<0.001, ****p<0.0001) Error bars indicate standard error of mean.

5.4 Discussion and Conclusion

The *trombone* model was initially identified during ABR screening of Ageing Screen pedigrees, exhibiting a hearing deficit at nine months of age, which progressed further by twelve months of age. I have undertaken a comprehensive longitudinal study of this model and have shown that at two and six months of age, *Slc4a10*$^{trmb/trmb}$ mice have similar ABR thresholds compared to their *Slc4a10*$^{+/+}$ and *Slc4a10*$^{+/trmb}$ littermates. However, by nine months of age the *Slc4a10*$^{trmb/trmb}$ mice have elevated ABR thresholds (~15-20dB increase) when compared to *Slc4a10*$^{+/+}$ and *Slc4a10*$^{+/trmb}$ littermates across all frequencies tested. By twelve months of age, the ABR thresholds were further elevated in *Slc4a10*$^{trmb/trmb}$ mice (~30dB increase). Analysis of the progressive hearing loss in the *Slc4a10*$^{trmb/trmb}$ mice confirmed no significant change in auditory function between two and six months of age, however there is a significant decline in auditory function between six and nine months of age, and between nine and twelve months of age. At twelve months of age a hearing threshold difference of ≥20dB is detected at 8, 16, and 32 kHz compared to 2 and 6 month thresholds, indicating *trombone* is a model of progressive mild age-related hearing loss.

Ultrastructural studies were undertaken to investigate the integrity of the cochlear sensory epithelium. These studies demonstrated a similar number of sensory hair cells to be present in *Slc4a10*$^{trmb/trmb}$ mice as their *Slc4a10*$^{+/+}$ and *Slc4a10*$^{+/trmb}$ littermates at two or six months of age, with no gross morphological changes observed. However, by nine months of age degeneration of the sensory hair cells was observed in *Slc4a10*$^{trmb/trmb}$ mice,

with further loss of cells by 12 months of age. No loss of hair cells was observed in the *Slc4a10*$^{+/+}$ and *Slc4a10*$^{+/trmb}$ littermate control mice. Thus, the results of the longitudinal ultrastructural study show that the hearing loss phenotype is concomitant with hair cell loss, suggesting that the hearing impairment observed in the *trombone* model is due to reduced auditory transduction occurring as a result of cochlear hair cell loss.

Immunolabelling studies identified that Slc4a10, the protein encoded by the gene mutated in *trombone*, is expressed in the cochlear lateral wall of normal hearing mice. In particular, the protein is localized to the type II and V fibrocytes of the spiral ligament. Interestingly, initial studies identified a lack of expression of Slc4a10 in these fibrocytes of *Slc4a10*$^{trmb/trmb}$ mice at 12 months of age. My longitudinal studies have shown that Slc4a10 is consistently expressed in the lateral wall fibrocytes of *Slc4a10*$^{+/+}$ and *Slc4a10*$^{+/trmb}$ mice at 2, 6, 9 and 12 months of age, suggesting it likely has a 'maintenance' function in these cells. However, Slc4a10 expression is not found in *Slc4a10*$^{trmb/trmb}$ mice at any age tested. Lack of immunolabelling suggests that the *trombone* mutation either leads to mis-folding of the protein such that the antibody epitope is no longer recognized, or destabilization, such that the protein is broken down. Either way the mutation is most likely to cause a loss-of-function of Slc4a10, which based on the expression profile observed in normal hearing mice appears to be required throughout life.

Histological analyses suggest that chronic loss of Slc4a10 does not lead to degeneration of the spiral ligament fibrocytes, as no reduction in fibrocyte number is found between *Slc4a10*$^{+/+}$, *Slc4a10*$^{+/trmb}$ and *Slc4a10*$^{trmb/trmb}$ mice.

However, morphological analyses of the adjacent stria vascularis show a reduced cross-sectional surface area in *Slc4a10*$^{trmb/trmb}$ mice when compared to their *Slc4a10*$^{+/+}$ and *Slc4a10*$^{+/trmb}$ littermates. This finding suggests that loss of Slc4a10 in the spiral ligament somehow affects the stria vascularis. Nuclei counts show a similar number of cells within the stria vascularis of *Slc4a10*$^{+/+}$, *Slc4a10*$^{+/trmb}$ and *Slc4a10*$^{trmb/trmb}$ mice, and therefore the reduced surface area could be due to compaction of the strial layers rather than a loss of cells. Whilst the stria vascularis and spiral ligament are distinct structures they function together to allow potassium recycling within the cochlea, a prerequisite for endolymph production and generation of the endocochlear potential.

Indeed, endocochlear potential measurements undertaken at 2, 9 and 12 months, show that *Slc4a10*$^{trmb/trmb}$ mice have chronically reduced endocochlear potential values compared to their *Slc4a10*$^{+/+}$ and *Slc4a10*$^{+/trmb}$ littermates. This phenotype is consistent with both the chronically reduced strial surface area phenotype and the immunolabelling results, but precedes the auditory phenotype. Thus, taken together my longitudinal studies suggest that whilst the *trombone* hearing deficit is due to sensory hair cell loss, this hair cell loss is likely caused by chronic stress due to failure to produce endolymph of the correct composition.

5.4.1 The role of the stria vascularis in auditory function

In the cochlear, the sensory cells are apically bathed in a potassium-rich extracellular fluid known as the endolymph, the ionic composition of which is essential for auditory transduction. Endolymph homeostasis and the

maintenance of the positive endocochlear potential requires the stria vascularis (Trowe et al., 2011). The stria vascularis is a highly vascularised, energetic epithelial structure on the cochlear lateral wall and is composed of three cell layers.

The marginal cells of the stria vascularis are primarily involved in the transport of potassium ions (K^+). The basolateral membrane of marginal cells contain high levels of Na^+/K^+-ATPase (both α- and β- isoforms) which transport K^+ into the cell in exchange for sodium ions (Na^+). The apical membranes of marginal cells contain a K^+ channel formed by two subunits, the KCNE1 regulatory protein and the KCNQ1 channel protein (Vetter et al., 1996). This channel provides the pathway through which K^+ is secreted into the endolymph (Forge and Wright, 2002). During development, high levels of K^+ are found in the endolymph with the marginal cells showing high Na/K-ATPase activity, even before an EP can be recorded. A similar system exists in the vestibular system where the marginal cells exhibit an identical morphology and physiology however no positive potential equivalent to the EP in recordable. This suggests that whilst the role of the marginal cells are to transport K^+ and maintain the concentration of K^+ in the endolymph, the generation of EP is a separate phenomenon regulated by the intermediate and/or basal cells (Forge and Wright, 2002).

The intermediate cells of the stria vascularis are made of the melanocytes derived from the neural crest. They contain a variety of enzymes which function to detoxify oxidative wastes (Spector and Carr, 1979). Coupled with the presence of melanin, the intermediate cells are thought to play a role in protecting the stria vascularis under conditions of stress. However,

studies have also shown a role for the intermediate cells in the generation and maintenance of the endocochlear potential. In the viable dominant spotting mouse mutant, a neural crest defect leads to a reduced number of intermediate cells and there is no EP generated (Steel and Barkway, 1989). In this model, all other cells of the stria are intact, suggesting that the lack of EP is due to the absent intermediate cells (Schulte and Steel, 1994).

The basal cells border the spiral ligament and are mesenchymal-derived. During development, tight junctions are formed between the basal cells which coincide with the initial onset of measurable EPs suggesting that these tight junctions are necessary to provide the electrical insulation required for the generation and maintenance of the EP (Forge and Wright, 2002). In addition, there are also a large number of gap junctions present between adjacent basal cells, basal and intermediate cells and basal cells and fibrocytes in the spiral ligament. The fibrocytes take up K^+ from the perilymph and it is thought that the gap junctions between the fibrocytes and the basal cells create a pathway whereby the K^+ can enter the strial cells. This intracellular communication provided by gap junctions is thought to be important for the maintenance of EP.

The functional role of the stria vascularis has previously been studied in detail through inherited disorders linked with hearing impairment. Ion transport disruption by marginal cells have been implicated as causing a spectrum of syndromes including Jervell and Lange-Nielsen syndrome (Neyroud et al., 1997, Schulze-Bahr et al., 1997) and Bartter syndrome (Birkenhager et al., 2001). The loss of the potassium channel Kir4.1 from the intermediate cells has also be known to result in hearing impairment in

humans due to a complete ablation of the endocochlear potential causing SeSAME syndrome (Bockenhauer et al., 2009, Marcus et al., 2002, Scholl et al., 2009). The lack of differentiated intermediate cells in the stria vascularis affects the differentiation and migration of neural rest derived melanocytes causing sensorineural deafness (Schrott and Spoendlin, 1987, Steel and Barkway, 1989, Tachibana, 1999, Tachibana et al., 1992). In addition, studies have shown that loss of the protein Claudin11 from the basal cells obstructs the generation of EP resulting in hearing loss (Gow et al., 2004, Kitajiri et al., 2004).

In the *trombone* model, immunolabelling studies have shown the strial marginal cells to be present in homozygous mice at two and twelve months of age, indicating that marginal cell-mediated K^+ transport is likely unaffected. Also, the fact that an EP is generated in the homozygous *trombone* mice, albeit very reduced, suggests that the integrity of the epithelial border established by these cells is intact.

Kir4.1 labelling in homozygous mice at two months of age indicate that the intermediate cells are present. However, the immunolabelling appears to diminish by 12 months of age. Given the nuclei count data this is unlikely to be due to loss of intermediate cells, but instead a reduction in expression of Kir4.1 by these cells. The Kir4.1 channel is reported to be the rate-limiting pathway for K^+ secretion by the stria vascularis, hence it is essential for the generation of the EP, with mice lacking this channel unable to generate an EP (Marcus et al., 2002). Despite the presence of Kir4.1, at 2 months of age homozygous *trombone* mice already display a reduced EP compared to wildtype and heterozygous mice. Importantly, the reduction in Kir4.1

immunoreactivity observed in homozygous *trombone* mice occurring between 2 and 12 months is not associated with a concomitant further reduction in EP values in these mice. These data suggest that intermediate cell dysfunction is not the underlying cause of the reduced EP in the homozygous mice.

The expression levels of Glut1 however, appear to be reduced in the homozygous mice at both two and twelve months of age suggesting a possible loss of basal cells. The consequences of this are two- fold. Firstly, the lack of functional basal cells could result in the lack of electrical insulation needed by the stria vascularis in order to generate and maintain the endocochlear potential. This would explain the chronically reduced EP seen in homozygous mice at two months of age. In addition, the lack of basal cells would also result in the loss of the intracellular transport route for K^+ from the fibrocytes to the stria vascularis, which in turn could affect the ionic composition of the endolymph.

5.4.2 *trombone*

The results obtained suggest that trombone is a model of progressive late-onset hearing loss, with elevated hearing thresholds apparent by nine months of age and become further elevated by 12 months of age.

Longitudinal characterisation studies show that, although the hearing loss manifests by nine months of age, there are obvious morphological and biochemical deficits present from two months of age. Based on the data I have collected and the phenotypes observed, the following mechanism is hypothesised for the hearing impairment identified in the *trombone* model.

The spiral ligament fibrocytes are known to play an important role in the uptake of K^+ from the perilymph and recycling it to the stria vascularis. As such, they play a pivotal role in the pathway that enables the generation and maintenance of the EP. In the *trombone* model, there is no immunoreactivity for Slc4a10 seen in the type II and V fibrocytes of homozygous mice. Nuclei counts have shown that there is not a reduction in fibrocyte number in these mice and therefore it is likely due to a lack of functional Slc4a10 protein. Loss of this NCBT will lead to dysregulated control of intracellular pH, which will undoubtedly affect fibrocyte function. This dysfunction will in turn likely lead to a reduction in K^+ transport to the basal cells of the stria vascularis.

As mentioned previously, the stria vascularis plays a pivotal role in the secretion of K^+ into the endolymph and in the generation and maintenance of the EP. The secretion of K^+ by the stria vascularis is normally rate limited by the potassium channel Kir4.1, which is expressed in the intermediate cells. However, immunolabelling studies have shown that the reduced EP seen in the *trombone* model at 2 months of age is not due to reduced Kir4.1 expression in the intermediate cells. In addition, immunolabelling studies have also confirmed the presence of marginal cells in homozygous *trombone* mice suggesting that the reduction in EP is not due to loss of marginal cells. However, immunolabelling studies have indicated a lack of Glut1 expression in the basal cells of homozygous *trombone* mice. This may be due to absence of this cell layer, or it may be due to a reduction in the expression of Glut1 in these basal cells.

The basal cells of the stria vascularis and the fibrocytes of the spiral ligament form a syncytium. Thus, creating an intracellular pathway whereby K^+ taken up from the perilymph by the fibrocytes can be transported to the strial basal cells. Dysfunction of the fibrocytes due to loss of Slc4a10 could therefore also lead to dysfunction of the basal cells. Impaired K^+ transport to the stria vascularis would limit the rate of K^+ secretion into the endolymph, which in turn would cause a reduction in EP. As mention previously, the rate of K^+ secretion by the stria vascularis is normally limited by Kir4.1. Interestingly, whilst there is a reduction in Kir4.1 immunoreactivity between 2 and 12 months of age in homozygous *trombone* mice, there is no change in EP measurements taken at these ages. This would perhaps suggest that Kir4.1 is not rate-limiting in these homozygous mice, which would be the case if K^+ transport to the stria vascularis is drastically reduced.

How the chronically reduced EP leads to hair cell loss is still unclear, but one can suppose that alteration in the ionic balance of the endolymph may stress the sensory hair cells, which eventually leads to their degeneration.

5.4.3 Conclusion

The data obtained confirms trombone as a model of late-onset progressive hearing loss due to a mutation in the gene Slc4a10. I hypothesise that sensory hair cell loss in the trombone model is secondary to the strial and EP phenotypes observed. However, it is the eventual degeneration of the sensory hair cells that results in the elevated hearing thresholds observed in homozygous trombone mice. In order to fully understand the mechanism underlying the phenotypes observed, further molecular and genetic studies will need to be undertaken.

Chapter 6

Discussion and Conclusion

The aim of my DPhil study was to utilize the Harwell Ageing Screen in order to identify mouse models of age-related hearing loss. It was hoped that characterization of these models would increase understanding of the genetics and pathobiology of this common condition for which currently very little is known. During my studies I have identified two models, MP90 and MPC96 (subsequently named *trombone*).

MP90 is a model of late-onset hearing loss that was identified by ABR phenotyping at nine months of age. Whole genome mapping was undertaken and a candidate interval identified. In an attempt to determine the underlying genetic lesion next generation sequencing was employed. However, all of the ENU-induced lesions identified within the candidate interval are in non-coding regions. To facilitate the cloning of the causative genetic lesion, this line will need to be rederived using frozen sperm from the founder G1 male, and additional mice bred to allow further phenotyping, inheritance testing and mapping studies. However, due to the late-onset nature of the phenotype and the time constraints associated with breeding and ageing test cohorts, this model was not pursued further. I

decided to concentrate my efforts on the second model I identified – *trombone.*

The *trombone* model was identified by ABR phenotyping with a subset of mice exhibiting elevated ABR thresholds at nine month of age, which were further elevated by 12 months of age. Whole genome mapping and next generation sequencing studies were undertaken and these helped to identify one coding mutation within the novel hearing loss gene *Slc4a10*, causing a missense mutation in the encoded Slc4a10 protein (Leu647Pro).

Slc4a10 is a member of the solute carrier 4 (SLC4) group of membrane transport proteins that play an important role in regulating cellular pH. This group of proteins is made up of five Na^+ couples HCO_3^- transporters (NCBTs) and three Na^+ independent $Cl^-HCO_3^-$ exchangers. Slc4a10 is a NCBT which functions to transport bicarbonate into the cell thereby maintaining intracellular pH. There are four known splice variants of *Slc4a10* with the *trombone* mutation being present in all isoforms.

To fully assess the onset and progression of the hearing loss phenotype and to allow the underlying pathological consequences of the *trombone* mutation to be investigated additional test cohorts were bred and utilized for secondary phenotyping studies at 2, 6, 9 and 12 months of age. My studies have shown that *trombone* mice have normal looking cochlear morphology at a young age, but display sensory hair cell loss as they age, which is likely the cause of the increased hearing thresholds. However, my studies also show that this cell loss occurs subsequent to the chronically

reduced endocochlear potential in *trombone* mice, which is due to loss of Slc4a10 in the spiral ligament fibrocytes.

Prior to this investigation, *Slc4a10* has not been reported to be associated with auditory dysfunction in the mouse or in human studies. Previous research has focused on the expression of *Slc4a10* in adult mouse brain and its effect on the choroid plexus (Song et al., 2014, Christensen et al., 2013, Damkier and Praetorius, 2012, Liu et al., 2011). However, more recent studies of a *Slc4a10* targeted knockout (KO) mouse mutant (*Slc4a10*$^{-/-}$) have identified a role for Slc4a10 in maintaining intracellular chloride and bicarbonate concentration in retinal neurons. Demonstrating that loss of Slc4a10 in the retina leads to impaired visual function in the *Slc4a10*$^{-/-}$ KO mouse (Hilgen et al., 2012). To ascertain if the *Slc4a10*$^{trmb/trmb}$ mice also display a retinal phenotype I sent mice to a collaborator (Dr Alun Barnard, University of Oxford) for assessment using electroretinography (ERG). The *trombone* model is on a mixed genetic background involving the C3H.Pde6b+ line. The presence of the *Gpr179*^{nob5} allele in this line renders them unsuitable for ERG studies (Balmer et al., 2013, Hoelter et al., 2008) because of a severe and confounding effect of this mutation on ERG function. Therefore I requested that frozen sperm from the G1 founder of MPC96 be used in a rederivation of the line, backcrossing to C57BL/6J a strain suitable for ERG studies. The ERG analysis **(Supplementary Figure 2)** showed that *trombone* mice display a very similar, albeit milder, retinal phenotype to the *Slc4a10*$^{-/-}$ KO mice. The similar phenotype is encouraging as it would suggest that my previous supposition that the *trombone* allele causes loss-of-function is correct.

Reasons why the *trombone* model have a milder ERG phenotype than the targeted KO are: residual function of Slc4a10 protein in *trombone* vs no protein in KO; age of testing (12 weeks for *trombone* vs 12 months for KO); background strain (mainly C57BL/6J for *trombone* vs no detail given for KO); and, numbers tested (5x WT and 5x Hom *trombone* vs 2x WT and 3x KO).

Interestingly, Slc4a7, another NCBT closely related to Slc4a10, has been linked to retinal impairment and auditory dysfunction. Slc4a7 also acts to maintain intracellular pH playing a vital role in the efficient disposal of acid (H^+) generated by neuronal and sensory receptor activity, which is an essential requisite of sensory transduction. Mice lacking Slc4a7 (*Slc4a7* knockout) develop blindness and auditory impairment due to degeneration of sensory receptors in the eye and the inner ear, respectively (Bok et al., 2003). Auditory impairment in these mice is present from one month of age, and is concomitant with loss of hair cells and morphological changes in the stria vascularis and spiral ligament. In addition to the very similar phenotype, the expression pattern of Slc4a7 is the same as Slc4a10, with expression in the type II and type V cochlear fibrocytes. It was hypothesised that impaired ion transport by the spiral ligament fibrocytes in *Slc4a7* KO mice may lead to hair cell degeneration and consequently auditory impairment.

Taken together, the data from these mouse models (the *Slc4a7* KO, the *Slc4a10* KO and *trombone*) demonstrate the importance of NCBTs in the function of the mammalian visual and auditory systems. It will be interesting to investigate the knockout models of the other three related

NCBTs (Slc4a4, Slc4a5 and Slc4a8) to study if they also have a role in visual and auditory function. Indeed, it would also be interesting to cross these models together to generate double heterozygous mice, and investigate for phenotypes. Also, whilst I am convinced the *Slc4a10*^{trmb} allele is the underlying genetic lesion responsible for the *trombone* auditory phenotype, it would be good to undertake a complementation test by crossing *trombone* with the *Slc4a10* KO to generate compound heterozygous mice (i.e. *Slc4a10*$^{trmb/-}$). If these mice also display a hearing deficit this would provide unequivocal evidence that Slc4a10 is required for mammalian auditory function. Unfortunately, I did not have access to the *Slc4a10* KO during my studies. In addition, it would be interesting to age the *Slc4a10*$^{trmb/+}$ mice further and assess their hearing as the EP data suggests there may be some decline in EP values with age in these mice **(Figure 5.15)**. Thus, potentially these mice may go on to develop hearing loss, but over a longer time period than the *Slc4a10*$^{trmb/trmb}$ mice. It might also be worth testing whether the *Slc4a10*$^{trmb/+}$ mice are more susceptible to noise-induced hearing loss compared to *Slc4a10*$^{+/+}$ littermate mice. Unfortunately, given the time constraints of my studentship I have not been able to undertake these additional studies.

Importantly, it will be critical to assess the contribution of Slc4a10 to human hearing loss. To this end, we are collaborating with research groups studying human age-related hearing loss. These groups are undertaking GWA studies for hearing function in adult humans and exome sequencing of familial presbycusis cases. Through the interrogation of their datasets we hope to establish whether Slc4a10 is involved in human hearing loss.

The mouse continues to be the predominant model organism for studying the auditory system. Historically, spontaneous and induced-models have led to the identification of numerous early-onset hearing loss genes, the majority of which have then subsequently been shown to be critical for auditory function in man. However, to date little is known about the genetics or pathology associated with age-related hearing loss. The mouse offers a great opportunity to elaborate upon the genes underlying this common condition. In particular being able to take tissues at various stages of disease progression is critical for our understanding of the pathological changes occurring within the cochlea as the condition develops, something that is just not possible in humans. The more we increase our knowledge of the genes, pathways, and pathology, the better placed we will be to develop therapeutic strategies to ameliorate age-related auditory decline.

6.1 Conclusion

My studies demonstrate the utility of undertaking a phenotype-driven approach, using recurrent auditory screening, for the identification of mouse models of age-related hearing loss. Through the characterization of one of these models I have established that Slc4a10 is required for normal auditory function in the mouse. The data generated lead me to suggest that *trombone* is a novel model of strial presbycusis (also called metabolic presbycusis), which is believed to be the most common form of age-related hearing loss in the human population. This model offers an opportunity to explore potential therapeutic interventions, such as lentiviral gene therapy. As such, further functional characterization of this model promises to increase our understanding of the pathobiology associated with age-related hearing loss.

References

ACEVEDO-AROZENA, A., WELLS, S., POTTER, P., KELLY, M., COX, R. D. & BROWN, S. D. 2008. ENU mutagenesis, a way forward to understand gene function. *Annu Rev Genomics Hum Genet,* 9**,** 49-69.

ANDO, M. & TAKEUCHI, S. 1999. Immunological identification of an inward rectifier K+ channel (Kir4.1) in the intermediate cell (melanocyte) of the cochlear stria vascularis of gerbils and rats. *Cell Tissue Res,* 298**,** 179-83.

ANNIKO, M. 1976. Surface structure of stria vascularis in the guinea pig cochlea. Normal morphology and atoxyl-induced pathologic changes. *Acta Otolaryngol,* 82**,** 343-53.

ASSAD, J. A., SHEPHERD, G. M. & COREY, D. P. 1991. Tip-link integrity and mechanical transduction in vertebrate hair cells. *Neuron,* 7**,** 985-94.

BAEK, J. S., BAE, E. J., LEE, S. Y., PARK, S. S., KIM, S. Y., JUNG, K. N. & NOH, C. I. 2010. Jervell and Lange-Nielsen syndrome: novel compound heterozygous mutations in the KCNQ1 in a Korean family. *J Korean Med Sci,* 25**,** 1522-5.

BALMER, J., JI, R., RAY, T. A., SELBER, F., GASSMANN, M., PEACHEY, N. S., GREGG, R. G. & ENZMANN, V. 2013. Presence of the Gpr179(nob5) allele in a C3H-derived transgenic mouse. *Mol Vis,* 19**,** 2615-25.

BIELEFELD, E. C., TANAKA, C., CHEN, G. D. & HENDERSON, D. 2010. Age-related hearing loss: is it a preventable condition? *Hear Res,* 264**,** 98-107.

BIRKENHAGER, R., OTTO, E., SCHURMANN, M. J., VOLLMER, M., RUF, E. M., MAIER-LUTZ, I., BEEKMANN, F., FEKETE, A., OMRAN, H., FELDMANN, D., MILFORD, D. V., JECK, N., KONRAD, M., LANDAU, D., KNOERS, N. V., ANTIGNAC, C., SUDBRAK, R., KISPERT, A. & HILDEBRANDT, F. 2001. Mutation of BSND causes Bartter syndrome with sensorineural deafness and kidney failure. *Nat Genet,* 29**,** 310-4.

BOCKENHAUER, D., FEATHER, S., STANESCU, H. C., BANDULIK, S., ZDEBIK, A. A., REICHOLD, M., TOBIN, J., LIEBERER, E., STERNER, C., LANDOURE, G., ARORA, R., SIRIMANNA, T., THOMPSON, D., CROSS, J. H., VAN'T HOFF, W., AL MASRI, O., TULLUS, K., YEUNG, S., ANIKSTER, Y., KLOOTWIJK, E., HUBANK, M., DILLON, M. J., HEITZMANN, D., ARCOS-BURGOS, M., KNEPPER, M. A., DOBBIE, A., GAHL, W. A., WARTH, R., SHERIDAN, E. & KLETA, R. 2009. Epilepsy, ataxia, sensorineural deafness, tubulopathy, and KCNJ10 mutations. *N Engl J Med,* 360**,** 1960-70.

BOETTGER, T., HUBNER, C. A., MAIER, H., RUST, M. B., BECK, F. X. & JENTSCH, T. J. 2002. Deafness and renal tubular acidosis in mice lacking the K-Cl co-transporter Kcc4. *Nature,* 416**,** 874-8.

BOETTGER, T., RUST, M. B., MAIER, H., SEIDENBECHER, T., SCHWEIZER, M., KEATING, D. J., FAULHABER, J., EHMKE, H., PFEFFER, C., SCHEEL, O., LEMCKE, B., HORST, J., LEUWER, R., PAPE, H. C., VOLKL, H., HUBNER, C. A. & JENTSCH, T. J. 2003. Loss of K-Cl co-transporter KCC3 causes deafness, neurodegeneration and reduced seizure threshold. *EMBO J,* 22**,** 5422-34.

BOK, D., GALBRAITH, G., LOPEZ, I., WOODRUFF, M., NUSINOWITZ, S., BELTRANDELRIO, H., HUANG, W., ZHAO, S., GESKE, R., MONTGOMERY, C., VAN SLIGTENHORST, I., FRIDDLE, C., PLATT, K., SPARKS, M. J., PUSHKIN, A., ABULADZE, N., ISHIYAMA, A., DUKKIPATI, R., LIU, W. & KURTZ, I. 2003. Blindness and auditory impairment caused by loss of the sodium bicarbonate cotransporter NBC3. *Nat Genet,* 34**,** 313-9.

BORON, W. F., CHEN, L. & PARKER, M. D. 2009. Modular structure of sodium-coupled bicarbonate transporters. *J Exp Biol,* 212**,** 1697-706.

BOWL, M. R. & DAWSON, S. J. 2014. The Mouse as a Model for Age-Related Hearing Loss - A Mini-Review. *Gerontology*.

BROWN, A. C. 1874. The Sense of Rotation and the Anatomy and Physiology of the Semicircular Canals of the Internal Ear. *J Anat Physiol,* 8**,** 327-31.

BROWN, S. D., HARDISTY-HUGHES, R. E. & MBURU, P. 2008. Quiet as a mouse: dissecting the molecular and genetic basis of hearing. *Nat Rev Genet,* 9**,** 277-90.

CASIMIRO, M. C., KNOLLMANN, B. C., YAMOAH, E. N., NIE, L., VARY, J. C., JR., SIRENKO, S. G., GREENE, A. E., GRINBERG, A., HUANG, S. P., EBERT, S. N. & PFEIFER, K. 2004. Targeted point mutagenesis of mouse Kcnq1: phenotypic analysis of mice with point mutations that cause Romano-Ward syndrome in humans. *Genomics,* 84**,** 555-64.

CASSELBRANT, M. L., MANDEL, E. M., FALL, P. A., ROCKETTE, H. E., KURS-LASKY, M., BLUESTONE, C. D. & FERRELL, R. E. 1999. The heritability of otitis media: a twin and triplet study. *JAMA,* 282**,** 2125-30.

CHARIZOPOULOU, N., LELLI, A., SCHRADERS, M., RAY, K., HILDEBRAND, M. S., RAMESH, A., SRISAILAPATHY, C. R., OOSTRIK, J., ADMIRAAL, R. J., NEELY, H. R., LATOCHE, J. R., SMITH, R. J., NORTHUP, J. K., KREMER, H., HOLT, J. R. & NOBEN-TRAUTH, K. 2011. Gipc3 mutations associated with audiogenic seizures and sensorineural hearing loss in mouse and human. *Nat Commun,* 2**,** 201.

CHEESEMAN, M. T., TYRER, H. E., WILLIAMS, D., HOUGH, T. A., PATHAK, P., ROMERO, M. R., HILTON, H., BALI, S., PARKER, A., VIZOR, L., PURNELL, T., VOWELL, K., WELLS, S., BHUTTA, M. F., POTTER, P. K. & BROWN, S. D. 2011. HIF-VEGF pathways are critical for chronic otitis media in Junbo and Jeff mouse mutants. *PLoS Genet,* 7**,** e1002336.

CHEN, L. M., CHOI, I., HADDAD, G. G. & BORON, W. F. 2007. Chronic continuous hypoxia decreases the expression of SLC4A7 (NBCn1) and SLC4A10 (NCBE) in mouse brain. *Am J Physiol Regul Integr Comp Physiol,* 293**,** R2412-20.

CHEN, L. M., KELLY, M. L., ROJAS, J. D., PARKER, M. D., GILL, H. S., DAVIS, B. A. & BORON, W. F. 2008. Use of a new polyclonal antibody to study the distribution and glycosylation of the sodium-coupled bicarbonate transporter NCBE in rodent brain. *Neuroscience,* 151**,** 374-85.

CHRISTENSEN, I. B., GYLDENHOLM, T., DAMKIER, H. H. & PRAETORIUS, J. 2013. Polarization of membrane associated proteins in the choroid plexus epithelium from normal and slc4a10 knockout mice. *Front Physiol,* 4**,** 344.

CHRISTENSEN, K., FREDERIKSEN, H. & HOFFMAN, H. J. 2001. Genetic and environmental influences on self-reported reduced hearing in the old and oldest old. *J Am Geriatr Soc,* 49**,** 1512-7.

COHEN-SALMON, M., MAXEINER, S., KRUGER, O., THEIS, M., WILLECKE, K. & PETIT, C. 2004. Expression of the connexin43- and connexin45-encoding genes in the developing and mature mouse inner ear. *Cell Tissue Res,* 316**,** 15-22.

CONCEPCION, D., SEBURN, K. L., WEN, G., FRANKEL, W. N. & HAMILTON, B. A. 2004. Mutation rate and predicted phenotypic target sizes in ethylnitrosourea-treated mice. *Genetics,* 168**,** 953-9.

COREY, D. P. & HUDSPETH, A. J. 1979. Ionic basis of the receptor potential in a vertebrate hair cell. *Nature,* 281**,** 675-7.

CROUCH, J. J., SAKAGUCHI, N., LYTLE, C. & SCHULTE, B. A. 1997. Immunohistochemical localization of the Na-K-Cl co-transporter (NKCC1) in the gerbil inner ear. *J Histochem Cytochem,* 45**,** 773-8.

CROUCH, J. J. & SCHULTE, B. A. 1995. Expression of plasma membrane Ca-ATPase in the adult and developing gerbil cochlea. *Hear Res,* 92**,** 112-9.

DAMKIER, H. H., AALKJAER, C. & PRAETORIUS, J. 2010. Na+-dependent HCO3- import by the slc4a10 gene product involves Cl- export. *J Biol Chem,* 285**,** 26998-7007.

DAMKIER, H. H. & PRAETORIUS, J. 2012. Genetic ablation of Slc4a10 alters the expression pattern of transporters involved in solute movement in the mouse choroid plexus. *Am J Physiol Cell Physiol,* 302**,** C1452-9.

DAUWERSE, J. G., DIXON, J., SELAND, S., RUIVENKAMP, C. A., VAN HAERINGEN, A., HOEFSLOOT, L. H., PETERS, D. J., BOERS, A. C., DAUMER-HAAS, C., MAIWALD, R., ZWEIER, C., KERR, B., COBO, A. M., TORAL, J. F., HOOGEBOOM, A. J., LOHMANN, D. R., HEHR, U., DIXON, M. J., BREUNING, M. H. & WIECZOREK, D. 2011. Mutations in genes encoding subunits of RNA polymerases I and III cause Treacher Collins syndrome. *Nat Genet,* 43**,** 20-2.

DEL CASTILLO, I., MORENO-PELAYO, M. A., DEL CASTILLO, F. J., BROWNSTEIN, Z., MARLIN, S., ADINA, Q., COCKBURN, D. J., PANDYA, A., SIEMERING, K. R., CHAMBERLIN, G. P., BALLANA, E., WUYTS, W., MACIEL-GUERRA, A. T., ALVAREZ, A., VILLAMAR, M., SHOHAT, M., ABELIOVICH, D., DAHL, H. H., ESTIVILL, X., GASPARINI, P., HUTCHIN, T., NANCE, W. E., SARTORATO, E. L., SMITH, R. J., VAN CAMP, G., AVRAHAM, K. B., PETIT, C. & MORENO, F. 2003. Prevalence and evolutionary origins of the del(GJB6-D13S1830) mutation in the DFNB1 locus in hearing-impaired subjects: a multicenter study. *Am J Hum Genet,* 73**,** 1452-8.

DELPIRE, E., LU, J., ENGLAND, R., DULL, C. & THORNE, T. 1999. Deafness and imbalance associated with inactivation of the secretory Na-K-2Cl co-transporter. *Nat Genet,* 22**,** 192-5.

DELPIRE, E. & MOUNT, D. B. 2002. Human and murine phenotypes associated with defects in cation-chloride cotransport. *Annu Rev Physiol,* 64**,** 803-43.

DIXON, M. J., GAZZARD, J., CHAUDHRY, S. S., SAMPSON, N., SCHULTE, B. A. & STEEL, K. P. 1999. Mutation of the Na-K-Cl co-transporter gene Slc12a2 results in deafness in mice. *Hum Mol Genet,* 8**,** 1579-84.

DRAYTON, M. & NOBEN-TRAUTH, K. 2006. Mapping quantitative trait loci for hearing loss in Black Swiss mice. *Hear Res,* 212**,** 128-39.

DROR, A. A. & AVRAHAM, K. B. 2009. Hearing loss: mechanisms revealed by genetics and cell biology. *Annu Rev Genet,* 43**,** 411-37.

ERICHSEN, S., ZUO, J., CURTIS, L., RAREY, K. & HULTCRANTZ, M. 1996. Na,K-ATPase alpha- and beta-isoforms in the developing cochlea of the mouse. *Hear Res,* 100**,** 143-9.

ESTEVEZ, R., BOETTGER, T., STEIN, V., BIRKENHAGER, R., OTTO, E., HILDEBRANDT, F. & JENTSCH, T. J. 2001. Barttin is a Cl- channel beta-subunit crucial for renal Cl- reabsorption and inner ear K+ secretion. *Nature,* 414**,** 558-61.

FECHNER, F. P., BURGESS, B. J., ADAMS, J. C., LIBERMAN, M. C. & NADOL, J. B., JR. 1998. Dense innervation of Deiters' and Hensen's cells persists after chronic deefferentation of guinea pig cochleas. *J Comp Neurol,* 400**,** 299-309.

FEE, W. E., JR. 1980. Aminoglycoside ototoxicity in the human. *Laryngoscope,* 90**,** 1-19.

FELDING, J. U., RASMUSSEN, J. B. & LILDHOLDT, T. 1987. Gas composition of the normal and the ventilated middle ear cavity. *Scand J Clin Lab Invest Suppl,* 186**,** 31-41.

FETTIPLACE, R. & HACKNEY, C. M. 2006. The sensory and motor roles of auditory hair cells. *Nat Rev Neurosci,* 7**,** 19-29.

FLAGELLA, M., CLARKE, L. L., MILLER, M. L., ERWAY, L. C., GIANNELLA, R. A., ANDRINGA, A., GAWENIS, L. R., KRAMER, J., DUFFY, J. J., DOETSCHMAN, T., LORENZ, J. N., YAMOAH, E. N., CARDELL, E. L. & SHULL, G. E. 1999. Mice lacking the basolateral Na-K-2Cl cotransporter have impaired epithelial chloride secretion and are profoundly deaf. *J Biol Chem,* 274**,** 26946-55.

FORGE, A. 1984. Gap junctions in the stria vascularis and effects of ethacrynic acid. *Hear Res,* 13**,** 189-200.

FORGE, A. & WRIGHT, T. 2002. The molecular architecture of the inner ear. *Br Med Bull,* 63**,** 5-24.

FRANSEN, E., BONNEUX, S., CORNEVEAUX, J. J., SCHRAUWEN, I., DI BERARDINO, F., WHITE, C. H., OHMEN, J. D., VAN DE HEYNING, P., AMBROSETTI, U., HUENTELMAN, M. J., VAN CAMP, G. & FRIEDMAN, R. A. 2014. Genome-wide association analysis demonstrates the highly polygenic character of age-related hearing impairment. *Eur J Hum Genet*.

FRANSEN, E., LEMKENS, N., VAN LAER, L. & VAN CAMP, G. 2003. Age-related hearing impairment (ARHI): environmental risk factors and genetic prospects. *Exp Gerontol,* 38**,** 353-9.

FRIEDMAN, R. A., VAN LAER, L., HUENTELMAN, M. J., SHETH, S. S., VAN EYKEN, E., CORNEVEAUX, J. J., TEMBE, W. D., HALPERIN, R. F., THORBURN, A. Q., THYS, S., BONNEUX, S., FRANSEN, E., HUYGHE, J., PYYKKO, I., CREMERS, C. W., KREMER, H., DHOOGE, I., STEPHENS, D., ORZAN, E., PFISTER, M., BILLE, M., PARVING, A., SORRI, M., VAN DE HEYNING, P. H., MAKMURA, L., OHMEN, J. D., LINTHICUM, F. H., JR., FAYAD, J. N., PEARSON, J. V., CRAIG, D. W., STEPHAN, D. A. & VAN CAMP, G. 2009. GRM7 variants confer susceptibility to age-related hearing impairment. *Hum Mol Genet,* 18**,** 785-96.

FRIEDMANN, I., FRASER, G. R. & FROGGATT, P. 1966. Pathology of the ear in the cardioauditory syndrome of Jervell and Lange-Nielsen (recessive deafness with electrocardiographic abnormalities). *J Laryngol Otol,* 80**,** 451-70.

GATES, G. A. 2012. Central presbycusis: an emerging view. *Otolaryngol Head Neck Surg,* 147**,** 1-2.

GATES, G. A., COBB, J. L., LINN, R. T., REES, T., WOLF, P. A. & D'AGOSTINO, R. B. 1996. Central auditory dysfunction, cognitive dysfunction, and dementia in older people. *Arch Otolaryngol Head Neck Surg,* 122**,** 161-7.

GATES, G. A. & MILLS, J. H. 2005. Presbycusis. *Lancet,* 366**,** 1111-20.

GIFFARD, R. G., LEE, Y. S., OUYANG, Y. B., MURPHY, S. L. & MONYER, H. 2003. Two variants of the rat brain sodium-driven chloride bicarbonate exchanger (NCBE): developmental expression and addition of a PDZ motif. *Eur J Neurosci,* 18**,** 2935-45.

GIROTTO, G., PIRASTU, N., SORICE, R., BIINO, G., CAMPBELL, H., D'ADAMO, A. P., HASTIE, N. D., NUTILE, T., POLASEK, O., PORTAS, L., RUDAN, I., ULIVI, S., ZEMUNIK, T., WRIGHT, A. F., CIULLO, M., HAYWARD, C., PIRASTU, M. & GASPARINI, P. 2011. Hearing function and thresholds: a genome-wide association study in European isolated populations identifies new loci and pathways. *J Med Genet,* 48**,** 369-74.

GORLIN, R. J., TORIELLO, H. V. & COHEN, M. M. 1995. *Hereditary Hearing Loss and Its Syndromes*, Oxford University Press.

GOW, A., DAVIES, C., SOUTHWOOD, C. M., FROLENKOV, G., CHRUSTOWSKI, M., NG, L., YAMAUCHI, D., MARCUS, D. C. & KACHAR, B. 2004. Deafness in Claudin 11-null mice reveals the critical contribution of basal cell tight junctions to stria vascularis function. *J Neurosci,* 24**,** 7051-62.

GROUP, T. T. C. 1996. Positional cloning of a gene involved in the pathogenesis of Treacher Collins syndrome. The Treacher Collins Syndrome Collaborative Group. *Nat Genet,* 12**,** 130-6.

HALL, D. J., SKERRETT, E. J. & THOMAS, W. D. 1978. Critical point drying for scanning electron microscopy: a semi-automatic method of preparing biological specimens. *J Microsc,* 113**,** 277-90.

HARDELIN, J.-P., LEVILLIERS, J. & PETIT, C. 2001. Deafness: Hereditary. *eLS.* John Wiley & Sons, Ltd.

HARDISTY-HUGHES, R. E., PARKER, A. & BROWN, S. D. 2010. A hearing and vestibular phenotyping pipeline to identify mouse mutants with hearing impairment. *Nat Protoc,* 5**,** 177-90.

HARDISTY-HUGHES, R. E., TATEOSSIAN, H., MORSE, S. A., ROMERO, M. R., MIDDLETON, A., TYMOWSKA-LALANNE, Z., HUNTER, A. J., CHEESEMAN, M. & BROWN, S. D. 2006. A mutation in the F-box gene, Fbxo11, causes otitis media in the Jeff mouse. *Hum Mol Genet,* 15**,** 3273-9.

HENDERSON, D., BIELEFELD, E. C., HARRIS, K. C. & HU, B. H. 2006. The role of oxidative stress in noise-induced hearing loss. *Ear Hear,* 27**,** 1-19.

HENRY, K. R. 1979. Auditory brainstem volume-conducted responses: origins in the laboratory mouse. *J Am Aud Soc,* 4**,** 173-8.

HEQUEMBOURG, S. & LIBERMAN, M. C. 2001. Spiral ligament pathology: a major aspect of age-related cochlear degeneration in C57BL/6 mice. *J Assoc Res Otolaryngol,* 2**,** 118-29.

HIBINO, H., HIGASHI-SHINGAI, K., FUJITA, A., IWAI, K., ISHII, M. & KURACHI, Y. 2004. Expression of an inwardly rectifying K+ channel, Kir5.1, in specific types of fibrocytes in the cochlear lateral wall suggests its functional importance in the establishment of endocochlear potential. *Eur J Neurosci,* 19**,** 76-84.

HIBINO, H., HORIO, Y., INANOBE, A., DOI, K., ITO, M., YAMADA, M., GOTOW, T., UCHIYAMA, Y., KAWAMURA, M., KUBO, T. & KURACHI, Y. 1997. An ATP-dependent inwardly rectifying potassium channel, KAB-2 (Kir4. 1), in cochlear stria vascularis of inner ear: its specific subcellular localization and correlation with the formation of endocochlear potential. *J Neurosci,* 17**,** 4711-21.

HIBINO, H. & KURACHI, Y. 2006. Molecular and physiological bases of the K+ circulation in the mammalian inner ear. *Physiology (Bethesda),* 21**,** 336-45.

HIBINO, H., NIN, F., TSUZUKI, C. & KURACHI, Y. 2010. How is the highly positive endocochlear potential formed? The specific architecture of the stria vascularis and the roles of the ion-transport apparatus. *Pflugers Arch,* 459**,** 521-33.

HILDING, D. A. & GINZBERG, R. D. 1977. Pigmentation of the stria vascularis. The contribution of neural crest melanocytes. *Acta Otolaryngol,* 84**,** 24-37.

HILGEN, G., HUEBNER, A. K., TANIMOTO, N., SOTHILINGAM, V., SEIDE, C., GARRIDO, M. G., SCHMIDT, K. F., SEELIGER, M. W., LOWEL, S., WEILER, R., HUBNER, C. A. & DEDEK, K. 2012. Lack of the sodium-driven chloride bicarbonate exchanger NCBE impairs visual function in the mouse retina. *PLoS One,* 7**,** e46155.

HOELTER, S. M., DALKE, C., KALLNIK, M., BECKER, L., HORSCH, M., SCHREWE, A., FAVOR, J., KLOPSTOCK, T., BECKERS, J., IVANDIC, B., GAILUS-DURNER, V., FUCHS, H., HRABE DE ANGELIS, M., GRAW, J. & WURST, W. 2008. "Sighted C3H" mice--a tool for analysing the influence of vision on mouse behaviour? *Front Biosci,* 13**,** 5810-23.

HOUSLEY, G. D., MARCOTTI, W., NAVARATNAM, D. & YAMOAH, E. N. 2006. Hair cells--beyond the transducer. *J Membr Biol,* 209**,** 89-118.

HTTP://HEARINGIMPAIRMENT.JAX.ORG/TABLE2.HTML. Available: [Accessed 25/11/2014].

HTTP://WWW.BIOON.COM/BIOLINE/NEUROSCI/COURSE/AUDVEST.HTML. Available: [Accessed 25/11/2014].

HTTP://WWW.BRITANNICA.COM/EBCHECKED/TOPIC/626968/VESTIBULAR-SYSTEM. Available: [Accessed 25/11/2014].

HTTP://WWW.MICHELLEWYATT.COM/ENT-SURGERY/EAR-SURGERY/GROMMET-SURGERY. Available: [Accessed 25/11/2014].

HUBNER, C. A., HENTSCHKE, M., JACOBS, S. & HERMANS-BORGMEYER, I. 2004. Expression of the sodium-driven chloride bicarbonate exchanger NCBE during prenatal mouse development. *Gene Expr Patterns,* 5**,** 219-23.

HUDSPETH, A. J. 1989. How the ear's works work. *Nature,* 341**,** 397-404.

HUDSPETH, A. J. 1997. How hearing happens. *Neuron,* 19**,** 947-50.

HUNTER-DUVAR, I. M. 1978. A technique for preparation of cochlear specimens for assessment with the scanning electron microscope. *Acta Otolaryngol Suppl,* 351**,** 3-23.

IKEDA, K. & MORIZONO, T. 1989. Electrochemical profiles for monovalent ions in the stria vascularis: cellular model of ion transport mechanisms. *Hear Res,* 39**,** 279-86.

ISAACSON, J. E. & VORA, N. M. 2003. Differential diagnosis and treatment of hearing loss. *Am Fam Physician,* 68**,** 1125-32.

IWASA, K. H., MIZUTA, K., LIM, D. J., BENOS, D. J. & TACHIBANA, M. 1994. Amiloride-sensitive channels in marginal cells in the stria vascularis of the guinea pig cochlea. *Neurosci Lett,* 172**,** 163-6.

JACOBS, S., RUUSUVUORI, E., SIPILA, S. T., HAAPANEN, A., DAMKIER, H. H., KURTH, I., HENTSCHKE, M., SCHWEIZER, M., RUDHARD, Y., LAATIKAINEN, L. M., TYYNELA, J., PRAETORIUS, J., VOIPIO, J. & HUBNER, C. A. 2008. Mice with targeted Slc4a10 gene disruption have small brain ventricles and show reduced neuronal excitability. *Proc Natl Acad Sci U S A,* 105**,** 311-6.

JAHNKE, K. 1975. The fine structure of freeze-fractured intercellular junctions in the guinea pig inner ear. *Acta Otolaryngol Suppl,* 336**,** 1-40.

JAWOREK, T. J., BHATTI, R., LATIEF, N., KHAN, S. N., RIAZUDDIN, S. & AHMED, Z. M. 2012. USH1K, a novel locus for type I Usher syndrome, maps to chromosome 10p11.21-q21.1. *J Hum Genet,* 57**,** 633-7.

JOHNSEN, T., JORGENSEN, M. B. & JOHNSEN, S. 1986. Mondini cochlea in Pendred's syndrome. A histological study. *Acta Otolaryngol,* 102**,** 239-47.

JOHNSON, K. R., ERWAY, L. C., COOK, S. A., WILLOTT, J. F. & ZHENG, Q. Y. 1997. A major gene affecting age-related hearing loss in C57BL/6J mice. *Hear Res,* 114**,** 83-92.

JOHNSON, K. R., GAGNON, L. H., LONGO-GUESS, C. & KANE, K. L. 2012. Association of a citrate synthase missense mutation with age-related hearing loss in A/J mice. *Neurobiol Aging,* 33**,** 1720-9.

JOHNSON, K. R., LONGO-GUESS, C., GAGNON, L. H., YU, H. & ZHENG, Q. Y. 2008. A locus on distal chromosome 11 (ahl8) and its interaction with Cdh23 ahl underlie the early onset, age-related hearing loss of DBA/2J mice. *Genomics,* 92**,** 219-25.

JOHNSON, K. R. & ZHENG, Q. Y. 2002. Ahl2, a second locus affecting age-related hearing loss in mice. *Genomics,* 80**,** 461-4.

JOHNSON, K. R., ZHENG, Q. Y., BYKHOVSKAYA, Y., SPIRINA, O. & FISCHEL-GHODSIAN, N. 2001. A nuclear-mitochondrial DNA interaction affecting hearing impairment in mice. *Nat Genet,* 27**,** 191-4.

JOHNSON, K. R., ZHENG, Q. Y. & ERWAY, L. C. 2000. A major gene affecting age-related hearing loss is common to at least ten inbred strains of mice. *Genomics,* 70**,** 171-80.

JOHNSTONE, B. M., PATUZZI, R., SYKA, J. & SYKOVA, E. 1989. Stimulus-related potassium changes in the organ of Corti of guinea-pig. *J Physiol,* 408**,** 77-92.

KEAYS, D. A., CLARK, T. G. & FLINT, J. 2006. Estimating the number of coding mutations in genotypic- and phenotypic-driven N-ethyl-N-nitrosourea (ENU) screens. *Mamm Genome,* 17**,** 230-8.

KELLER, J. M., NEELY, H. R., LATOCHE, J. R. & NOBEN-TRAUTH, K. 2011. High-frequency sensorineural hearing loss and its underlying genetics (Hfhl1 and Hfhl2) in NIH Swiss mice. *J Assoc Res Otolaryngol,* 12**,** 617-31.

KELLER, J. M. & NOBEN-TRAUTH, K. 2012. Genome-wide linkage analyses identify Hfhl1 and Hfhl3 with frequency-specific effects on the hearing spectrum of NIH Swiss mice. *BMC Genet,* 13**,** 32.

KHARKOVETS, T., DEDEK, K., MAIER, H., SCHWEIZER, M., KHIMICH, D., NOUVIAN, R., VARDANYAN, V., LEUWER, R., MOSER, T. & JENTSCH, T. J. 2006. Mice with altered KCNQ4 K+ channels implicate sensory outer hair cells in human progressive deafness. *EMBO J,* 25**,** 642-52.

KIKUCHI, T., ADAMS, J. C., MIYABE, Y., SO, E. & KOBAYASHI, T. 2000a. Potassium ion recycling pathway via gap junction systems in the mammalian cochlea and its interruption in hereditary nonsyndromic deafness. *Med Electron Microsc,* 33**,** 51-6.

KIKUCHI, T., KIMURA, R. S., PAUL, D. L., TAKASAKA, T. & ADAMS, J. C. 2000b. Gap junction systems in the mammalian cochlea. *Brain Res Brain Res Rev,* 32**,** 163-6.

KITAJIRI, S., MIYAMOTO, T., MINEHARU, A., SONODA, N., FURUSE, K., HATA, M., SASAKI, H., MORI, Y., KUBOTA, T., ITO, J., FURUSE, M. & TSUKITA, S. 2004. Compartmentalization established by claudin-11-based tight junctions in stria vascularis is required for hearing through generation of endocochlear potential. *J Cell Sci,* 117**,** 5087-96.

KONISHI, T., HAMRICK, P. E. & WALSH, P. J. 1978. Ion transport in guinea pig cochlea. I. Potassium and sodium transport. *Acta Otolaryngol,* 86**,** 22-34.

KONISHI, T. & MENDELSOHN, M. 1970. Effect of ouabain on cochlear potentials and endolymph composition in guinea pigs. *Acta Otolaryngol,* 69**,** 192-9.

KROS, C. 1996. Physiology of Mammalian Cochlear Hair Cells. *In:* DALLOS, P., POPPER, A. & FAY, R. (eds.) *The Cochlea.* Springer New York.

KUSAKARI, J., ISE, I., COMEGYS, T. H., THALMANN, I. & THALMANN, R. 1978. Effect of ethacrynic acid, furosemide, and ouabain upon the endolymphatic potential and upon high energy phosphates of the stria vascularis. *Laryngoscope,* 88**,** 12-37.

LATOCHE, J. R., NEELY, H. R. & NOBEN-TRAUTH, K. 2011. Polygenic inheritance of sensorineural hearing loss (Snhl2, -3, and -4) and organ of Corti patterning defect in the ALR/LtJ mouse strain. *Hear Res,* 275**,** 150-9.

LAUTERMANN, J., TEN CATE, W. J., ALTENHOFF, P., GRUMMER, R., TRAUB, O., FRANK, H., JAHNKE, K. & WINTERHAGER, E. 1998. Expression of the gap-junction connexins 26 and 30 in the rat cochlea. *Cell Tissue Res,* 294**,** 415-20.

LAWRENCE, M., WOLSK, D. & LITTON, W. B. 1961. Circulation of the inner ear fluids. *Ann Otol Rhinol Laryngol,* 70**,** 753-76.

LIU, X. Z., XIA, X. J., ADAMS, J., CHEN, Z. Y., WELCH, K. O., TEKIN, M., OUYANG, X. M., KRISTIANSEN, A., PANDYA, A., BALKANY, T., ARNOS, K. S. & NANCE, W. E. 2001. Mutations in GJA1 (connexin 43) are associated with non-syndromic autosomal recessive deafness. *Hum Mol Genet,* 10**,** 2945-51.

LIU, X. Z. & YAN, D. 2007. Ageing and hearing loss. *J Pathol,* 211**,** 188-97.

LIU, Y., XU, J. Y., WANG, D. K., BORON, W. F. & CHEN, L. M. 2011. Expression and distribution of NBCn2 (Slc4a10) splice variants in mouse brain: cloning of novel variant NBCn2-D. *Brain Res,* 1390**,** 33-40.

MARCUS, D. C., MARCUS, N. Y. & THALMANN, R. 1981. Changes in cation contents of stria vascularis with ouabain and potassium-free perfusion. *Hear Res,* 4**,** 149-60.

MARCUS, D. C., ROKUGO, M. & THALMANN, R. 1985. Effects of barium and ion substitutions in artificial blood on endocochlear potential. *Hear Res,* 17**,** 79-86.

MARCUS, D. C., WU, T., WANGEMANN, P. & KOFUJI, P. 2002. KCNJ10 (Kir4.1) potassium channel knockout abolishes endocochlear potential. *Am J Physiol Cell Physiol,* 282**,** C403-7.

MASHIMO, T., ERVEN, A. E., SPIDEN, S. L., GUENET, J. L. & STEEL, K. P. 2006. Two quantitative trait loci affecting progressive hearing loss in 101/H mice. *Mamm Genome,* 17**,** 841-50.

MERCHANT, S. N., RAVICZ, M. E., PURIA, S., VOSS, S. E., WHITTEMORE, K. R., JR., PEAKE, W. T. & ROSOWSKI, J. J. 1997. Analysis of middle ear mechanics and application to diseased and reconstructed ears. *Am J Otol,* 18**,** 139-54.

MILLAN, J. M., ALLER, E., JAIJO, T., BLANCO-KELLY, F., GIMENEZ-PARDO, A. & AYUSO, C. 2011. An update on the genetics of usher syndrome. *J Ophthalmol,* 2011**,** 417217.

MILLS, J. H. & GOING, J. A. 1982. Review of environmental factors affecting hearing. *Environ Health Perspect,* 44**,** 119-27.

MIZUTA, K., ADACHI, M. & IWASA, K. H. 1997. Ultrastructural localization of the Na-K-Cl cotransporter in the lateral wall of the rabbit cochlear duct. *Hear Res,* 106**,** 154-62.

MORITA, Y., HIROKAWA, S., KIKKAWA, Y., NOMURA, T., YONEKAWA, H., SHIROISHI, T., TAKAHASHI, S. & KOMINAMI, R. 2007. Fine mapping of Ahl3 affecting both age-related and noise-induced hearing loss. *Biochem Biophys Res Commun,* 355**,** 117-21.

MORSLI, H., CHOO, D., RYAN, A., JOHNSON, R. & WU, D. K. 1998. Development of the mouse inner ear and origin of its sensory organs. *J Neurosci,* 18**,** 3327-35.

NAGTEGAAL, A. P., SPIJKER, S., CRINS, T. T. & BORST, J. G. 2012. A novel QTL underlying early-onset, low-frequency hearing loss in BXD recombinant inbred strains. *Genes Brain Behav*.

NEMOTO, M., MORITA, Y., MISHIMA, Y., TAKAHASHI, S., NOMURA, T., USHIKI, T., SHIROISHI, T., KIKKAWA, Y., YONEKAWA, H. & KOMINAMI, R. 2004. Ahl3, a third locus on mouse chromosome 17 affecting age-related hearing loss. *Biochem Biophys Res Commun,* 324**,** 1283-8.

NEYROUD, N., TESSON, F., DENJOY, I., LEIBOVICI, M., DONGER, C., BARHANIN, J., FAURE, S., GARY, F., COUMEL, P., PETIT, C., SCHWARTZ, K. & GUICHENEY, P. 1997. A novel mutation in the potassium channel gene KVLQT1 causes the Jervell and Lange-Nielsen cardioauditory syndrome. *Nat Genet,* 15**,** 186-9.

NOBEN-TRAUTH, K., LATOCHE, J. R., NEELY, H. R. & BENNETT, B. 2010. Phenotype and genetics of progressive sensorineural hearing loss (Snhl1) in the LXS set of recombinant inbred strains of mice. *PLoS One,* 5**,** e11459.

NOBEN-TRAUTH, K., ZHENG, Q. Y. & JOHNSON, K. R. 2003. Association of cadherin 23 with polygenic inheritance and genetic modification of sensorineural hearing loss. *Nat Genet,* 35**,** 21-3.

NOLAN, L. S., MAIER, H., HERMANS-BORGMEYER, I., GIROTTO, G., ECOB, R., PIRASTU, N., CADGE, B. A., HUBNER, C., GASPARINI, P., STRACHAN, D. P., DAVIS, A. & DAWSON, S. J. 2013. Estrogen-related receptor gamma and hearing function: evidence of a role in humans and mice. *Neurobiol Aging,* 34**,** 2077 e1-9.

NOLAN, P. M., PETERS, J., VIZOR, L., STRIVENS, M., WASHBOURNE, R., HOUGH, T., WELLS, C., GLENISTER, P., THORNTON, C., MARTIN, J., FISHER, E., ROGERS, D., HAGAN, J., REAVILL, C., GRAY, I., WOOD, J., SPURR, N., BROWNE, M., RASTAN, S., HUNTER, J. & BROWN, S. D. 2000. Implementation of a large-scale ENU mutagenesis program: towards increasing the mouse mutant resource. *Mamm Genome,* 11**,** 500-6.

OHLEMILLER, K. K. 2004. Age-related hearing loss: the status of Schuknecht's typology. *Curr Opin Otolaryngol Head Neck Surg,* 12**,** 439-43.

OHLEMILLER, K. K. 2006. Contributions of mouse models to understanding of age- and noise-related hearing loss. *Brain Res,* 1091**,** 89-102.

PAPARELLA, M. M., MORIZONO, T. & MATSUNAGA, T. 1992. Kyoshiro yamakawa, md, and temporal bone histopathology of meniere's patient reported in 1938: Commemoration of the centennial of his birth. *Archives of Otolaryngology–Head & Neck Surgery,* 118**,** 660-662.

PARKER, M. D., MUSA-AZIZ, R., ROJAS, J. D., CHOI, I., DALY, C. M. & BORON, W. F. 2008. Characterization of human SLC4A10 as an electroneutral Na/HCO3 cotransporter (NBCn2) with Cl- self-exchange activity. *J Biol Chem,* 283**,** 12777-88.

PARKINSON, N., HARDISTY-HUGHES, R. E., TATEOSSIAN, H., TSAI, H. T., BROOKER, D., MORSE, S., LALANE, Z., MACKENZIE, F., FRAY, M., GLENISTER, P., WOODWARD, A. M., POLLEY, S., BARBARIC, I., DEAR, N., HOUGH, T. A., HUNTER, A. J., CHEESEMAN, M. T. & BROWN, S. D. 2006. Mutation at the Evi1 locus in Junbo mice causes susceptibility to otitis media. *PLoS Genet,* 2**,** e149.

PETIT, C., LEVILLIERS, J. & HARDELIN, J. P. 2001. Molecular genetics of hearing loss. *Annu Rev Genet,* 35**,** 589-646.

PETIT, C. & WEIL, D. 2001. Deafness. *eLS.* John Wiley & Sons, Ltd.

PITTLER, S. J. & BAEHR, W. 1991. Identification of a nonsense mutation in the rod photoreceptor cGMP phosphodiesterase beta-subunit gene of the rd mouse. *Proc Natl Acad Sci U S A,* 88**,** 8322-6.

PRAETORIUS, J., NEJSUM, L. N. & NIELSEN, S. 2004. A SCL4A10 gene product maps selectively to the basolateral plasma membrane of choroid plexus epithelial cells. *Am J Physiol Cell Physiol,* 286**,** C601-10.

PUJOL, R. & LAVIGNE-REBILLARD, M. 1995. Sensory and neural structures in the developing human cochlea. *Int J Pediatr Otorhinolaryngol,* 32 Suppl**,** S177-82.

PURVES, D. 2001. *Neuroscience,* Sunderland, Mass. ; [Great Britain], Sinauer Associates.

QUWAILID, M. M., HUGILL, A., DEAR, N., VIZOR, L., WELLS, S., HORNER, E., FULLER, S., WEEDON, J., MCMATH, H., WOODMAN, P., EDWARDS, D., CAMPBELL, D., RODGER, S., CAREY, J., ROBERTS, A., GLENISTER, P., LALANNE, Z., PARKINSON, N., COGHILL, E. L., MCKEONE, R., COX, S., WILLAN, J., GREENFIELD, A., KEAYS, D., BRADY, S., SPURR, N., GRAY, I., HUNTER, J., BROWN, S. D. & COX, R. D. 2004. A gene-driven ENU-based approach to generating an allelic series in any gene. *Mamm Genome,* 15**,** 585-91.

RAMSAY, H. A. & LINTHICUM, F. H., JR. 1994. Mixed hearing loss in otosclerosis: indication for long-term follow-up. *Am J Otol,* 15**,** 536-9.

RAPHAEL, Y. & ALTSCHULER, R. A. 2003. Structure and innervation of the cochlea. *Brain Res Bull,* 60**,** 397-422.

REHM, H. L. & MORTON, C. C. 1999. A new age in the genetics of deafness. *Genet Med,* 1**,** 295-302; quiz 303.

RONAGHI, M. 2001. Pyrosequencing sheds light on DNA sequencing. *Genome Res,* 11**,** 3-11.

RUSSELL, W. L., HUNSICKER, P. R., CARPENTER, D. A., CORNETT, C. V. & GUINN, G. M. 1982. Effect of dose fractionation on the ethylnitrosourea induction of specific-locus mutations in mouse spermatogonia. *Proc Natl Acad Sci U S A,* 79**,** 3592-3.

RUSSELL, W. L., KELLY, E. M., HUNSICKER, P. R., BANGHAM, J. W., MADDUX, S. C. & PHIPPS, E. L. 1979. Specific-locus test shows ethylnitrosourea to be the most potent mutagen in the mouse. *Proc Natl Acad Sci U S A,* 76**,** 5818-9.

RZADZINSKA, A. K., SCHNEIDER, M. E., DAVIES, C., RIORDAN, G. P. & KACHAR, B. 2004. An actin molecular treadmill and myosins maintain stereocilia functional architecture and self-renewal. *J Cell Biol,* 164**,** 887-97.

SAIKI, R. K., SCHARF, S., FALOONA, F., MULLIS, K. B., HORN, G. T., ERLICH, H. A. & ARNHEIM, N. 1985. Enzymatic amplification of beta-globin genomic sequences and restriction site analysis for diagnosis of sickle cell anemia. *Science,* 230**,** 1350-4.

SAKAGUCHI, N., CROUCH, J. J., LYTLE, C. & SCHULTE, B. A. 1998. Na-K-Cl cotransporter expression in the developing and senescent gerbil cochlea. *Hear Res,* 118**,** 114-22.

SALT, A. N., MELICHAR, I. & THALMANN, R. 1987. Mechanisms of endocochlear potential generation by stria vascularis. *Laryngoscope,* 97**,** 984-91.

SALT, A. N. & OHYAMA, K. 1993. Accumulation of potassium in scala vestibuli perilymph of the mammalian cochlea. *Ann Otol Rhinol Laryngol,* 102**,** 64-70.

SAMBROOK, J., FRITSCH, E. F. & MANIATIS, T. 1989. *Molecular cloning : a laboratory manual,* Cold Spring Harbor, N.Y., Cold Spring Harbor Laboratory.

SCHLINGMANN, K. P., KONRAD, M., JECK, N., WALDEGGER, P., REINALTER, S. C., HOLDER, M., SEYBERTH, H. W. & WALDEGGER, S. 2004. Salt wasting and deafness resulting from mutations in two chloride channels. *N Engl J Med,* 350**,** 1314-9.

SCHNEIDER, C. A., RASBAND, W. S. & ELICEIRI, K. W. 2012. NIH Image to ImageJ: 25 years of image analysis. *Nat Methods,* 9**,** 671-5.

SCHOLL, U. I., CHOI, M., LIU, T., RAMAEKERS, V. T., HAUSLER, M. G., GRIMMER, J., TOBE, S. W., FARHI, A., NELSON-WILLIAMS, C. & LIFTON, R. P. 2009. Seizures, sensorineural deafness, ataxia, mental retardation, and electrolyte imbalance (SeSAME syndrome) caused by mutations in KCNJ10. *Proc Natl Acad Sci U S A,* 106**,** 5842-7.

SCHROTT, A. & SPOENDLIN, H. 1987. Pigment anomaly-associated inner ear deafness. *Acta Otolaryngol,* 103**,** 451-7.

SCHUKNECHT, H. F. 1955. Presbycusis. *Laryngoscope,* 65**,** 402-19.

SCHUKNECHT, H. F. & GACEK, M. R. 1993. Cochlear pathology in presbycusis. *Ann Otol Rhinol Laryngol,* 102**,** 1-16.

SCHULTE, B. A. & ADAMS, J. C. 1989. Distribution of immunoreactive Na+,K+-ATPase in gerbil cochlea. *J Histochem Cytochem,* 37**,** 127-34.

SCHULTE, B. A. & STEEL, K. P. 1994. Expression of alpha and beta subunit isoforms of Na,K-ATPase in the mouse inner ear and changes with mutations at the Wv or Sld loci. *Hear Res,* 78**,** 65-76.

SCHULZE-BAHR, E., WANG, Q., WEDEKIND, H., HAVERKAMP, W., CHEN, Q., SUN, Y., RUBIE, C., HORDT, M., TOWBIN, J. A., BORGGREFE, M., ASSMANN, G., QU, X., SOMBERG, J. C., BREITHARDT, G., OBERTI, C. & FUNKE, H. 1997. KCNE1 mutations cause jervell and Lange-Nielsen syndrome. *Nat Genet,* 17**,** 267-8.

SHIN, J. B., LONGO-GUESS, C. M., GAGNON, L. H., SAYLOR, K. W., DUMONT, R. A., SPINELLI, K. J., PAGANA, J. M., WILMARTH, P. A., DAVID, L. L., GILLESPIE, P. G. & JOHNSON, K. R. 2010. The R109H variant of fascin-2, a developmentally regulated actin crosslinker in hair-cell stereocilia, underlies early-onset hearing loss of DBA/2J mice. *J Neurosci,* 30**,** 9683-94.

SHOTWELL, S. L., JACOBS, R. & HUDSPETH, A. J. 1981. Directional sensitivity of individual vertebrate hair cells to controlled deflection of their hair bundles. *Ann N Y Acad Sci,* 374**,** 1-10.

SMITH, R. J. H., SHEARER, A. E., HILDEBRAND, M. S. & VAN CAMP, G. 1993. Deafness and Hereditary Hearing Loss Overview.

SONG, X., YAMASAKI, M., MIYAZAKI, T., KONNO, K., UCHIGASHIMA, M. & WATANABE, M. 2014. Neuron type- and input pathway-dependent expression of Slc4a10 in adult mouse brains. *Eur J Neurosci,* 40**,** 2797-810.

SPECTOR, G. J. & CARR, C. 1979. The ultrastructural cytochemistry of peroxisomes in the guinea pig cochlea: a metabolic hypothesis for the stria vascularis. *Laryngoscope,* 89**,** 1-38.

SPICER, S. S. & SCHULTE, B. A. 1996. The fine structure of spiral ligament cells relates to ion return to the stria and varies with place-frequency. *Hear Res,* 100**,** 80-100.

STEEL, K. P. & BARKWAY, C. 1989. Another role for melanocytes: their importance for normal stria vascularis development in the mammalian inner ear. *Development,* 107**,** 453-63.

STERKERS, O., SAUMON, G., TRAN BA HUY, P. & AMIEL, C. 1982. K, Cl, and H2O entry in endolymph, perilymph, and cerebrospinal fluid of the rat. *Am J Physiol,* 243**,** F173-80.

SUBHA, S. T. & RAMAN, R. 2006. Role of impacted cerumen in hearing loss. *Ear Nose Throat J,* 85**,** 650, 652-3.

TACHIBANA, M. 1999. Sound needs sound melanocytes to be heard. *Pigment Cell Res,* 12**,** 344-54.

TACHIBANA, M., HARA, Y., VYAS, D., HODGKINSON, C., FEX, J., GRUNDFAST, K. & ARNHEITER, H. 1992. Cochlear disorder associated with melanocyte anomaly in mice with a transgenic insertional mutation. *Mol Cell Neurosci,* 3**,** 433-45.

TAKEUCHI, S. & ANDO, M. 1998a. Dye-coupling of melanocytes with endothelial cells and pericytes in the cochlea of gerbils. *Cell Tissue Res,* 293**,** 271-5.

TAKEUCHI, S. & ANDO, M. 1998b. Inwardly rectifying K+ currents in intermediate cells in the cochlea of gerbils: a possible contribution to the endocochlear potential. *Neurosci Lett,* 247**,** 175-8.

TANG, W., ZHANG, Y., CHANG, Q., AHMAD, S., DAHLKE, I., YI, H., CHEN, P., PAUL, D. L. & LIN, X. 2006. Connexin29 is highly expressed in cochlear Schwann cells, and it is required for the normal development and function of the auditory nerve of mice. *J Neurosci,* 26**,** 1991-9.

TASAKI, I. & SPYROPOULOS, C. S. 1959. Stria vascularis as source of endocochlear potential. *J Neurophysiol,* 22**,** 149-55.

TEELE, D. W., KLEIN, J. O. & ROSNER, B. 1989. Epidemiology of otitis media during the first seven years of life in children in greater Boston: a prospective, cohort study. *J Infect Dis,* 160**,** 83-94.

TEUBNER, B., MICHEL, V., PESCH, J., LAUTERMANN, J., COHEN-SALMON, M., SOHL, G., JAHNKE, K., WINTERHAGER, E., HERBERHOLD, C., HARDELIN, J. P., PETIT, C. & WILLECKE, K. 2003. Connexin30 (Gjb6)-deficiency causes severe hearing impairment and lack of endocochlear potential. *Hum Mol Genet,* 12**,** 13-21.

THOMAS, K. R. & CAPECCHI, M. R. 1987. Site-directed mutagenesis by gene targeting in mouse embryo-derived stem cells. *Cell,* 51**,** 503-12.

TROWE, M. O., MAIER, H., PETRY, M., SCHWEIZER, M., SCHUSTER-GOSSLER, K. & KISPERT, A. 2011. Impaired stria vascularis integrity upon loss of E-cadherin in basal cells. *Dev Biol,* 359**,** 95-107.

TROWE, M. O., MAIER, H., SCHWEIZER, M. & KISPERT, A. 2008. Deafness in mice lacking the T-box transcription factor Tbx18 in otic fibrocytes. *Development,* 135**,** 1725-34.

UHLMANN, R. F., LARSON, E. B., REES, T. S., KOEPSELL, T. D. & DUCKERT, L. G. 1989. Relationship of hearing impairment to dementia and cognitive dysfunction in older adults. *JAMA,* 261**,** 1916-9.

VAN LAER, L., HUYGHE, J. R., HANNULA, S., VAN EYKEN, E., STEPHAN, D. A., MAKI-TORKKO, E., AIKIO, P., FRANSEN, E., LYSHOLM-BERNACCHI, A., SORRI, M., HUENTELMAN, M. J. & VAN CAMP, G. 2010. A genome-wide association study for age-related hearing impairment in the Saami. *Eur J Hum Genet,* 18**,** 685-93.

VERILLAUD, B., GUILLERE, L., WILLIAMS, M. T., EL BAKKOURI, W. & AYACHE, D. 2011. Middle ear osteoma: a rare cause of conductive hearing loss with normal tympanic membrane. *Rev Laryngol Otol Rhinol (Bord),* 132**,** 159-61.

VETTER, D. E., MANN, J. R., WANGEMANN, P., LIU, J., MCLAUGHLIN, K. J., LESAGE, F., MARCUS, D. C., LAZDUNSKI, M., HEINEMANN, S. F. & BARHANIN, J. 1996. Inner ear defects induced by null mutation of the isk gene. *Neuron,* 17**,** 1251-64.

VON BEKESY, G. 1952. Resting potentials inside the cochlear partition of the guinea pig. *Nature,* 169**,** 241-2.

VON BÉKÉSY, G. & WEVER, E. G. 1960. *Experiments in hearing*, McGraw-Hill Book Co Inc.

WADA, J., KAMBAYASHI, J., MARCUS, D. C. & THALMANN, R. 1979. Vascular perfusion of the cochlea: effect of potassium-free and rubidium-substituted media. *Arch Otorhinolaryngol,* 225**,** 79-81.

WANG, C. Z., YANO, H., NAGASHIMA, K. & SEINO, S. 2000. The Na+-driven Cl-/HCO3- exchanger. Cloning, tissue distribution, and functional characterization. *J Biol Chem,* 275**,** 35486-90.

WANG, Z., LI, H., MOSS, A. J., ROBINSON, J., ZAREBA, W., KNILANS, T., BOWLES, N. E. & TOWBIN, J. A. 2002. Compound heterozygous mutations in KvLQT1 cause Jervell and Lange-Nielsen syndrome. *Mol Genet Metab,* 75**,** 308-16.

WANGEMANN, P. 2002. K+ cycling and the endocochlear potential. *Hear Res,* 165**,** 1-9.

WANGEMANN, P. 2006. Supporting sensory transduction: cochlear fluid homeostasis and the endocochlear potential. *J Physiol,* 576**,** 11-21.

WANGEMANN, P., LIU, J. & MARCUS, D. C. 1995. Ion transport mechanisms responsible for K+ secretion and the transepithelial voltage across marginal cells of stria vascularis in vitro. *Hear Res,* 84**,** 19-29.

WATERSTON, R. H., LINDBLAD-TOH, K., BIRNEY, E., ROGERS, J., ABRIL, J. F., AGARWAL, P., AGARWALA, R., AINSCOUGH, R., ALEXANDERSSON, M., AN, P., ANTONARAKIS, S. E., ATTWOOD, J., BAERTSCH, R., BAILEY, J., BARLOW, K., BECK, S., BERRY, E., BIRREN, B., BLOOM, T., BORK, P., BOTCHERBY, M., BRAY, N., BRENT, M. R., BROWN, D. G., BROWN, S. D., BULT, C., BURTON, J., BUTLER, J., CAMPBELL, R. D., CARNINCI, P., CAWLEY, S., CHIAROMONTE, F., CHINWALLA, A. T., CHURCH, D. M., CLAMP, M., CLEE, C., COLLINS, F. S., COOK, L. L., COPLEY, R. R., COULSON, A., COURONNE, O., CUFF, J., CURWEN, V., CUTTS, T., DALY, M., DAVID, R., DAVIES, J., DELEHAUNTY, K. D., DERI, J., DERMITZAKIS, E. T., DEWEY, C., DICKENS, N. J., DIEKHANS, M., DODGE, S., DUBCHAK, I., DUNN, D. M., EDDY, S. R., ELNITSKI, L., EMES, R. D., ESWARA, P., EYRAS, E., FELSENFELD, A., FEWELL, G. A., FLICEK, P., FOLEY, K., FRANKEL, W. N., FULTON, L. A., FULTON, R. S., FUREY, T. S., GAGE, D., GIBBS, R. A., GLUSMAN, G., GNERRE, S., GOLDMAN, N., GOODSTADT, L., GRAFHAM, D., GRAVES, T. A., GREEN, E. D., GREGORY, S., GUIGO, R., GUYER, M., HARDISON, R. C., HAUSSLER, D., HAYASHIZAKI, Y., HILLIER, L. W., HINRICHS, A., HLAVINA, W., HOLZER, T., HSU, F., HUA, A., HUBBARD, T., HUNT, A., JACKSON, I., JAFFE, D. B., JOHNSON, L. S., JONES, M., JONES, T. A., JOY, A., KAMAL, M., KARLSSON, E. K., et al. 2002. Initial sequencing and comparative analysis of the mouse genome. *Nature,* 420**,** 520-62.

WITTWER, C. T., REED, G. H., GUNDRY, C. N., VANDERSTEEN, J. G. & PRYOR, R. J. 2003. High-resolution genotyping by amplicon melting analysis using LCGreen. *Clin Chem,* 49**,** 853-60.

XIA, A., KATORI, Y., OSHIMA, T., WATANABE, K., KIKUCHI, T. & IKEDA, K. 2001. Expression of connexin 30 in the developing mouse cochlea. *Brain Res,* 898**,** 364-7.

XIAO, Z., YANG, Z., LIU, X. & XIE, D. 2011. Impaired membrane targeting and aberrant cellular localization of human Cx26 mutants associated with inherited recessive hearing loss. *Acta Otolaryngol,* 131**,** 59-66.

ZELANTE, L., GASPARINI, P., ESTIVILL, X., MELCHIONDA, S., D'AGRUMA, L., GOVEA, N., MILA, M., MONICA, M. D., LUTFI, J., SHOHAT, M., MANSFIELD, E., DELGROSSO, K., RAPPAPORT, E., SURREY, S. & FORTINA, P. 1997. Connexin26 mutations associated with the most common form of non-syndromic neurosensory autosomal recessive deafness (DFNB1) in Mediterraneans. *Hum Mol Genet,* 6**,** 1605-9.

ZHENG, J., SHEN, W., HE, D. Z., LONG, K. B., MADISON, L. D. & DALLOS, P. 2000. Prestin is the motor protein of cochlear outer hair cells. *Nature,* 405**,** 149-55.

ZHENG, Q. Y., DING, D., YU, H., SALVI, R. J. & JOHNSON, K. R. 2009. A locus on distal chromosome 10 (ahl4) affecting age-related hearing loss in A/J mice. *Neurobiol Aging,* 30**,** 1693-705.

ZHENG, Q. Y., JOHNSON, K. R. & ERWAY, L. C. 1999. Assessment of hearing in 80 inbred strains of mice by ABR threshold analyses. *Hear Res,* 130**,** 94-107.

ZIDANIC, M. & BROWNELL, W. E. 1990. Fine structure of the intracochlear potential field. I. The silent current. *Biophys J,* 57**,** 1253-68.

ZIELHUIS, G. A., HEUVELMANS-HEINEN, E. W., RACH, G. H. & VAN DEN BROEK, P. 1989. Environmental risk factors for otitis media with effusion in preschool children. *Scand J Prim Health Care,* 7**,** 33-8.

Supplementary Information

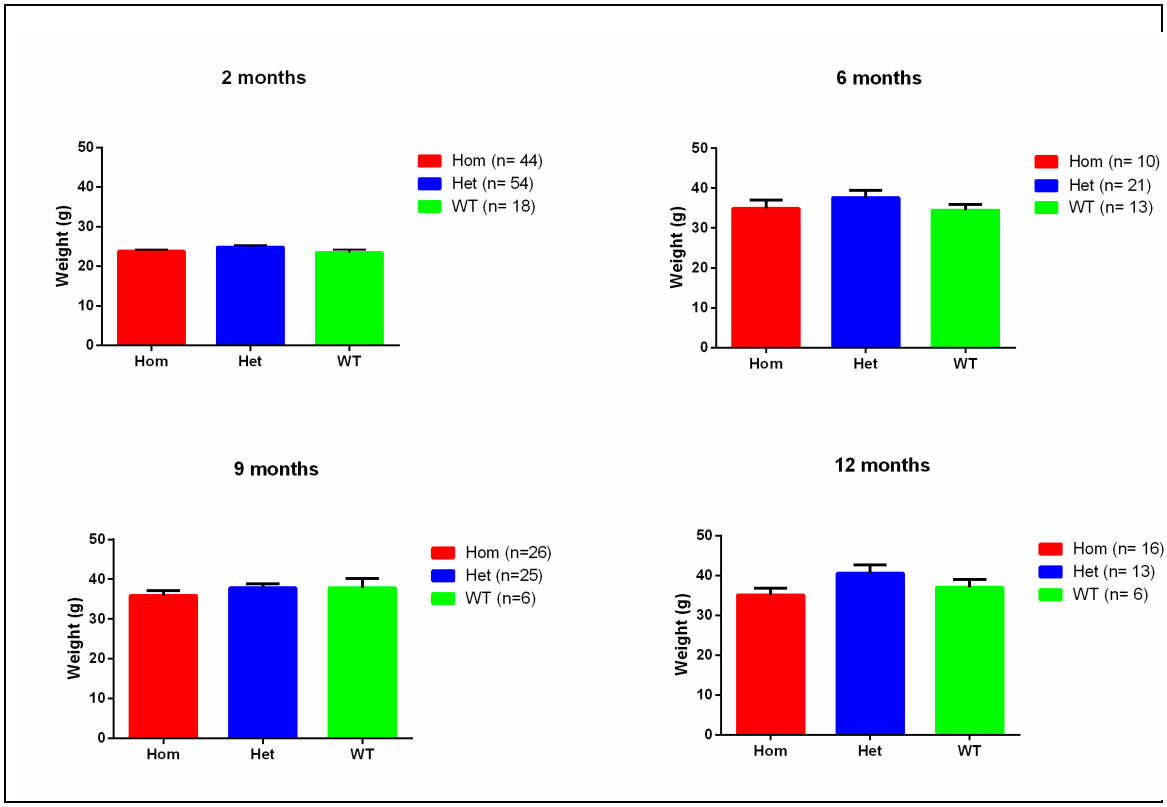

Figure S1: Weight data of *trombone* mice at two, six, nine and 12 months of age
There was no difference seen in the average weight of homozygous mice when compared to heterozygous and wildtype mice at all of the ages analysed. Error bars indicate standard error of mean, SEM.

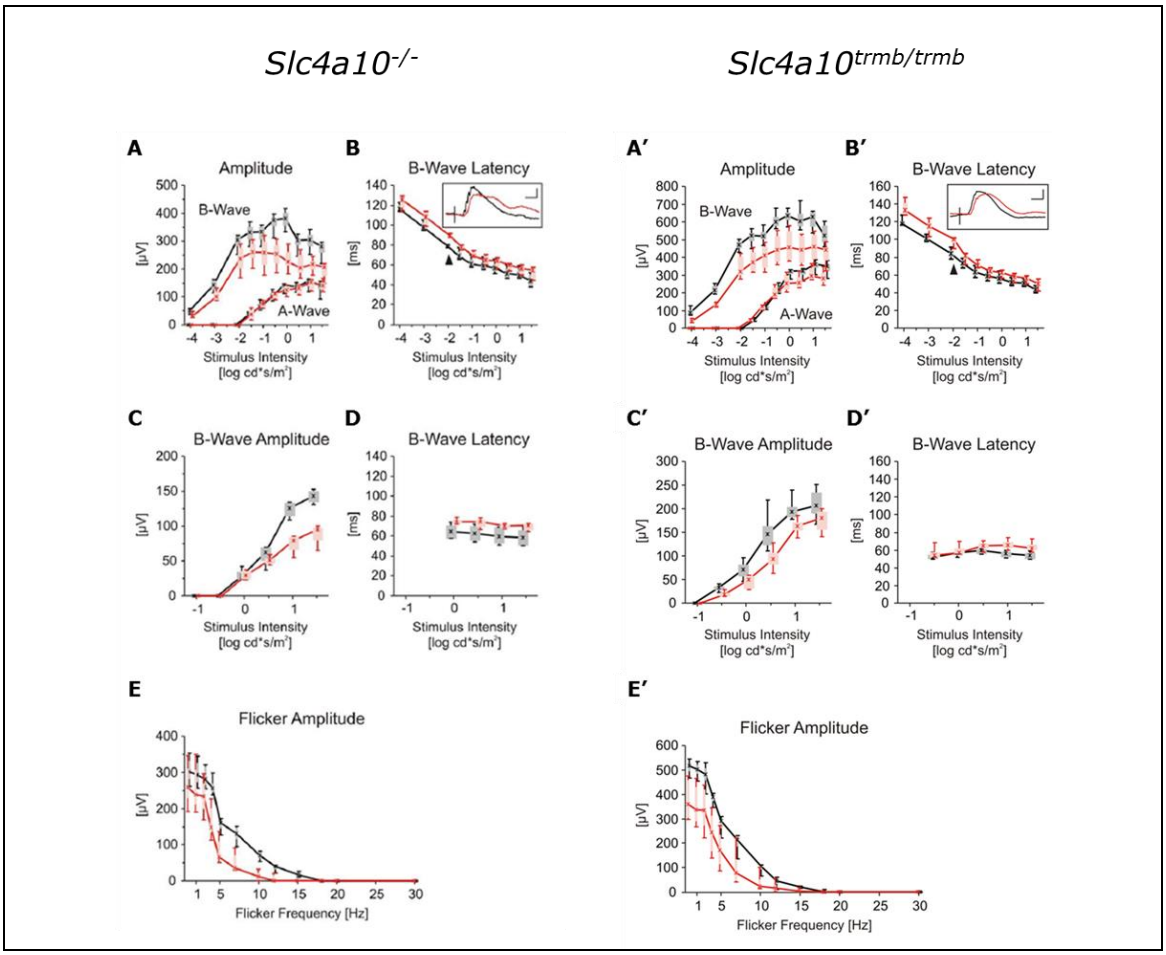

Figure S2: Comparison of Electroretinography results between *Slc4a10*$^{-/-}$ and *Slc4a10*$^{trmb/trmb}$

[A-E] Single flash ERG recordings from *Slc4a10*$^{+/+}$ (black) (n=2) and *Slc4a10*$^{-/-}$ (red) (n=3) mice at 12 months of age were conducted for increasing intensities under dark-adapted (scotopic) and light-adapted (photopic) conditions (Hilgen et al., 2012). Results showed that in *Slc4a10*$^{-/-}$ mice, scoptopic b-wave but not a-wave amplitudes were reduced [A] and b-wave latencies were increased [B], when compared to *Slc4a10*$^{+/+}$ littermates. Under photopic conditions, b-wave amplitudes [C] and b-wave latencies [D] of *Slc4a10*$^{-/-}$ mice were similarly affected. ERG recordings of a flicker frequency series (flash intensity G: −2 log cd*s/m2; I: 0.5 log cd*s/m2) under scotopic conditions showed that the flicker amplitudes [E] of *Slc4a10*$^{-/-}$ mice decreased at much lower flash frequencies than that of *Slc4a10*$^{+/+}$ littermate controls [E].

[A'-E'] To assess the effect of the *trombone* mutation on retinal function, ERG recordings were conducted on *Slc4a10*$^{+/+}$ (black) (n=5) and *Slc4a10*$^{trmb/trmb}$ (red) (n=5) mice at 12 weeks of age [A'-E']. Results for *Slc4a10*$^{trmb/trmb}$ in comparison are similar to those obtained by (Hilgen et al., 2012) *Slc4a10*$^{-/-}$ mice, albeit the difference from their respective wildtype controls is more mild in the *trombone* mice. Under scotopic conditions, b-wave amplitudes, but not a-wave amplitudes were reduced [A'] and b-wave latencies were increased [B']. Under photopic conditions, b-wave amplitudes [C'] and b-wave latencies [D'] of *Slc4a10*$^{-/-}$ mice were similarly affected. Flicker amplitudes [E'] of *Slc4a10*$^{trmb/trmb}$ mice also decrease at much lower flash frequencies thatn *Slc4a10*$^{+/+}$ littermates.

In all quantitative plots, boxes indicate the 25% and 75% quantile range, whiskers indicate the 5% and 95% quantiles, and solid lines connect the medians of the data.
Slc4a10$^{-/-}$ data from (Hilgen et al., 2012)

ERG recordings on *Slc4a10*$^{trmb/trmb}$ were conducted by Dr. Alun Barnard at the Nuffield Laboratory of Ophthalmology, University of Oxford.